Y 3.AT7:
36/11-1

REACTOR AND FUEL-PROCESSING TECHNOLOGY

A Quarterly Technical Progress Review

ILLINOIS STATE LIBRARY
JUN 3 - 1968
U. S. Supt. of Documents Deposit

Prepared for DIVISION OF TECHNICAL INFORMATION, U. S. ATOMIC ENERGY COMMISSION,
by ARGONNE NATIONAL LABORATORY

Winter 1967-1968

● VOLUME 11

● NUMBER 1

TECHNICAL PROGRESS REVIEWS

The United States Atomic Energy Commission publishes the Technical Progress Reviews to meet the needs of industry and government for concise summaries of current nuclear developments. Each journal digests and evaluates the latest findings in a specific area of nuclear technology and science. *Nuclear Safety* is a bimonthly journal; the other three are quarterly journals.

Isotopes and Radiation Technology
P. S. Baker, A. F. Rupp, and Associates
Isotopes Information Center, Oak Ridge National Laboratory

Nuclear Safety
Wm. B. Cottrell, W. H. Jordan, J. P. Blakely, and Associates
Nuclear Safety Information Center, Oak Ridge National Laboratory

Reactor and Fuel-Processing Technology
Argonne National Laboratory

Reactor Materials
E. M. Simons and Associates
Battelle Memorial Institute

All are available from the U. S. Government Printing Office. See the back cover for ordering instructions.

The views expressed in this publication do not necessarily represent those of the United States Atomic Energy Commission, its divisions or offices, or of any Commission advisory committee or contractor.

Availability of Reports Cited in This Review

United States Atomic Energy Commission (USAEC) reports are available at USAEC depository libraries and are sold by the Clearinghouse for Federal Scientific and Technical Information (CFSTI), National Bureau of Standards, U. S. Department of Commerce, 5285 Port Royal Road, Springfield, Va. 22151. All reports sold by CFSTI are $3.00 for printed copy and $0.65 for microfiche. Each separately bound part of a report is priced as a separate report. Some reports may not be available because of their preliminary nature; however, the information contained in them will generally be found in later progress or topical reports on the subject.

Other U. S. Government agency reports identified in this journal generally are available from CFSTI.

Private-organization reports should be requested from the originator.

United Kingdom Atomic Energy Authority (UKAEA) and Atomic Energy of Canada Limited (AECL) reports are available at USAEC depository libraries. UKAEA reports are sold by Her Majesty's Stationery Office, London; AECL reports are sold by the Scientific Document Distribution Office, Atomic Energy of Canada Limited, Chalk River, Ontario, Canada. UKAEA and AECL reports issued after March 1, 1967, are sold by CFSTI to purchasers in the United States and its territories.

Contents

Reactor and Fuel-Processing Technology
Vol. 11, No. 1, Winter 1967–1968

REACTOR SAFETY
Highlights of the Aix Conference on Fast Reactor Safety
C. E. Dickerman 1

DESIGN AND CONSTRUCTION PRACTICE
Further Developments in Containment-Building Electrical Penetrations
Fred Verber 5

Realistic Data Are Needed for Mechanical Analysis of Reactor Fuel Elements
Richard A. Valentin 13

OPERATING EXPERIENCE
Operational Problems and Solutions
Rolf C. Skaardal 17

FLUID AND THERMAL TECHNOLOGY
Thermophysical Properties of Sodium — Recommended Values
Gerald H. Golden, John V. Tokar, and David Miller 27

AQUEOUS PROCESSING
Research and Development on Aqueous Processing
C. E. Stevenson and D. M. Paige 49

NONAQUEOUS PROCESSING
Volatility Processes
J. J. Barghusen 54

Compact Pyrochemical Processes
W. E. Miller and R. K. Steinenberg 60

WASTE DISPOSAL
Progress in Waste-Disposal Research and Development
Phillip Fineman 65

Issued quarterly by the U. S. Atomic Energy Commission. Use of funds for printing this publication approved by the Director of the Bureau of the Budget on July 8, 1966.

Reactor and Fuel-Processing Technology

is a quarterly review of developments in reactor and reactor fuel technology. As such, this journal reports and interprets progress in the reactor field in terms of its significance to the reactor designer, operator, and fuel-cycle specialist. Articles either summarize and critically evaluate recently reported developments or review the "state of the art" of a particular topic. Both types of articles reference reports and publications that merit study; readers are urged to consult the references for additional information and the judgments of the original authors. If a reader has information that causes his evaluation to reinforce, modify, or contradict the opinions of our reviewers, he is encouraged to write to the Editor.

The scope of the journal encompasses:

CONCEPTS and APPLICATIONS: Progress in evaluating the applicability and economics of various reactor types and systems (including unconventional approaches), as well as of fuel resources and cycles, for utility central-station generation of electricity, auxiliary power, process radiation and heat, desalting, and propulsion — and for terrestrial, undersea, aerospace, and other advanced uses.

ANALYSIS and EXPERIMENTATION: Advancements in the techniques of reactor physics, fluid and thermal technology, energy conversion, fuel elements, materials, mechanics, control and dynamics, and reactor safety.

SYSTEMS and COMPONENTS: Experience as reflected in design and construction practice, components, systems technology, and operating performance of various specific types of reactors — including pressurized- and boiling-water reactors, molten-salt, organic-, gas-, and liquid-metal-cooled reactors, as well as generally applicable aspects of research and test reactors.

FUEL PROCESSING: Recent research and development on fuel aqueous processing, nonaqueous processing, waste disposal, and processing safety.

This journal is prepared by Argonne National Laboratory at the request of the Division of Technical Information of the U. S. Atomic Energy Commission. At Argonne, the Reactor Engineering Division (L. J. Koch, Director) and the Chemical Engineering Division (R. C. Vogel, Director) have the principal responsibility for the preparation of *Reactor and Fuel-Processing Technology*, with the regular assistance of the Reactor Physics Division (R. A. Avery, Director) and the Idaho Division (M. Novick, Director) and the occasional assistance of other divisions (Metallurgy, Chemistry, and Reactor Operations). Thus, unless noted otherwise, the reviewers and authors of articles are Laboratory staff members. The editors welcome interpretive review articles contributed by authors outside the Laboratory.

Editor, *James J. Dutton*
Advisory Editor, *David H. Lennox*
Managing Editor, *Karl K. Brown*
Co-Editor (Fuel Processing), *Joseph Royal*
Associate Editor (Physics), *Raymond Gold*
Assistant Editor, *Paul H. Gregory*

Argonne National Laboratory

Highlights of the Aix Conference on Fast Reactor Safety

By C. E. Dickerman

A general spirit that safety problems offer no basic obstacle to development of sodium-cooled fast reactors permeated the recent International Conference on Fast Reactor Safety held at Aix-en-Provence, France.[1] Speaker after speaker called for vigorous moves to develop large fast power reactors. W. McCarthy, of the Power Reactor Development Company, Fermi reactor, admonished that the fast breeder should become the standard reactor of the future: "the reactor our children will know."

Unlike the 1965 fast reactor safety conference at Argonne,[2] when reactivity coefficients were given the most technical attention, this September 1967 Aix conference was noted by the vigorous attention to the models for describing and calculating transient sodium boiling and expulsion by vaporization. The interest culminated in an informal meeting of the sodium investigators attending, who recommended that a conference on sodium boiling should be held as a follow-up. These developments will be reported in detail in a subsequent article.

Problems of fuel meltdown, sodium-vapor explosion, and malfunction detection are recognized but now are considered comparable to those of high-power-density thermal reactors. D. Okrent of Argonne cautioned against overlooking safety problems and observed that experience has shown that the unexpected often does occur. G. Denielou of the French Commissariat à l'Énergie Atomique summed up his feelings by noting that problems discussed seem to be essentially the same as for thermal reactors. F. Farmer of the UKAEA continued in a parallel vein by expressing the U. K. attitude that the fast reactor is proving to be "just another highly rated reactor" system.

Topics discussed include the physics of both local and generalized accidents, neutronics, critical experiments, sodium boiling, loss of coolant, reactor operation, and accident detection. The low ratio of steam papers (4) to sodium papers (63) reflected the actual emphasis of the discussions. Of the national programs represented at the conference, only the German program gave comparable emphasis to both steam-cooled reactors and sodium-cooled reactors.

Steam-Cooled Reactors, Briefly

The steam-cooled system has evolved into a direct cycle, with the reactor supplying superheated steam to the turbine; thus it more closely resembles gas-cooled-reactor designs than sodium-cooled fast reactors.

A paper from BelgoNucléaire focused on safety aspects of direct steam cycles.[3] Two German papers[4,5] and a U. S. paper[6] presented detailed considerations of equipment and control characteristics of the coupled reactor–turbine system.

The conference papers showed clearly the relative stage of development of steam-cooled fast reactors—systems now in the design-study stages—and liquid-metal-cooled fast reactors, which first moved to the operating stage a generation ago with Experimental Breeder Reactor I (EBR-I). No significant safety advantages of the steam systems were apparent.

Liquid-Metal Systems

It is apparent from the desire for details, both in experimental studies and in theoretical analyses, that the technology of liquid-metal-cooled fast breeder reactors is much more advanced than is the technology of steam-cooled breeders. In the liquid-metal systems, the central questions relate to meltdown, core compaction, and sodium behavior as they are characterized by experiment, analysis, and operating fast reactor experience.

MELTDOWN EXPERIMENTS

Three papers on experimental studies of core behavior under accident conditions were presented.

First was an Argonne report on its Transient Reactor Test (TREAT) reactor-transient studies, which featured descriptions and analyses of recent meltdown experiments in sodium loops.[7] The loop tests were performed on metallic, EBR-II driver fuel pins, run both as single pins and in small seven-pin clusters. Fuel-failure thresholds were reviewed in terms of a basic single-pin model. Rapid sodium expulsion, sharp pressure spikes, and extensive secondary movement of fuel and coolant were reported. TREAT was designed specifically for short transients, with durations of the order of a few seconds.

The second paper, from Cadarache, described the CEA program under way to set up a sodium loop for slow (up to 10 min) oxide-fuel meltdown experiments on the Cabri swimming-pool reactor.[8] The test loop being developed is designed for experiments on single fuel pins, with a capability for expansion to three-pin clusters by means of minor changes. The goal is meltdown experiments on full subassemblies, and a reference case of a seven-subassembly cluster was given as the eventual loop design basis.

Next was a BelgoNucléaire report[9] that analyzed results of a power excursion on oxide fuel in a sodium loop. The analysis was performed as part of the BelgoNucleaire studies on their proposed transient test reactor Briseis.

CORE-COMPACTION ACCIDENTS

It has become traditional for fast reactor safety sessions to include papers on the calculation of nuclear explosions that result from superprompt-critical reactivity insertions brought about by meltdown and core compaction during a less severe accident. A German paper[10] presented results from calculations on a mock-up of the core pin geometry for the core disassembly. Their geometry model was chosen as an improvement over the usual hypothetical fluid assumed for such computations. The paper by Lord[11] considered effects of geometry changes, but with a conventional core material description. In general, the calculations indicate that a value of about 500 lb "TNT equivalent" is a reasonable basis for containment design of prototype-size fast reactors.

What Core Behavior? Core behavior leading to the explosion phase was not detailed in these explosion-calculation papers. If a nuclear explosion is assumed to result from an initiating, less-severe accident involving all (or a large part) of a core, it is necessary to examine the course of the initiating accident, including the degree of coherence in fuel failure, of fuel and coolant movement, and, finally, of possible secondary collapse of fuel remains; if the accident is assumed to result from a severe localized accident (such as subassembly blockage and meltdown at power), it is necessary to consider the severity and speed of propagation of damage and degree of coherence of secondary movements. Thus it is clear—to this reviewer, at least—that the biggest current problem in the maximum-accident nuclear explosion calculations is the description of core behavior leading to the maximum accident. A related problem is the adequacy of the physical description of the core during the explosion.

SODIUM VAPORIZATION

Special attention was given to the problem of rapid energy transfer from hot finely divided fuel fragments to sodium. The resulting work done by the expansion of sodium vapor is analogous to a steam explosion such as those generated in the BORAX and SPERT experimental water-reactor destructive tests. Farmer (United Kingdom) observed in his panel talk (at the conclusion of the conference) that the thermal energy remaining in a fast reactor core after a maximum-accident explosion is very large and that it is possible to calculate a sodium-vapor explosion as severe as the (assumed) previous nuclear excursion. Hence the United Kingdom considered it as important to design containment for a sodium-vapor explosion as to design for a core vaporization explosion.

Models. MacFarlane[12] described calculations with a coupled code system that combines transient heat transfer, two-phase coolant hydrodynamics using an annular flow model, and neutron kinetics. Although the paper was presented to display a significant advance in the development of accident analysis techniques, the conference interest in details of transient sodium boiling was so strong that the vigorous discussion following the paper was almost exclusively on the two-phase hydrodynamics module of the coupled code system!

A contrasting model, of sodium slug expulsion, was incorporated into a Karlsruhe sodium-voiding code, the BLOW code, which was described in the paper by Peppler.[13] The BLOW model was developed on the basis of analyses of experiments performed by Grass and coworkers at Ispra[14] and was also related to results obtained by LeGonidec under CEA auspices.[15]

The effects of two-phase compressibility phenomena on transient sodium behavior and analyses of data were discussed by Fauske.[16] Liquid-metal superheat values reported[14] ranged up to 800°C, with widely varying but lower values reported by French,[15] Argonne,[17] Atomics International,[18] and Casaccia[19] workers. However, Pinchera[19] pointed out that under realistic core conditions the effective value of superheat might be rather low.

The theory of transient vaporization and condensation of sodium was discussed in some detail by Peppler,[13] Judd,[20] and Kosky.[21] For the models he used, Judd[20] found that dynamics of void growth were relatively insensitive to changes in geometry ranging

from a single spherical bubble to many spherical bubbles.

The general problem of sodium behavior during a core accident is still not well defined. Because of the scope and complexity of the subject, the Aix sodium papers will be discussed in greater detail in separate reviews on reactor safety implications of superheat[22] and on coolant-ejection mechanisms.[23]

Sodium Release. Consequences of sodium release during an accident also were considered. A paper by Morewitz[24] reported data and analyses of aerosol generation and behavior during a sodium fire. Their results showed that the presence of sodium oxide particles produced a significant scavenging action on the fuel aerosols. Deschamps and Rygaert[25] described related experiments on iodine distribution following a simulated sodium release. Containment of plutonium aerosols was discussed by Heller.[26]

OPERATING EXPERIENCE

A high point of the conference was the session on actual operating experience with the Dounreay, Rapsodie, BR-5, and Fermi fast reactors.

Dounreay. Phillips[27] reviewed the history of the Dounreay reactor, which was shut down by a NaK leak shortly before the conference. The paper was essentially a discussion of the well-known use of this facility as a fast-flux testing reactor. There was little more than an acknowledgment concerning the NaK leak; however, the leak has recently been located in one of 24 links between the primary coolant circuit and the reactor vessel.[28] Repair of the leak is expected to require "some months," apparently as a result of accessibility and radiation problems.

Rapsodie. Gajac and Reynes[29] told of problems encountered in the commissioning and startup of the French Rapsodie reactor, including thermal-stress difficulties in the original design and an inadvertent release of sodium. The actual reactor operation was reported to be smooth; in fact, current French optimism on the state of the fast-breeder-reactor art was such that the prototype Phenix reactor has been designed without a sealed containment building.[30]

BR-5. Orlov[31] told of the variety of difficulties met and overcome in the operation of the Russian BR-5 reactor. The report presented new information on BR-5 experience, such as extensive oxide plugging of the core following exposure of a drained core to air, gas entrapment in the primary system, and leaks in the liquid-metal heat exchanger.

Fermi. Most interest in the operating experience was generated by the review of the partial meltdown in the Fermi reactor. McCarthy[32] described the sequence of events in the incident, which occurred a year before the meeting, and announced that the cause—an unidentified object in the inlet plenum—had been found just prior to the conference. As follow-up papers to the Fermi review, there were analyses on thermocouple response in Fermi to core abnormalities[33] and analyses of instrumentation that could have detected the Fermi meltdown (which occurred on startup) in its early stages.[34] The Fermi operators have been quite timely and candid in their reports on the incident. A somewhat condensed version of their Aix report[32] has been published.[35]

References

Except for Refs. 2, 22, 23, 28, and 35, all references are papers in Ref. 1.

1. Proceedings of the International Conference on Fast Reactor Safety, Aix-en-Provence, France, September 19–22, 1967, to be published.
2. Proceedings of the Conference on Safety, Fuels and Core Design in Large Fast Power Reactors, October 11–14, 1965, USAEC Report ANL-7120, Argonne National Laboratory, 1965.
3. J. Chermanne and M. Stievenart, Safety Reflections Concerning the Use of Direct Cycles in Fast Reactors.
4. F. J. Erbacher et al., Influence of the Design and Arrangement of the Components in Various Cycles on the Safety of Steam Cooled Reactors.
5. W. Frisch et al., Safety Aspects of Steam Cooled Fast Breeder Reactors.
6. K. Hikido, H. J. Rubenstein, and D. B. Sherer, Safety Considerations for Steam Cooled Fast Reactors.
7. C. E. Dickerman and L. E. Robinson, Fuel Meltdown Experiments in TREAT.
8. H. Blanc, N. Lyons, and J. P. Millot, The Cabri Sodium Loop.
9. C. Deschamps et al., Analysis of the Thermal and Hydraulic Behavior of Sodium During a Prompt Power Excursion.
10. K. Thurnay, H. Kusters, and D. Braess, Improvement in Second Excursion Calculations.
11. R. M. Lord, Effect of Core Configuration on the Explosive Yields from Large Sodium Cooled Fast Reactors.
12. D. MacFarlane et al., Theoretical Studies of the Response of Fast Reactors During Sodium Boiling Accidents.
13. W. Peppler et al., Sodium Boiling and Fast Reactor Safety.
14. G. Grass, H. Kottowski, and K. Spiller, Superheat Measurement and Study of Liquid Metal Boiling.
15. LeGonidec et al., Experimental Studies on Sodium Boiling.
16. H. Fauske, Two-Phase Compressibility in Liquid Metal Systems.
17. R. Holtz and R. Singer, On the Superheating of Sodium and the Generation of Pressure Pulses.
18. D. Logan et al., Boiling Liquid Metals and Two-Phase Flow Investigations.
19. G. Pinchera et al., Experimental Boiling Studies Related to Fast Reactor Safety.
20. A. Judd, Boiling and Condensation of Sodium in Relation to Fast Reactor Safety.
21. P. Kosky, Some Aspects of Boiling and Vapor Voidage Growth Problems in a Liquid Metal Cooled Reactor.
22. H. Fauske, Superheating of Liquid Metals in Relation to Fast Reactor Safety, to be published.
23. H. Fauske, A Discussion on Proposed Coolant Ejection Mechanisms for Use in Fast Reactor Safety Analyses, to be published.

24. H. Morewitz, Sodium Burning, Aerosol Generation, and Control of Fission Product Release During an Accident.
25. C. Deschamps and J. Rygaert, Behavior of Fission Products in the Atmosphere Surrounding a Sodium Cooled Fast Reactor in Case of Accidental Coolant Fire.
26. F. Heller, W. Hafele, and W. Schikarski, The Principle of Double Containment and the Behavior of Aerosols in Its Relation to the Safety of Reactors with a High Plutonium Inventory.
27. J. Phillips, Minimizing the Hazards Associated with the Use of the Dounreay Fast Reactor as an Irradiation Facility.
28. *Nucleonics Week*, p.8, Dec. 14, 1967.
29. G. Gajac and L. Reynes, Experience Gained from the Final Construction Phase and the Attainment of Power of the Rapsodie Reactor.
30. G. Denielou et al., Phenix — Main Safety Criteria — Consequences for the Reactor Design.
31. V. Orlov et al., Problems in the Operations of the BR-5 Reactor.
32. W. McCarthy, Jr., and W. Jens, A Review of the Fermi Reactor Fuel Damage Incident and a Preliminary Assessment of Its Significance to the Design and Operation of Sodium Cooled Reactors.
33. A. Friedland, Relation Between Maximum Core Coolant Temperatures and Outlet Thermocouple Readings for Plugged Subassemblies.
34. E. Volk et al., Malfunction Detection in Fast Reactors.
35. W. McCarthy, Jr., and W. Jens, Enrico Fermi Fast Breeder, *Nucl. News*, 10(11): 54 (November 1967).

Further Developments in Containment-Building Electrical Penetrations

By Fred Verber

New information about the electrical penetration systems in the Fermi,[1] Peach Bottom,[2] and Dresden 2 (Ref. 3) nuclear power stations supplements that presented previously in this journal.[4] Specifically, this article considers some electrical penetration problems and solutions experienced during plant operations at Fermi and at Peach Bottom, describes fire-protection modifications to the penetrations and to the electrical design at Peach Bottom following the occurrence of a fire, and presents recent developments in the design of the Dresden 2 electrical penetration system and assemblies.

Fermi

Figures 1 to 3 are views of Fermi electrical penetrations from inside and outside the reactor building. This containment vessel is designed for an internal

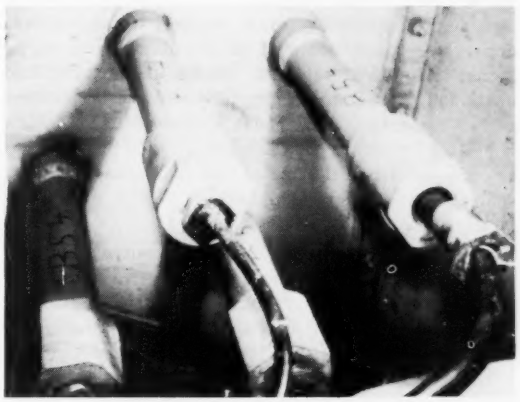

Fig. 2 Packing nut being installed (right) on outside end of Fermi penetration nozzle.[1]

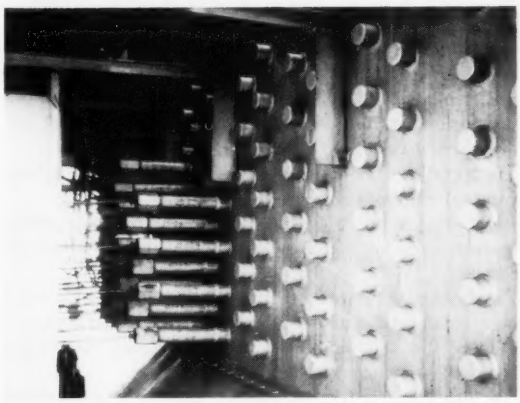

Fig. 1 Some Fermi electrical penetrations and spares are viewed from outside reactor containment building.[1]

Fig. 3 Inner end of two Fermi penetrations, showing both tubing connections for continuously monitoring for leakage and extrusion of backup sealant.[1]

pressure of 32 psig. The cluster of penetrations shown in Fig. 1 is part of a total of 517 penetrations (approximately 325 in use) grouped above the operating floor in a sector of the building that is 35 ft long and 15 ft high. The penetration nozzles are spaced approximately 10 in. on centers. These nozzles carry cables for 4800-, 480-, and 120-volt and lower voltage circuits; cable diameters range from $\frac{1}{2}$ in. to 2 in.

Figure 2 shows two stages of the installation of a packing nut that seals the cable at the outside end of a penetration nozzle. Figure 3 shows an interior view of two penetrations. Note the extrusion of the backup sealant (trade name, Weatherban) on the penetration; also note the tubing connections for continuously monitoring the penetrations for leakage.

Cold-Weather Effects. As previously reported,[4] the application of Weatherban, a butyl-rubber resilient sealant, to the neoprene packaging rings and other parts of the penetration assembly contributed very significantly to the integrity of the penetration seals. But during extremely cold weather, the outer seal apparently loses some of its resiliency, and occasional leaks have resulted.[1] These seals were taken apart and reassembled using new packing and caulking with Weatherban. The header system, which supplies 5 psi air pressure continuously to each penetration, is equipped with a flowmeter that is checked daily for indications of increased leakage. Each month the penetrations are tested at 32 psig.

A leak-rate test of the electrical penetrations was conducted at 32 psig on Nov. 6, 1967, and the total leakage was 551 scf/day. After repairs were made on the penetrations with excessive leakage, a leak-rate test was performed later in the month, and the total leakage was 291 scf/day. This was followed by additional repairs. No repairs had been required during the preceding 7 months. During the year from February 1967 to February 1968, repairs were made on 11 of the 325 penetrations in use.[5,6]

Peach Bottom

Containment of the reactor and auxiliaries of the Peach Bottom Atomic Power Plant is provided by a steel vessel designed to withstand an internal pressure of 8 psig.

During plant construction a fire occurred in one of the U-tube cable penetrations inside the reactor containment building.[2] It started when hot weld metal dropped onto the cable penetrations as a platform was being constructed above them. Because of the fire, several modifications have been made to improve fire protection and plant safety.

About 1100 cables were damaged in the fire. Of these, the multiconductor control and instrument cables were insulated with polyethylene and jacketed with polyvinyl chloride, the power cables were insulated with butyl rubber and jacketed with polyvinyl chloride, and the thermocouple extension leads were jacketed with polyethylene. Tests showed that polyvinyl chloride will burn but will not support combustion at moderate temperatures. However, the polyethylene and the permagum, silicone, or thiokol filler materials in the cables are combustible.

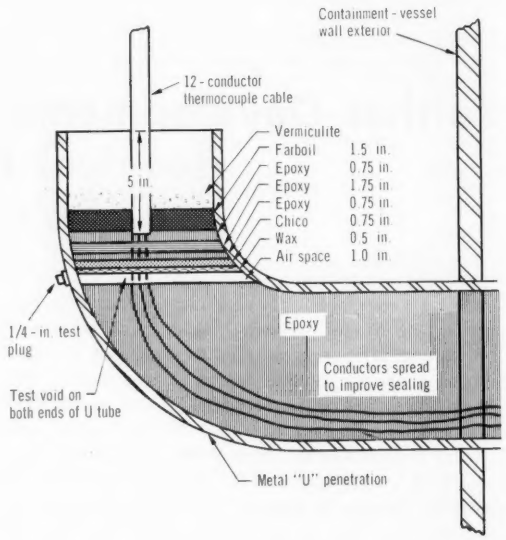

Fig. 4 Peach Bottom thermocouple-cable gas stop shows (a) vermiculite fire-proofing material added at ends of U-tube penetrations and (b) epoxy resin that replaced grout for sealing individual wires of unfilled multiconductor cables.[2]

FIRE-PROTECTION IMPROVEMENTS

Modifications made to improve plant safety include the following:

- For reliability, certain power and control cables were rerouted to segregate the circuits of essential redundant equipment.
- Horizontal runs of cable trays were covered for protection against falling objects and to prevent the spread of fire from one tray to another.
- Metal covers and fire stops were installed in long vertical runs of cable trays.
- Vermiculite, a fireproofing material, was added to both ends of the U-tube penetrations as shown in Fig. 4.
- Smoke detectors were installed in areas where electrical cables and equipment are concentrated, including the 480- and 2400-volt switchgear rooms and motor–generator sets.
- The CO_2 fire-extinguishing system was extended within the containment building to include areas where electrical cables are heavily concentrated.

Several other changes were made to improve leak-tightness of the cable penetrations:

- Epoxy resin was substituted for grout for sealing individual wires of unfilled multiconductor thermocouple cables after the outer jacket was removed (Fig. 4).
- Solid connectors were installed on single-conductor 600-volt cables to prevent leakage between strands of the conductor; the connector was covered by a heat-shrinking Raychem sealing sleeve (Fig. 5). This connector system was found to be very effective.
- Where leakage through cables was detected during tests, gas stops, as shown in Fig. 6, were added.

Individual leak-rate tests of all new penetrations showed the leakage to be insignificant. An integrated containment-building leak-rate test at 8 psi showed that the leak rate was less than the specified 0.2%/day and that the containment integrity of the building had not been impaired by the fire.

These modifications represent significant design improvements and safeguards, particularly in respect to fire protection of electrical equipment and wiring. Many of these features are applicable to—and should significantly improve equipment and wiring installations of—power-generating stations and industrial plants as well as reactor containment buildings.

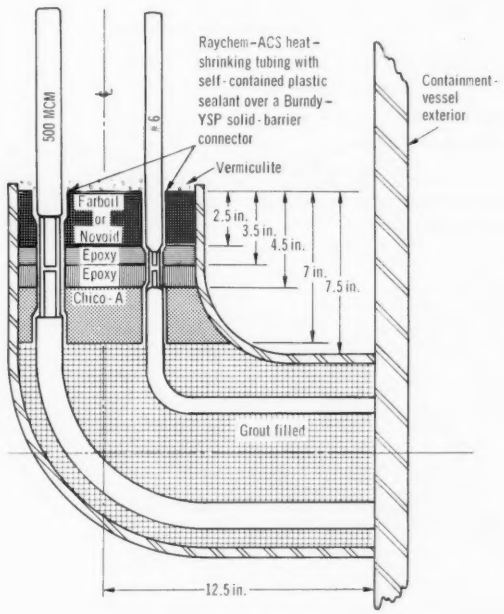

Fig. 5 Solid connectors installed on single-conductor unfilled cables prevent leakage between strands of conductor at Peach Bottom. Raychem heat-shrinking sealing sleeves cover connectors.

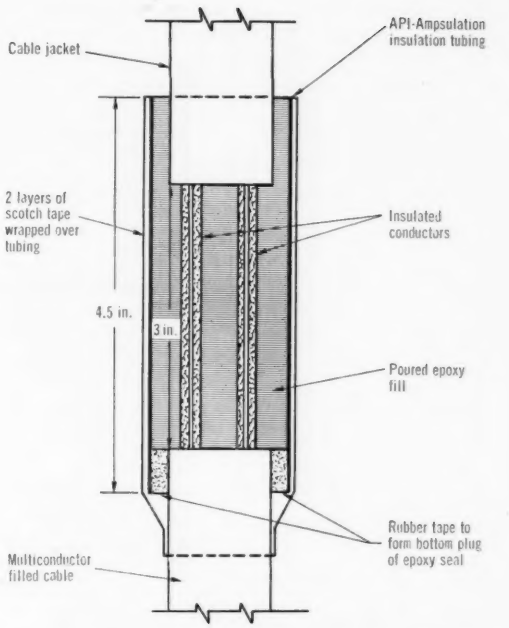

Fig. 6 Multiconductor gas stop was added to filled cables at Peach Bottom where leakage had been detected through cable.[2]

Dresden 2

The design of the electrical penetration system for the Dresden 2 primary containment system has advanced since the earlier description.[4] The primary containment design employs a pressure-suppression system that includes a steel pressure-vessel dry well containing the reactor vessel and recirculation system. The design internal pressure of the dry well is 62 psig. A reactor building provides secondary containment; it encloses the primary containment system and reactor servicing and auxiliary equipment. The design internal pressure of the reactor building is 0.25 psig. The electrical cables entering the building will pass through ducts sealed in the wall; soft sealing materials will be used around these cables.

As shown in Table 1, there are a total of 8376 conductors penetrating the dry-well structure in the present development of the Dresden 2 design; of these, 5568 are for control-rod-position indication, 448 for reactor gamma and neutron monitoring, 2348 for 120- and 440-volt power, control, and instrumentation circuits, and 12 for high-voltage (4160-volt) power circuits. Approximately 18% of the conductors are spares.

At an early stage of the design, a total of 63 electrical penetrations were contemplated. As the table indicates, the number of penetrations has been reduced to 20. In addition, seven spare penetration sleeves are provided (Figs. 7 and 8) in the dry-well structure.

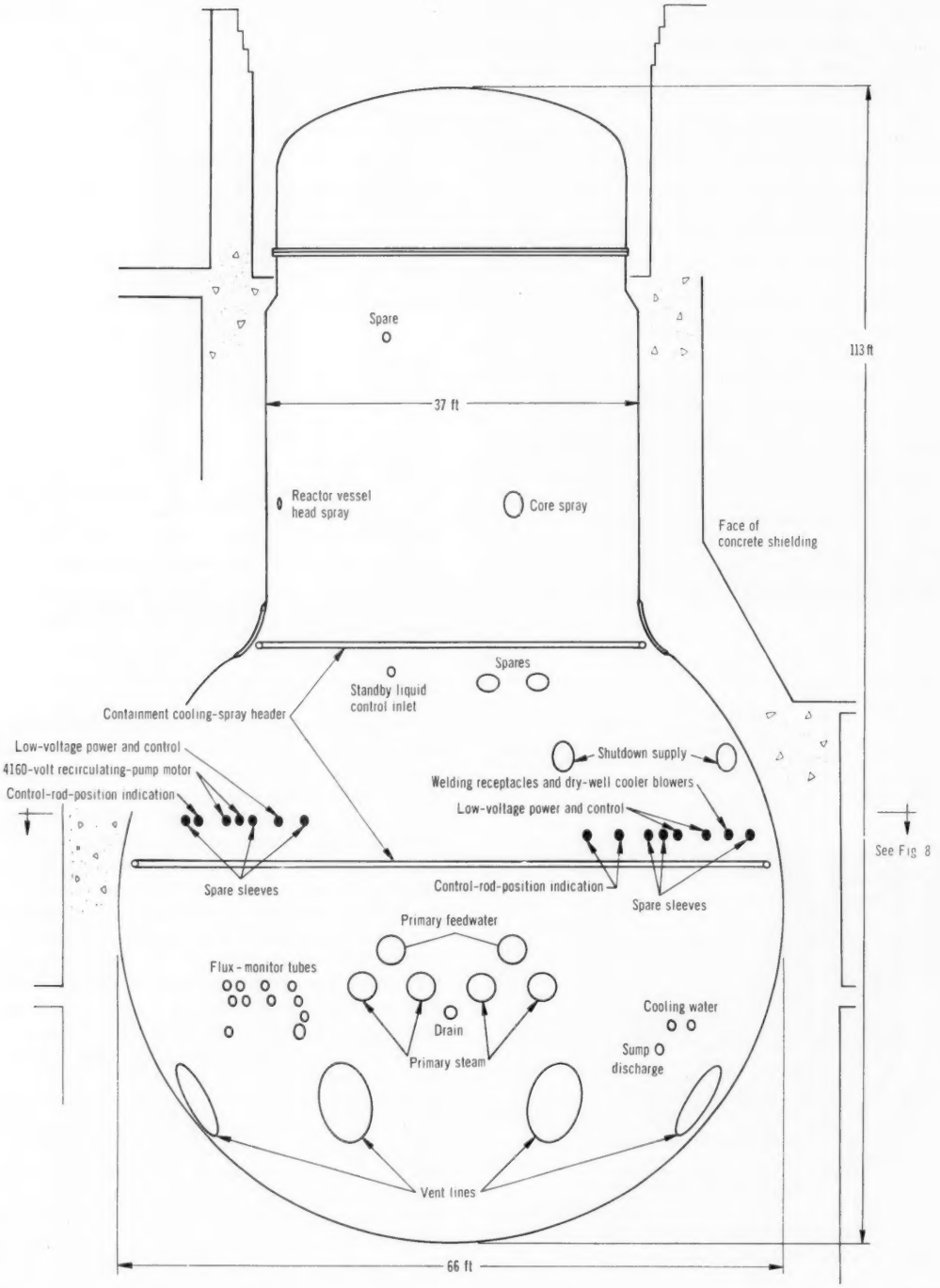

Fig. 7 Cutaway of Dresden 2 dry-well structure shows electrical penetration assemblies.[3] Openings for other service penetrations are also shown.

Table 1 DRESDEN 2 ELECTRICAL PENETRATION SYSTEM[3]

Type of penetration assembly	Quantity	Service	Range of conductor sizes	Total number of conductors	No. of spare conductors
Low-voltage power and control cable penetration	6	120-, 240-, and 480-volt power, valves, limit switches, thermocouples, controls	#14 to #0 wires, #20 thermocouple wire, 400-MCM bare ground wire	2348	1006
Low-voltage power and control cable penetration	6	Control-rod-position indication	Thirty-two 27-conductor #18 wires plus 1 pair of Chromel–Alumel thermocouples per penetration	5568	435
High-voltage power cable penetration	4	4160-volt recirculating-pump drive motors	Three 1000-MCM, single-conductor cables per penetration	12	0
Shielded-cable penetration	4	Reactor neutron and gamma monitoring	Fifty-one type RG-108 A/U shielded pairs; 5 coaxial triple-shielded cables	448	96
Totals	20			8376	1537

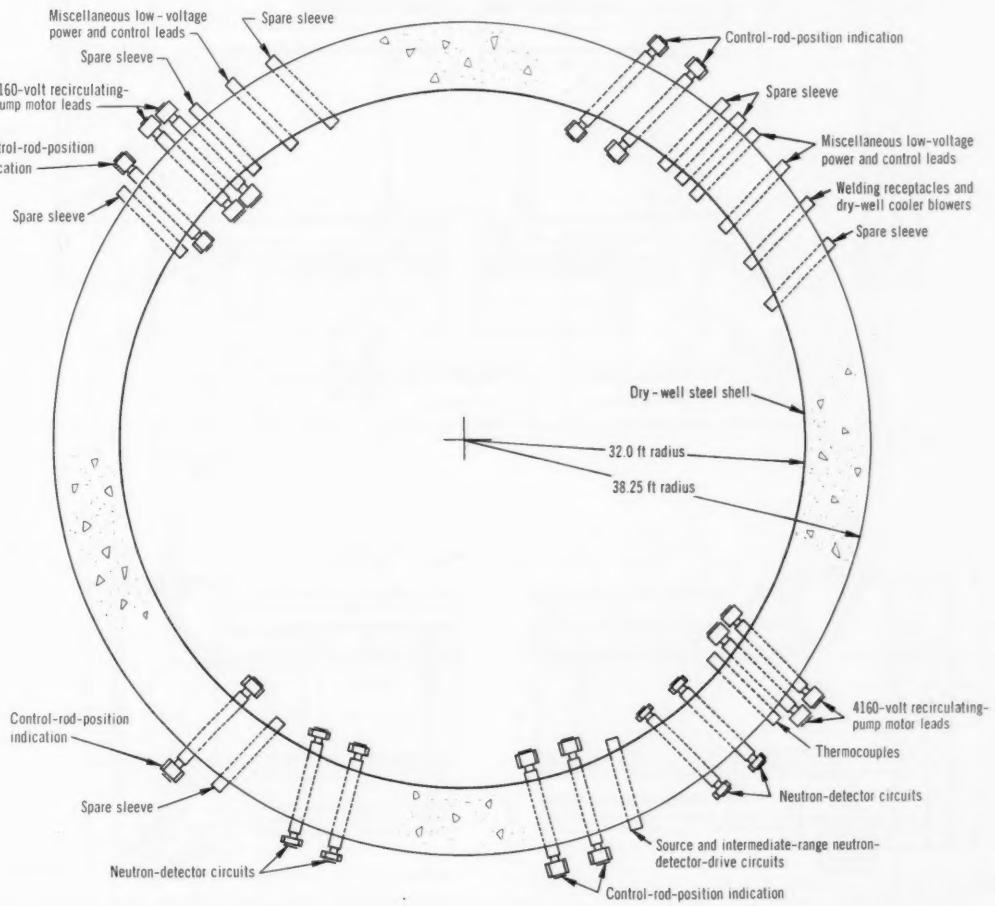

Fig. 8 Horizontal section through Dresden 2 dry-well structure (at level shown in Fig. 7) shows relative location of all 20 electrical penetration assemblies and seven spare sleeves.[3]

TYPES OF PENETRATIONS

A family of three commercially available standard types of electrical penetration assemblies, as developed by General Electric Company for application in the nuclear power industry, will be used in the primary containment structure for Dresden 2. The basic configuration of the three types of assemblies is essentially the same. Each penetration assembly is inserted into a penetration nozzle (Fig. 9) that is part of the containment dry well; double seals are formed by the two header plates of the assembly, thus creating a pressure chamber that facilitates leak-rate testing and continuous monitoring. Each penetration assembly will be equipped with a drain valve and pressure gauge, as indicated in Fig. 9. The pressure chambers will be purged with dry nitrogen gas at 15 psig for monitoring during normal plant operation.

Each of the three types of penetration assemblies is designed to satisfy the needs of a particular group of electrical cables. The three types are categorized as follows:

Low-voltage power and control cable penetration. This penetration (Fig. 10) is used for a-c circuits up to 600 volts and wire sizes from AWG #18 to 4/0.

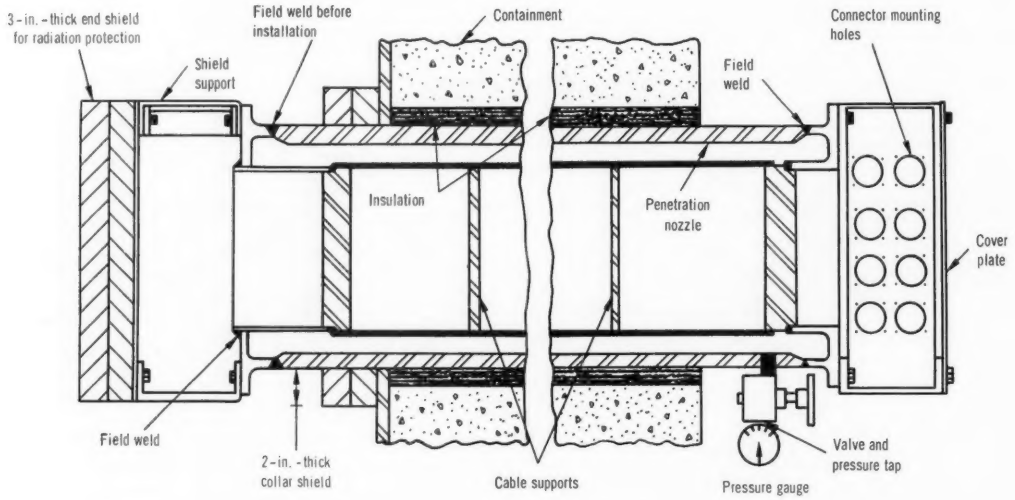

Fig. 9 Typical Dresden 2 electrical-penetration-assembly canister is inserted into nozzle on containment dry well.[3]

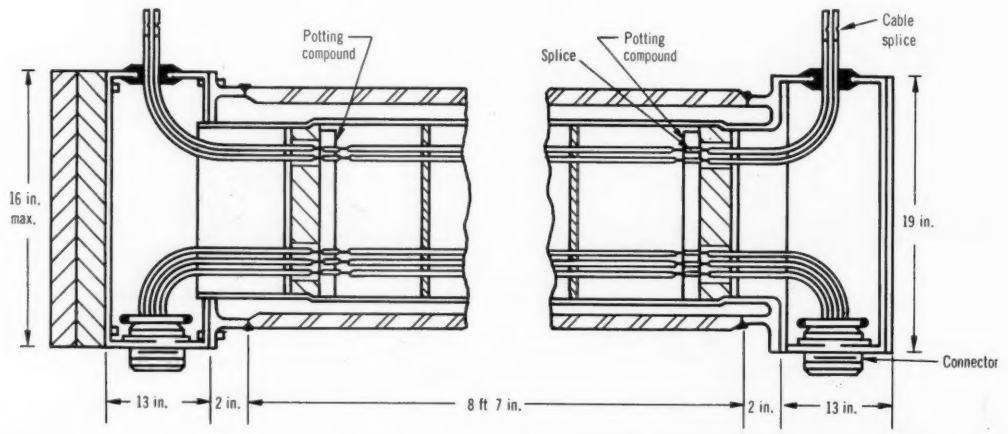

Fig. 10 Low-voltage power and control cable penetration[3] *at Dresden 2.*

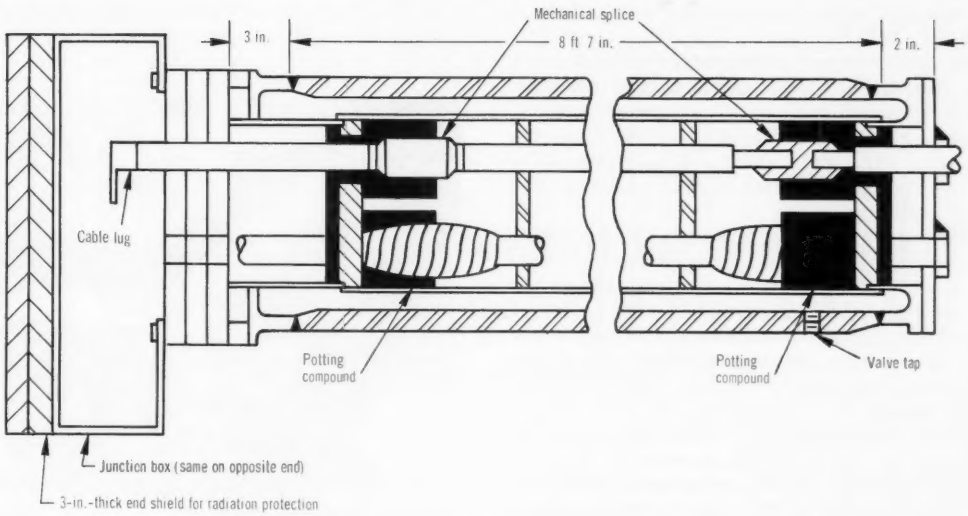

Fig. 11 High-voltage power cable penetration at Dresden 2 accommodates 4160-volt 3-phase motor leads.[3]

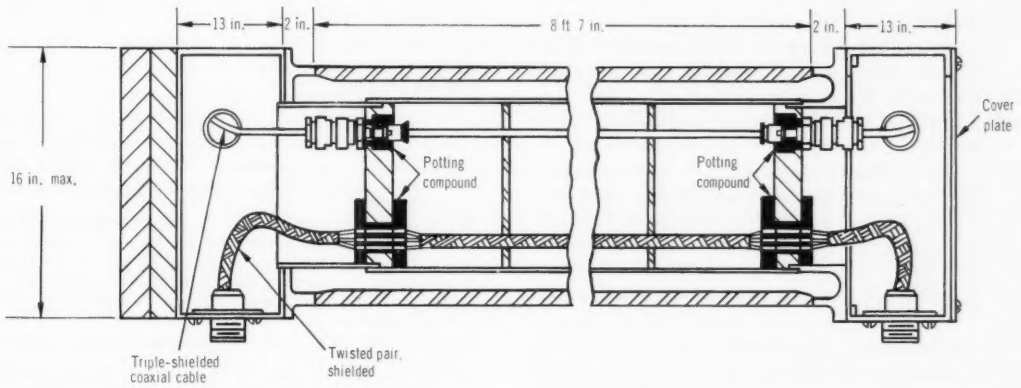

Fig. 12 Typical shielded-cable penetration at Dresden 2 handles reactor neutron-monitoring circuits.[3]

High-voltage power cable penetrations. This penetration (Fig. 11) accommodates circuit voltages up to 5000 volts and cable sizes up to 1000 MCM. Nonmagnetic stainless-steel header plates are used to eliminate the possibility of eddy-current heating (carbon-steel header plates are normally used in the other types of penetration assemblies). Three or six conductors per assembly is a typical conductor density for this penetration.

Shielded-cable penetration. Shielded signal cables are provided in this penetration (Fig. 12) to connect low-noise circuits between the reactor and control room. Coaxial connectors are mounted directly on the header plates and are isolated from ground. Single-, double-, or triple-shielded coaxial cables are used with these connectors and are normally used for circuits with a pulse output signal. Leads for reactor monitoring circuits with a d-c current signal consist of a twisted pair covered by a braid shield.

Figure 7 shows the design arrangement of a group of electrical penetration assemblies and other service openings on the dry-well structure. Figure 8 shows all 27 electrical penetrations.

Physical and operational characteristics of these three basic types of penetration assemblies are:

- The penetration assembly has a maximum leak rate of 1.16×10^{-6} cm^3/sec when pressurized to 63

psig with dry helium in an ambient temperature of 175° F.

• The assembly will continuously withstand an internal pressure of 125 psig during normal operation.

• The assembly maintains containment integrity continuously with the following conditions inside the containment (dry well): 150° F, –2 to 2 psig, 20 to 100% relative humidity, and 10 r/hr radiation dose (without shielding).

• The assembly will maintain containment integrity for at least 2 hr under the following maximum conditions inside the containment dry well: 320° F, 125 psig, and 100% relative humidity.

• Each conductor of the assembly is cut and reconnected in a solid mechanical splice at each header plate (best illustrated in Fig. 11). This eliminates leakage through the strands of the conductor. Splices and spaces surrounding the cables penetrating the header plate at each end of the assembly are buried in a potting compound, namely, a version of 3M Scotchcast epoxy resin No. 8. The resin is applied under a vacuum to eliminate voids that otherwise would be formed by trapped bubbles.

• The materials comprising the assembly are fire resistant and self-extinguishing in accordance with ASTM-D635.

• The penetration assembly is designed and fabricated in accordance with *ASME Boiler and Pressure Code*, Section III, Class B Vessel.

• As indicated in Fig. 9, cable boxes are installed on both ends of the assembly to accommodate the extension of cable leads in splices or in environmental resistant-type connectors. Figure 13 shows the factory termination of penetration cables in 10 connectors installed in a cable box mounted on one end of a penetration assembly.

• Protection against line-of-sight radiation is provided by end shields consisting of 3-in.-thick carbon-steel disks mounted on the shield support structure (Fig. 9) installed on the inside of the dry well; in addition to the disks, 2-in.-thick carbon-steel shielding is provided on the collars of the penetration assemblies.

I thank E. L. Alexanderson (of Power Reactor Development Company), R. F. Griffin (of Bechtel Corp.), and D. McDaniel and R. B. Hubbard (of General Electric Company) for providing information and for commenting on the manuscript.

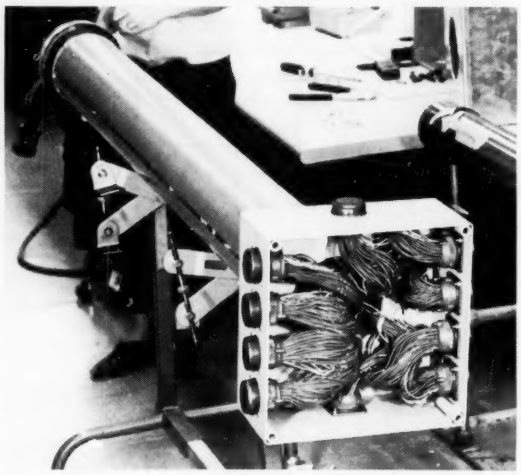

Fig. 13 Factory assembly of one type of penetration assembly to be used in Dresden 2. Note termination of cables in 10 connectors in cable box.

References

1. J. F. McCarthy, Compilation of Current Technical Experience at Enrico Fermi Atomic Power Plant, Monthly Report No. 7, February 1967, USAEC Report APDA-CFE-7, Atomic Power Development Associates, Inc., May 1967.
2. Final Semiannual Report of the Philadelphia Electric Company on the Peach Bottom Atomic Power Station, Appendix A, Jan. 11, 1966, Submitted to the USAEC Pursuant to Construction Permit No. CPPR-12; also Roger F. Griffin, Bechtel Corp., personal communication, May 16, 1967.
3. R. B. Hubbard, General Electric Company, personal communication, Oct. 6, 1967.
4. Fred Verber, Electrical Penetrations of Reactor Containment Buildings, *Power Reactor Tech. Reactor Fuel Process.*, 10(2): 122-135 (Spring 1967).
5. Power Reactor Development Company, Enrico Fermi Atomic Power Plant Report for November 1967, USAEC Report PRDC-EF-51.
6. E. L. Alexanderson, Power Reactor Development Company, personal communication, Dec. 6, 1967.

Realistic Data Are Needed for Mechanical Analysis of Reactor Fuel Elements

By Richard A. Valentin

As reactor design has progressed into the development of high-power-density systems with greater burnup and thermal efficiency, problems in the mechanical design of fuel elements have become more complex. One indication of this is the growing number of papers that show (1) application of rational methods of analysis to the theoretical prediction of thermal displacements, stresses, and strains, and (2) attempts to include radiation-induced creep and swelling effects in a more logical and less empirical manner. The analytical methods used in these studies have become more sophisticated and often include relatively recent developments from the mathematical theory of plasticity, viscoelasticity, and viscoplasticity.

Rather than attempting to survey comprehensively the extensive literature on the mechanical analysis of reactor fuel elements, this article discusses a few recent papers to illustrate the salient features and typical difficulties of such analyses. Noteworthy are the many assumptions needed to produce tractable problem formulations. A sequence of closely interrelated papers by Ma and his associates[1-5] is representative of this type of mechanical analysis. Of this group, we will consider "Mechanical Analysis for Solid Cylindrical Fuel Elements"[1] and "The Radiation Growth and Swelling Analysis for Cylindrical Fuel Elements During a Positive Reactor Period"[2] as typical examples.

Time Ranges. A point that deserves particular emphasis is the time range over which the analysis is to be applicable. Perhaps no other factor has such a profound influence on the mathematical models that can be employed and the analytical methods available for problem solutions. Although no truly satisfactory classification of time ranges can be stated, four rough classes will be used for illustration:

A. Very-short-term dynamic analysis of transient effects wherein one does not neglect inertia effects. In such problems, elastic wave propagation plays an important role in the behavior of the reactor. A typical example is the effect of wave propagation on the self-limiting behavior of pulsed fast reactors of the Godiva type (see Refs. 6 and 7). Time scales of this order, of course, preclude any interest in creep as the term is normally applied; however, it is conceivable that the safety analysis of such systems could include problems in the dynamic theory of plasticity or viscoplasticity.

B. Time scale defined by the limitations of quasi-static analysis. (The upper limit to times considered in this class is to some extent arbitrary but could probably be limited to a few seconds.) This includes times greater than those necessary for the attenuation and dispersion of elastic waves or the approximate solution of problems where wave propagation is known to be of minor importance; this class also includes most analyses of severe accidents where interaction between neutronics and mechanical behavior is limited to coupling through time derivatives of temperature by way of induced thermal displacements and the Doppler coefficient.

C. A broad and somewhat ill-defined time range having as its lower end times used in the analysis of less severe accidents and as its upper limit a time (perhaps minutes) sufficient to include mechanical effects noticed during controlled power oscillations, reactor shutdown procedures, etc. Perhaps the best scale definition would be one equivalent to the time associated with low-cycle thermal fatigue.

D. Very-long-time effects, say from several days to years, during which essentially steady-state conditions have existed. This is the range in which radiation-induced growth and creep are of greatest relative importance.

Problems of Class A will not be discussed further due to their extreme complexity, specialized nature, and relative lack of connection to questions of interest in the normal operation of power reactors.

Problems whose time scales fall into Class B are almost exclusively related to questions of reactor safety and thus fall outside the range of interest in this article; one exception would be the use of problems of Classes C and D as input to such safety analyses. The study of long-time effects as a means of specifying the initial deformation and stress field in a fuel rod at the time of initiation of a severe accident could be used to define a wide class of problems whose solutions, although using models and methods applicable to Classes C and D, are tailored to supply the specific information needed in forming a well-posed problem of Class B.

Discussion

The two papers[1,2] we will discuss in detail fall into Classes C and D. In Ref. 1, time enters only in an implicit fashion through various coefficients defining radiation-induced creep, swelling due to entrapped fission gas, etc.; thus it belongs in Class D. The problem treated in Ref. 2 has a range of times limited by what could be considered reasonable positive reactor periods (i.e., ~30 sec) and thus is within the range of Class C.

MECHANICAL ANALYSIS

The problem considered in Ref. 1 concerns theoretically predicting the stresses and strains in a solid, thinly clad, circular cylindrical fuel element. These changes are caused by thermal-cycling growth of uranium and its growth, swelling, and creep caused by irradiation. Although not explicitly stated, these effects are treated without reference to the elastic stress state of the fuel and cladding. That is, the analysis of all radiation effects is based on purely plastic considerations with no reference to, say, elastic-plastic boundaries that might exist solely as a result of the derived temperature field. As a result of this decoupling, elastic material properties such as Young's modulus and Poisson's ratio do not explicitly appear. It should also be noted that, although practicality dictates that various irradiation effects such as those mentioned be treated as separate phenomena, a satisfactory theoretical basis for this differentiation would be difficult to outline. Thus the separation must be considered to some extent as arbitrary.

Types of Dimensional Changes. As defined in Ref. 1, thermal-cycling growth is the gross dimensional change in the fuel material caused by the action of temperature cycles on the crystalline structure of the fuel. Such growth is a result of the basic anisotropic nature of the crystal structure.

Irradiation growth, a phenomenon that produces similar gross changes, also results from the anisotropy of the fuel but is that portion of the growth due solely to fuel burnup.

The term irradiation swelling identifies radiation-induced dimensional changes that are caused by fission-product gases being trapped within the fuel and lowering its density.

Irradiation creep separates long-term growth effects caused by the fuel creep rate being increased during fuel exposure to a severe neutron environment.

Satisfactory physical models for these growth effects will, no doubt, eventually become available as work in dislocation theory and similar disciplines begins to supply methods for relating microscopic behavior to observed macroscopic material properties. However, at present, one must rely almost entirely on empirical descriptions. For example, in Refs. 1 and 2, thermal-cycling growth and irradiation growth are included by noting that the ratio of final to initial length is approximately related to number of thermal cycles and percent burnup by an exponential relation derived from a fit to experimental data. Gross effects due to microstructure have been treated in much more exact terms than these in connection with the behavior of composite materials (e.g., Ref. 8), but such work has had little application in the nuclear field.

Heat-Generation Rate. If the heat-generation rate within a particular fuel element is to be considered, the local neutron flux must first be specified. If it is assumed that the diameter of a single fuel element is small when compared with the radial dimension of the reactor core, within the limitations of elementary diffusion theory, the flux distribution, ϕ, in a particular element is given by

$$\phi = AI_0(\beta r) \cos \eta z$$

where I_0 = the zero-order modified Bessel function of the first kind
A = a constant for a given element
β, η = constants
r, z = radial and axial coordinates relative to the element center

If this flux-distribution equation were used directly in an analytical development, the temperature and stress fields would be complicated. Therefore, except for very local effects, it is usually assumed that axial variations in flux are of minor importance. It is further assumed that the neutron-diffusion length is large relative to the radius of the fuel element, thus causing the radial dependence, $I_0(\beta r)$, to reduce to unity. This latter approximation is quite reasonable for a fast reactor system, although it may not be true in a thermal reactor. In the thermal system, however, the operating conditions are probably not so severe, the stresses are likely to be considered less, and the resulting errors are probably not of major

importance. The neglect of axial effects allows one to consider a plane strain formulation and, hence, greatly reduces the mathematical difficulties of the problem. Thus the flux has been reduced to a constant as a first approximation in the analysis, and the constant heat-generation rate may be computed immediately. After the assumption of constant thermal conductivity, radial symmetry, and known coolant properties at the element surface, the radial variation of the temperature can be obtained in a straightforward manner.

Deformation. In analyses of the radiation-induced plastic deformation of the fuel element, it is assumed that, in addition to the previously mentioned plane strain conditions, the fuel and cladding maintain constant densities and that there is no initial or plastic-yield-induced anisotropy. Further, both the cladding and the fuel are assumed to obey von Mises' yield criterion and to exhibit radiation-induced hardening that can be described in the same manner as conventional strain hardening. With these assumptions the displacement-strain equations, incompressibility condition, yield criterion, equilibrium, and boundary conditions provide sufficient information to allow an approximate solution for the state of stress in the fuel element if certain empirical material data are available.

Calculation Procedure. The calculation procedure may be roughly outlined as follows: Incompressibility allows the radial displacement to be obtained as an integral of the total thermal and radiation dilatation. With an empirical description of the radiation component of dilatation, which in Ref. 1 is assumed to vary exponentially with radial position so that the exponential coefficient is a small number that allows a simple power-series expansion of this term, integration then yields the radial displacement. This in turn gives the strain components in the fuel and cladding. If the shearing-yield-point stress (i.e., the second stress invariant at yield) is known from experiment, the radiation-induced strain hardening coefficient can be computed in terms of known quantities. Then sufficient information is available to allow computation of the stress state in the cladding and to obtain an iterative approximation to the radial variation of the stresses within the fuel.

Reservations. There are many theoretical reservations that could be expressed about the details of the computation method used in Ref. 1. However, it is perhaps more important to emphasize that all the results depend strongly on experimental data on effects that may be quite hard to isolate in practice. In particular, one should have detailed experimental knowledge of the radiation-induced dilatation of the fuel material and of the behavior of the yield surface under irradiation. In addition, even though the radiation-induced strain hardening of the material is specified by a derived quantity insofar as the analysis is concerned, it would seem prudent to check such derived results against experimental data before using this method of analysis as a design tool.

Evaluation. Overall, because of the numerous assumptions and the dependence on experimental knowledge that is difficult to obtain, it seems fair to state that serious reservations must be felt about the usefulness of these analytical methods to provide anything beyond a rough indication of the relative sensitivity of the true state of stress to various forms of radiation-induced deformation.

TRANSIENT GROWTH EFFECTS

The problem discussed in Ref. 2 is virtually identical with that of Ref. 1 with respect to fuel-rod geometry and method of analysis. However, the object in Ref. 2 is to study transient growth effects expected to be of importance during time ranges of the order of reasonable positive reactor periods. These are introduced into the analysis solely by including an exponential time dependence to multiply the spatially constant neutron flux. This makes the expression for the transient temperature field rather cumbersome and, of course, one now works in terms of strain rates rather than strains. But, other than such obvious modifications, the method of analysis in Ref. 1 is essentially repeated in Ref. 2. Hence all the assumptions and reservations discussed above remain pertinent.

In addition, one is faced with the more serious problem of justifying the method of analysis in time ranges of the order of a minute or less (the numerical example in Ref. 2 assumes a reactor period of 36 sec). It seems unrealistic to attempt to explain radiation-induced growth effects during such short periods without any experimental evidence concerning, for example, the plastic flow rules associated with the assumed yield criterion. Even if any mention of radiation effects is neglected, it is doubtful if the equivalent quasi-static plasticity problem for a clad cylinder exhibiting strain hardening could be solved in the manner outlined.

Summary

It seems that an invaluable "ground rule" to apply at the beginning of any theoretical transient mechanical analysis of reactor fuel elements is the need to include a demonstration that the mathematical model chosen applies to the time range under consideration. Further, unless the only interest of the study is to reveal the qualitative relation of various hypothesized physical-growth mechanisms to the state of stress in the fuel element, the analysis should not require experimental material data that are difficult or impossible to obtain in practice.

References

1. Benjamin M. Ma, Mechanical Analysis for Solid Cylindrical Fuel Elements of Nuclear Reactors, *Nucl. Eng. Design*, 3: 11-20 (1966).
2. Benjamin M. Ma, The Radiation Growth and Swelling Analysis for Cylindrical Fuel Elements During a Positive Reactor Period, *Nucl. Sci. Eng.*, 26: 99-109 (September 1966).
3. Benjamin M. Ma, Mechanical Analysis for Cylindrical Fuel Elements of a Fast Reactor for Use in a Lunar Power Plant, ASMS–SAE Air Transport and Space Meeting Production Forum, New York City, April 27–30, 1964, Paper 861B.
4. Benjamin M. Ma and Glenn Murphy, Radiation and Creep Analysis for Strain and Stress Distributions in Tubular Fuel Elements, *Nucl. Sci. Eng.*, 20: 536 (December 1964).
5. Benjamin M. Ma, Radiation and Creep Analysis of Strains and Stresses in Annular Fuel Elements, *Nucl. Struct. Eng.*, 1: 141 (1965).
6. J. Randles, Feedback Due to Elastic Waves and Doppler Coefficient During the Excursions of a Pulsed Fast Reactor, *J. Nucl. Energy, Parts A & B*, 20: 1-16 (1966).
7. V. F. Kolesov, On the Dynamics of a Spherically Symmetric Pulsed Fast System, *At. Energ.*, 14: 273-280 (March 1963).
8. Z. Hashin and S. Shtrikman, A Variational Approach to the Theory of the Elastic Behavior of Multiphase Materials, *J. Mech. Phys. Solids*, 11: 127-140 (1963).

Operational Problems and Solutions

By Rolf C. Skaardal

Several cases of reactor system component failure were reported at the July 1967 Conference on Reactor Operating Experience sponsored by the Reactor Operations Division of the American Nuclear Society (ANS). Such failures can be traced to errors in design, poor material selection, improper installation, and lack of testing; they should be of interest to reactor designers and are, therefore, reported here. Repair procedures and preparations for repairs as well as some equipment modifications are also taken into account in this article.

Failure of Mechanical Components

Component design and materials problems discussed here include the following:

- Hydriding of Zircaloy process tubes in a Hanford production reactor
- Fast-neutron damage in aluminum and beryllium core components
- Flow-induced vibration in heat-exchanger tubes
- Failure and replacement of shaft seals in a primary coolant pump

HYDRIDING OF ZIRCALOY PROCESS TUBES

Two years after retubing of two of Hanford's production reactors with Zircaloy-2 process tubes it was discovered that they were absorbing significant quantities of hydrogen.[1] The tubes are 1.8 in. in outside diameter by 0.037 in. in wall thickness and are about 47 ft long; cooling-water velocity within the tubes, which are surrounded by a mixture of helium and nitrogen, varies from 10 to 50 ft/sec. Continued use of these tubes appeared in question after one of them was removed and found to be very brittle. The existence of hydride was confirmed by metallurgical and chemical analyses of samples from this tube.

The hydride layer found on the inside, or water side, of the tube was about 0.004 in. thick and showed no significant difference in the appearance of longitudinal and transverse sections. Chemical analyses of the entire tube wall showed a total hydrogen content in the 1200- to 1400-ppm range, with approximately 50 ppm in the base metal itself. Recently a tube with a total hydrogen content of 4000 ppm was found.

No apparent direct correlation between total hydrogen content and residence time in the reactor has been found. However, the rate at which the hydrogen content of the base metal increases seems to be a uniform 25 to 30 ppm/year.[1]

Once the case layer has been removed, no gradient through the tube wall can be detected. The hydride platelets, or needles, have never been found to be oriented radially except at the Van Stone flange where the tube was cold rolled during installation.

System Conditions. It is common knowledge in the nuclear field that hydriding of Zircaloy may result from a high-temperature corrosion reaction with water or steam. Also, in some cases, it may result from a gas-phase reaction where moisture or hydrogen is an impurity in the atmosphere adjacent to Zircaloy. But in the Hanford case, the temperature of the coolant is too low to be responsible for corrosion reactions sufficient to account for the hydriding phenomenon. Also, there is no evidence to indicate that the reactor atmosphere could in any way contribute to the hydride found.

Laboratory tests have indicated that some hydrogen could be introduced into Zircaloy from low-temperature mixtures of hydrogen and water vapor.[2] However, the amount of hydrogen which would be introduced would be far below the levels encountered here. Exclusive of the case layer, the maximum hydrogen content found uniformly distributed in the base metal has been 175 ppm. The dissolving of this much hydrogen normally requires a temperature >300°C.

Electrolysis. References 2 to 4 indicate that, by making zirconium the cathode in an electrolytic cell where hot water is the electrolyte, hydrogen can be driven into or deposited on zirconium. Thus the problem might result from unexpected electric currents. However, it did not seem reasonable that the

magnitude of the electric currents would be sufficient to produce the observed hydriding even though (1) free electrons are available from radiolytic decomposition of the water, and (2) streaming potentials are caused by the high-velocity water.

Galvanic Coupling. Another possible source of current was the galvanic coupling of the Zircaloy tubes with the aluminum-clad fuel elements and aluminum dummy spacers. Preliminary tests verified that Zircaloy-2 would hydride in hot process water when electrically coupled to 6063 aluminum. The prevention of current flow, and thus the elimination of this cause of hydriding, requires either elimination of the couple or insulation of the two metals from each other.

Dummy elements made of different alternate materials, such as nickel-plated aluminum, stainless steel, Zircaloy, and carbon steel, were tested in the reactor. They all resulted in greatly reduced potentials or, as in the case of stainless steel, in a couple of reversed polarity.

All these materials, however, have serious drawbacks, such as high costs for the first three mentioned, a tendency for severe pitting corrosion of the nickel-plated aluminum, and a low corrosion resistance and high cross section for the carbon steel.

An Anodized Cure? The practical solution has been to insulate the tubes from the aluminum with a high-quality anodized coating on the aluminum. Although this has been done, detailed operating results are not yet available. Anodized coatings will break down eventually in hot water, but apparently a good coating will not allow significant hydriding during the normal residence time in the reactor. Further, anodized aluminum has none of the drawbacks mentioned above for the alternate metals.

The oxalic acid anodizing process is used and gives a hard scratch-resistant coat of at least 1-mil thickness. Such a coating has a resistance per square inch of approximately 225,000 ohms. After the pieces are anodized, they are sealed by autoclaving in water at 170°C for ½ hr.

Alternatives. If elimination of the galvanic currents fails to control hydrogen buildup, it will be necessary to remove the present case layer. Because the process tubes cannot be removed from the reactor, several in situ methods have been considered: (1) hot vacuum extraction, (2) chemical etching, and (3) mechanical removal by machining, grinding, or grit blasting.

Grit blasting is believed to be the most practical means. Trial attempts (both in the laboratory and in reactor) to remove given amounts of hydride from the tube walls have been fairly successful. Regardless, cleaning an entire reactor would be quite a large project; it would take several weeks and use about 500 tons of grit. The grit would become highly radioactive and could only be used once.

NEUTRON DAMAGE TO BERYLLIUM AND ALUMINUM CORE COMPONENTS

Fast-neutron damage and distortion of beryllium lattice components have long been recognized as a serious problem.[5,6] Recently, however, similar damage to Al–Cd shim safety rods (once assumed to be a permanent solution to shim safety-rod problems of this kind) was found in the Oak Ridge Research (ORR) Reactor.[5] In addition, two aluminum lattice pieces that held experimental facilities were also found to be distorted.

Bowing. In each case, bowing occurred—apparently from irradiation damage—with effects like those observed for fast-neutron damage to beryllium. This assumption is strengthened by test results of embrittled aluminum cladding from irradiated HFIR target rods, several of which have failed due to cracks in the cladding. In each instance at the ORR, the dimensional changes were sufficient to cause either improper fit of the component or interference with adjacent lattice pieces, or both.

The Al–Cd shim safety rods, located in lattice positions F-4 and F-6 of the ORR lattice (Fig. 1), failed to pass a manual check for freedom of movement prior to the reactor startup on Sept. 20, 1966.

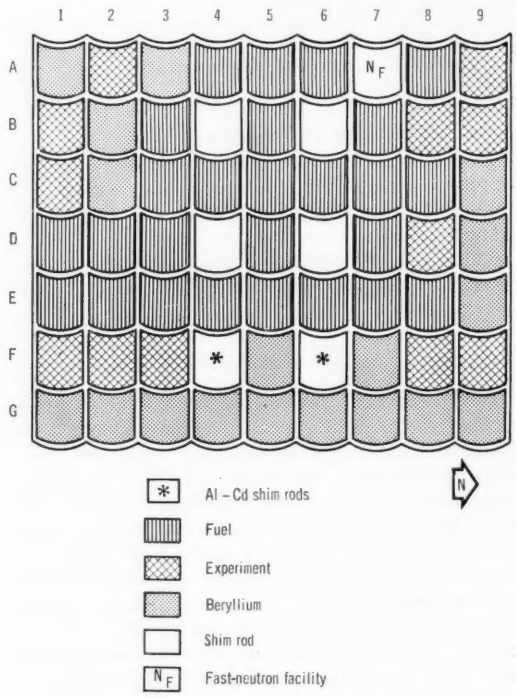

Fig. 1 The Al–Cd shim safety rods in positions F-4 and F-6 of the ORR lattice failed a manual check and subsequently were found to bow toward the fuel region.[5]

Figure 2 shows the normal alignment of these rods during operation. When the rods were checked with a straightedge they proved to be bowed toward the largest source of neutrons (the fuel region) as were Be–Cd rods that had been in the same lattice positions earlier.

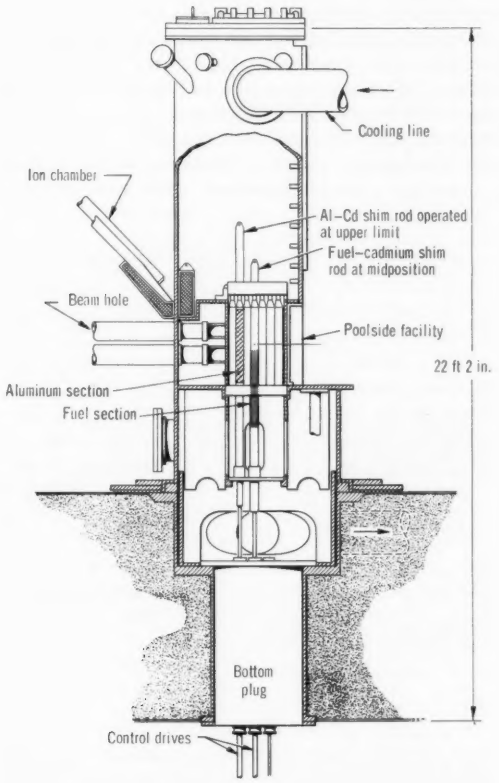

Fig. 2 Cross section of the ORR showing the alignment of the F-4 and F-6 Al–Cd shim rods.[5]

Measurements. Distortion of the aluminum portion of the rods (which were sectioned) was measured with a contour-measuring apparatus. This apparatus, Fig. 3, consists of a calibrated slide bar, a machined structural bed plate, a dial indicator with mounting clamps, and two vises for positioning the parts to be measured. Calibration curves were obtained with bar stock known to be flat to ±0.0005 in. Measurements of deflection were noted at 1-in. intervals parallel to the long axis of the aluminum section, and the data were adjusted from calibration curves.

Figure 4 shows the east–west measurements for the F-4 rod plotted as a function of distance from the top of the fuel region. (North–south deflections were relatively low, as expected.) The slight bowing toward the north is expected for the rod in position F-4, and similar results were found for the rod in F-6 because fuel was located in position F-7 during part of the irradiation period.

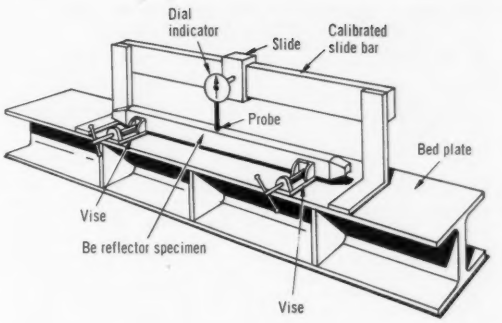

Fig. 3 Device used to measure bowing in ORR components.[5]

It is interesting to note that, for measurements on opposite sides of each rod, the maximum deflection is 5 to 10 mils greater on the side nearer the source. This characteristic has also been exhibited by damaged beryllium. Growth would be greatest in the region of highest flux and could indeed cause the aluminum (or beryllium) sections to be thicker near the center than at the ends.

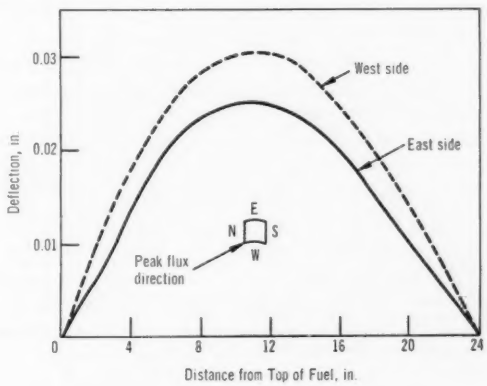

Fig. 4 Bowing measurements made on two sides of the Al–Cd rod in core position F-4.[5]

Table 1 lists observed deflections and estimated fast-neutron fluences. The data show that aluminum in core positions F-4 and F-6 bows at a rate of about 0.015 in./year—the rate for beryllium in the same positions is ~0.010 in./year.

Table 1 also contains measurements of bowing in two aluminum lattice pieces. These items were located on the periphery of the fuel region, specifically in lattice positions A-7 and D-8. One is essentially a

Table 1 IRRADIATION HISTORIES AND BOWING MEASUREMENTS[5] OF ALUMINUM LATTICE COMPONENTS IN THE ORR*

Component	Lattice position	Mwd	Fluence,† >1.0 Mev, neutrons/cm²	Bowing,‡ in.
Al–Cd shim rod, Al-3S	F-6	21,491	9.97×10^{21}	0.039
Al–Cd shim rod, Al-4S	F-4	21,491	9.22×10^{21}	0.030
Hydraulic tube No. 2	D-8	28,711	1.1×10^{22}	0.029
N_F tray	A-7	~67,549	1.8×10^{22}	0.060

*The ORR produces ~9400 Mwd(t)/year and operates at a nominal power of 30 Mw about 86% of the time.
†Estimates are based on measurements at the outer edge of a fuel element adjacent to a beryllium reflector piece.[13]
‡Bowing measurements given are the maximum measured values that occur on the side adjacent to the fuel region.

hollow aluminum box, and the other is an aluminum block with several drilled holes.

The hollow aluminum box (the N_F tray) was bowed in two directions as expected. The side away from the fuel bows less than does the side adjacent to the fuel, again indicating a "fattening" of the middle section of the lattice piece.

Damage of beryllium lattice pieces due to irradiation was established some 5 years ago in the ORR.[5] (A similar case of beryllium distortion occurred at the Materials Testing Reactor (MTR) where the beryllium section of a shim rod was found to be considerably bowed after 27,193 Mwd of irradiation.[6]) Table 2 gives the irradiation history and bowing measurements of damaged beryllium lattice components in the ORR.

Table 2 IRRADIATION HISTORIES AND BOWING MEASUREMENTS[5] OF BERYLLIUM LATTICE COMPONENTS IN THE ORR

Component	Lattice position	Mwd	Fluence,* >1.0 Mev, neutrons/cm²	Bowing,† in.
Be–Cd shim rod, Be-1S	F-6	24,323	10^{22}	0.031
Be–Cd shim rod, Be-2S	F-4	25,432	10^{22}	0.028
Be reflector, R-10	F-5	36,975	1.8×10^{22}	0.056

*Estimates are based on measurements at the outer edge of a fuel element adjacent to a beryllium reflector piece.[13]
†Bowing measurements given are the maximum measured values that occur on the side adjacent to the fuel region.

HEAT-EXCHANGER TUBE VIBRATIONS

Flow-induced vibrations and resulting damage of heat-exchanger tubes have in the last few years been recognized as a serious problem in need of thorough engineering attention. The most well-known case in this country probably concerns the Advanced Test Reactor (ATR).[7] Similar High Flux Beam Reactor (HFBR) experience has been reported.[8] However, in the HFBR case, the symptoms were recognized and the problem solved before any tube rupture occurred.

HFBR-Exchanger Design. The two HFBR primary coolers (Table 3 and Fig. 5) are U-tube counterflow exchangers with the heavy water on the tube side and cooling water on the shell side. Rattling noises were heard in these large coolers (68.5×10^6 Btu/hr) during an early test at rated secondary flow. Design similarities in size and baffle spacing which existed between these coolers and those of the ATR precipitated a study to determine the effect of reduced cooling-water flow. It was found that at about one-half rated flow the rattling disappeared.

Analysis indicated that the natural vibrational frequency of the tubes was sufficiently close to the driving frequency at rated cooling-water flow to cause some resonant vibrations. Because of the relatively long unsupported tube spans, the U bends were particularly suspect. Therefore it was decided to undertake a vibration survey to define the problem.

Table 3 DESIGN DATA FOR THE HFBR PRIMARY COOLERS*

	Tube side	Shell side
Fluid	D_2O	Cooling-tower water
Velocity, ft/sec	7.3	4.65
Rated flow, gal/min	9000	4000
Pressures		
Operating, psig	250	12
Drop at rated flow, psi	10	12
Temperatures at rated flow		
D_2O in, °F	134	
D_2O out, °F	120	
Cooling water in, °F		85
Cooling water out, °F		119
Number of U tubes	1350	
Tube specifications	$^3/_4$ in. in outside diameter × 16 BWG	
Tube-to-tube clearance, in.	$^3/_{16}$	
Tube pitch, in.	$\Delta^{15}/_{16}$	
Length between baffles, in.	$29^1/_8$	

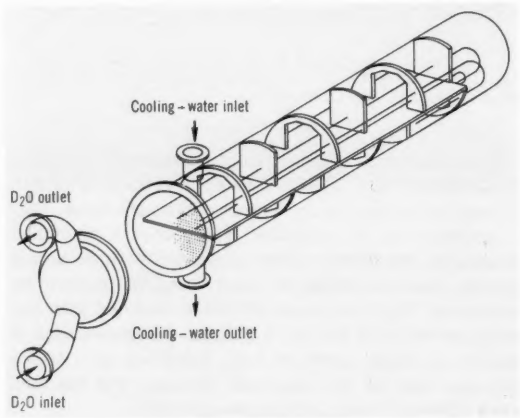

Fig. 5 Vibration in the as-designed HFBR primary coolers proved excessive; peak-to-peak amplitudes reached 0.150 in. at rated 4000 gal/min flow.[8]

Vibration Survey. Vibration-sensing elements were inserted into the previously drained and dried tubes of the cooler. The sensing elements were precalibrated piezoelectric-type accelerometers that could sense vibrations in two mutually perpendicular directions. The signals from the accelerometers were amplified, integrated, and recorded on an oscillograph. Twenty-nine tubes in one quadrant of one cooler were examined; measurements were made at several positions in each tube. Some of the tubes were selected in a random fashion—others because of the greater likelihood of vibrations (e.g., tubes near the cooling-water inlet nozzle). Longitudinal positions selected were usually the midpoints between the baffles. Measurements were not made in the curved section of the U tube because of the inaccessibility.

In tube positions where the unsupported length was two baffle spacings (~60 in.), the vibrational frequencies were 30 to 40 cps. Between the last baffle and the curved section of the U tube, however, the frequencies observed were between 5 and 15 cps. Where unsupported length was ~30 in., frequencies approached 140 cps.

View ports were cut into the side and U-bend end of the shells. Vibration visible through side ports did not appear serious. However, through the end ports, three of four tubes could be seen vibrating with substantial amplitudes. Motion pictures indicated amplitudes as high as 0.15 in. peak to peak at a flow of 4000 gal/min. No vibration was noted at 2000 gal/min.

The conclusions were that (1) there was little likelihood of dangerous vibrations in the straight sections of the tubes, (2) there was serious vibration in the U bends at rated flow, and (3) tube vibration at one-half rated flow appeared insignificant.

Revised Design. Reduction of tube vibration in the coolers without seriously limiting the heat-removal capability (it was necessary to increase primary-to-secondary log mean temperature difference by ~25%) was accomplished by cutting new outlet holes in the U-bend end of the coolers and splitting the cooling flow so that half the rated flow went through each shell pass. The goals were to restore cooling flow to its original value, to limit shell-side velocities to one-half of the original value over the straight section of the tubes, and to almost eliminate flow over the U bends (Fig. 6).

The modifications cost about $29,000 (20% of the initial cost of the exchangers) and were successful; at rated flow, no tube vibration has been detected.

Tube damage due to flow-induced vibrations in heat exchangers is a serious problem which has been given too little design consideration up to now. The HFBR case is another strong reminder that this must be done. Improved designs, analytical approaches, and in-shop testing procedures are being developed. For the new Argonne Advanced Research Reactor facility (for example), three 30-Mw heat exchangers are at present under contract negotiations. A full-scale mockup test is specified, and this contract will stipulate a manufacturer's guarantee against flow-induced vibrations.

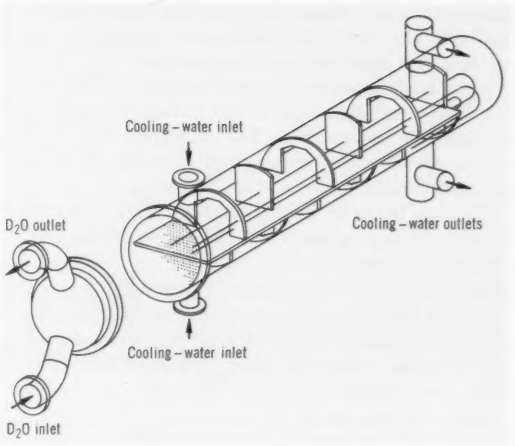

Fig. 6 Modified primary coolers for the HFBR almost eliminate flow over the U bends.[8]

CIRCULATION-PUMP SEAL FAILURE

When the Big Rock Point Nuclear Plant was restarted after a routine shutdown in November 1966, it became apparent that the shaft seals in the No. 2 circulation pump had failed.[9] In 1964 these controlled-leakage, mechanical shaft seals were changed from the original rotating hard-face Stellite to aluminum oxide (sapphire) for the No. 1 pump and to tungsten carbide for the No. 2 pump and had accumulated ~16,000 hr of operation when the tungsten carbide seals failed.

Planned Repairs. A schedule was laid out for replacing the failed seals in situ, with estimates of the time and number of personnel required to accomplish each step. On the basis of radiation levels (up to 2 r/hr in the working area) known from surveys conducted during the refueling outage, it was estimated that the job would require 16 men and could be done in about 12 hr of working time.

Repairmen were imported, briefed on radiation protection practices at Big Rock Point, and assigned a specific step in the seal-replacement procedure. They then studied their specific jobs with site personnel. Replacement parts were brought out, and, with drawings and pictures, each job was described in detail.

The work started at 8:00 a.m. on a Saturday, and the plant was expected to be back in full service by Monday. No problem was anticipated—contingencies had been included. But . . .

Complications. When the outer seal unit was examined, it was found that the tungsten carbide rotating seal face had shattered and caused severe damage to the pump shaft and other parts in the seal mechanism. This meant that the shaft would have to be removed and repaired or replaced. The magnitude of this job dictated that the entire pump be removed from the high-radiation pump room. The shattering of this seal is believed to have been caused by an insufficient seal-support arrangement, which later was redesigned by the pump manufacturer.

Radiation-Exposure Problems. The work required to remove the pump from the recirculating pump room was straightforward and did not demand a detailed briefing. When the pump was lifted free of its casing, the radiation reading was 20 r/hr at the impeller. The original location chosen for storing the pump was not suitable for this high radiation level; therefore the pump had to hang on the reactor crane until a suitable location was readied. While a pit on the refueling deck was being prepared, long-range decontamination techniques were employed to reduce the radiation reading at the impeller; this was lowered to approximately 9 r/hr but no further. The pump was then placed in the pit. Sheet lead was used to reduce the radiation field in the area. The men who had worked on this phase of the job had accumulated individual exposures of 1.8 to 2.7 r.

A stand was designed and fabricated to hold the pump in its normal upright position and also in an inverted position for impeller removal. The pump and stand were submerged in water (in a site-fabricated steel tank) to obtain a radiation shield and prevent airborne contamination. Sheet lead was also used where practicable during the pump disassembly to reduce the radiation field.

The job of disassembly and assembly required 3 weeks and was done by three groups of three men each. Each group worked 1 week on the job and accumulated an average exposure of 2.5 r in 40 hr of work. A plant engineer who supervised accumulated approximately 1.5 r during the 3-week period.

Pump Improvements. During reinstallation of the pump, several areas were noted in which modifications could save considerable time and exposure:

- Swagelok or similar fittings should be used on the seal-system controlled-leakage lines.
- Connectors should be used on the instrumentation leads.
- Provisions should be made to simplify draining and refilling bearing-oil reservoirs.
- Appendages should be minimized to ease lifting and lowering through tight spaces.

Work in Radiation Areas. Maintenance work on highly radioactive equipment or on equipment in high-radiation areas at Big Rock Point and other facilities leads to the following general conclusions:

(1) Procedures must be flexible but as detailed as possible.

(2) Skilled manpower with the required radiation-exposure history must be available. (As more of the utility's generating capacity becomes nuclear, the pool of outside personnel with low radiation exposures will decrease.)

(3) Equipment should be designed to facilitate maintenance. Plant layout must be aimed to reduce needless exposures that come from poor and improperly placed equipment.

(4) Key personnel should conduct a follow-up study immediately following each major job. Problem areas, solutions, and suggested solutions should be recorded.

Reactor Modifications

Ultimately, difficulties with components and materials lead to major reactor modifications.

PREPARATIONS FOR REPLACING A REACTOR VESSEL

Since first criticality in 1957, the NRU, a heavy-water-cooled and -moderated reactor (Fig. 7), has experienced significant corrosion in the aluminum reactor vessel.[10] As a result, much of the vessel—which was site assembled—may have to be replaced. Detailed plans have been developed and trial runs of removal and disposal operations have been made, often with full-scale mockups. A PERT program has been developed to make maximum use of manpower and resources. The program calls for full-time effort—24 hr/day, 7 days/week—during a reactor downtime of about 6 months. The prognosis, of course, is for successful completion.

Corrosion Damage. The NRU reactor-vessel aluminum sidewall is a rather complicated structure; it includes an annulus immediately outside the heavy-water vessel and, outside that, a light-water reflector. Corrosion is caused by water that leaks into the annulus from the reflector and from water-cooled assemblies irradiated in the annulus. An 8-ft-square aluminum window $\frac{1}{16}$ in. thick, used in lieu of the reflector in front of the graphite thermal column, has completely corroded through. If the sidewall of the reactor vessel should fail, attempts will be made to repair it in situ. Certain repairs, however, will not be possible.

Vessel Sidewall Details. The cylindrical aluminum sidewall, which is 0.188 to 0.313 in. thick, is sealed between top and bottom headers of stainless steel. The sidewall is secured to the two header flanges by 72 bolts at the top and 72 bolts at the bottom. These bolts shoulder on the headers and fasten to inserts in the sidewall flanges. To form a double seal, a metal-to-metal butt seal and a stainless-steel O-ring are used.

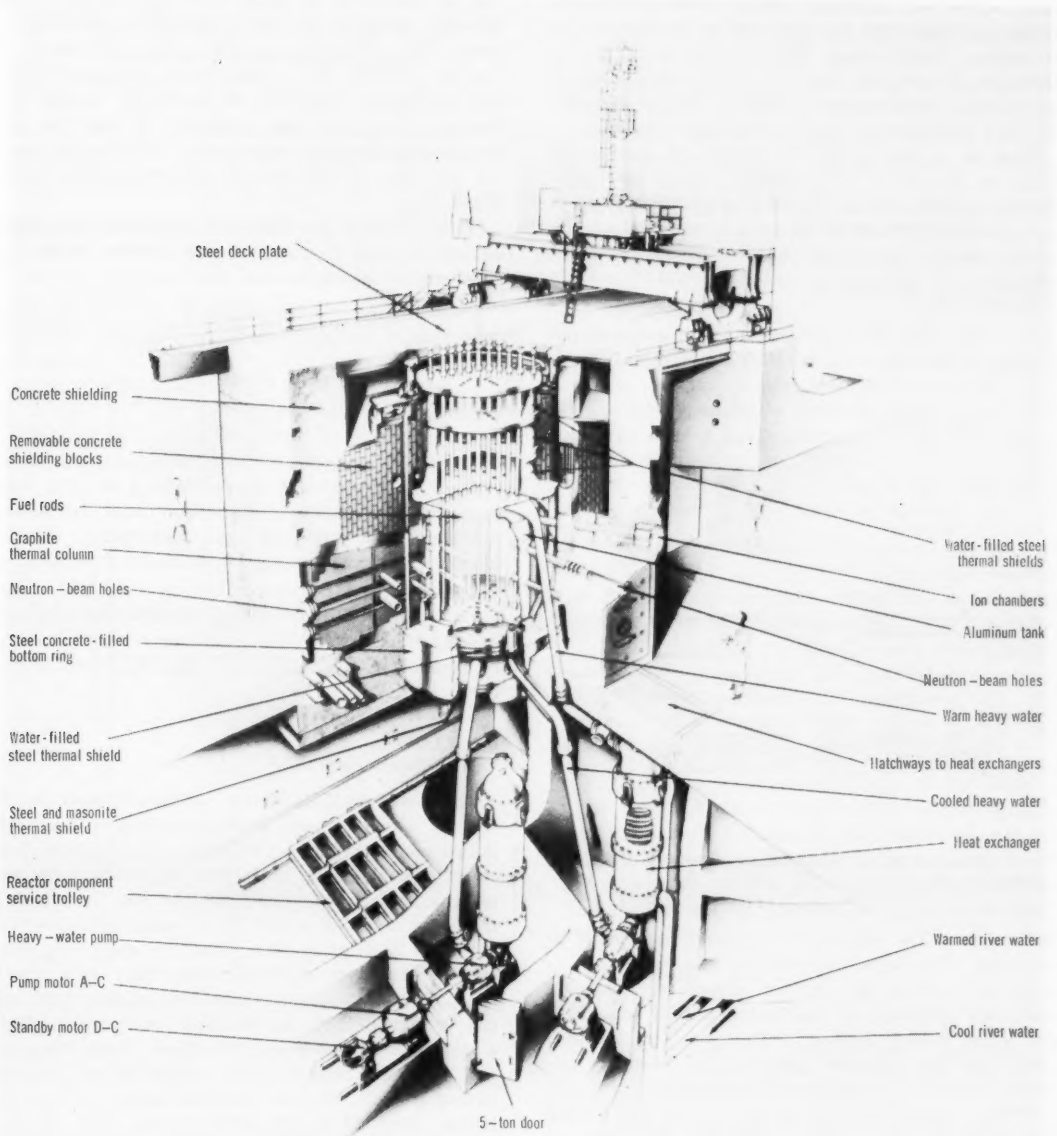

Fig. 7 Because of corrosion the aluminum reactor vessel in the Canadian NRU reactor may be replaced; preparations have been made.[10]

Another aluminum sidewall assembly has been delivered. Although similar to the original, it incorporates a new seal section made up of two $\frac{1}{8}$-in.-wide aluminum rings, one on each side of the bolt-circle centerline. These rings are integral parts of the aluminum flange and will mate to the seal surface of the existing stainless-steel header. Part of the preparatory program has been to ready this assembly.

Because of high-radiation fields, all operations must be conducted from behind heavy shielding. Planned facility design makes it possible to remove and retain behind shielding such large units as the bottom shield and bottom header. These units are anticipated to have contact radiation levels in excess of 20,000 r/hr.

Removal. Figure 8 shows the basic steps in the procedure for removing the sidewall assembly from

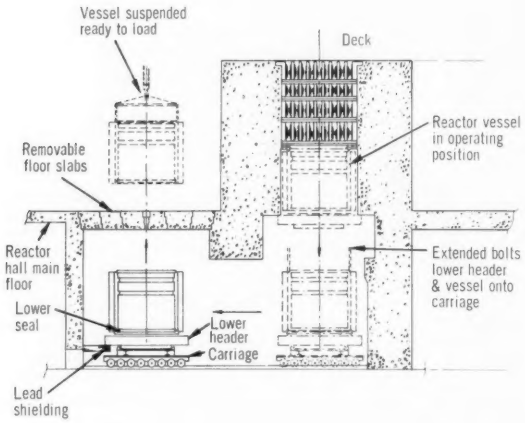

Fig. 8 Steps in the removal of the sidewall and lower header.[10]

the reactor. The 144 bolts at top and bottom must be removed. The upper shields and header remain in place as part of the reactor structure. Next, the aluminum sidewall and the bottom header and shield are again bolted together with three long capstan bolts that are operated from above. Then the assembly is (to be) lowered to a carriage.

Prior to these operations a steel skirt with a solid top equipped with a lifting yoke and fitted with an open-ended nylon bag will be hung at the ceiling of this room. When the carriage is properly positioned, the skirt will be lowered over the aluminum sidewall assembly and the lifting adapter secured to the vessel. After the floor slabs are lifted away, the disposable portion of the vessel will be enclosed in a metal and nylon container (for contamination control) and this package will be removed from the shielded area to the disposal skid positioned in the reactor hall. Operations will be viewed on closed-circuit television.

Disposal. One hundred days after reactor shutdown, the radiation fields from this 29,000-lb package are estimated to be about 350 r/hr at 25 ft—the distance behind a shielded vehicle at which it will be towed to a disposal area. The preferred vehicle to tow the package is a mobile crane equipped to hitch and disconnect remotely by hydraulic means. The disposal area has been prepared so that the tow vehicle can drive in, disconnect, and drive out, leaving the skid (a solid-tired flat-bed trailer) in the disposal pit.

Trial runs of the disposal procedure have been completed with a dummy vessel under winter and summer conditions.

Custom Tooling. Much special tooling is required. The most interesting is a very complex $100,000 surface-conditioning tool. Because the condition of the sealing surfaces on the stainless-steel headers is unknown, the conditioning tool must be able to inspect, brush, hone, grind, and clean as required to effect a 16-μin. surface finish. Now being tested, the tool is a three-armed spider with a vertical main drive stem. Tooling and inspection heads for various functions attach to each arm. A borescope viewing head and vacuum-cleaning facilities are provided.

The surface-conditioning tool is designed to operate in an environment of about 20,000 r/hr through a 4.7-in.-diameter vertical hole and to work on surfaces about 11 ft in diameter, 28 ft below the manned level.

INSTALLATION AND TESTING OF A STEEL POOL LINER

The Texas A&M University swimming-pool reactor facility has had pool leakage problems since the initial construction in 1961 (Ref. 11). Failure of the epoxy coating in the main pool section and the aluminum liner in the stall section was the result of improper installation and lack of adequate testing procedures. A solution was sought by contacting other pool-reactor operators concerning their liner experience.[12] When the pool leakage flow reached 1000 gal/day in March 1966, the decision was made to install a welded stainless-steel pool liner. Installation and related modifications were completed in a 4-month period at a cost of about $51,000; design cost is estimated at an additional $5000. (Some costs for pool and piping improvements are not included.)

Design. The walls of the 304 stainless-steel liner are constructed of 10-gauge sheet, and the floor is of $\frac{1}{4}$-in. plate. Drain channels in the concrete beneath the floor of the liner collect any leakage. Water from these channels drains into the radioactive waste-disposal system.

"Hat channels," Fig. 9, were formed from 10-gauge material and positioned vertically on the walls to facilitate vertical welding of the wall sheets. These

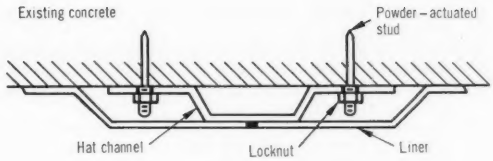

Fig. 9 "Hat channels," analogous to furring strips, were installed vertically on the concrete walls of a reactor pool to facilitate installation of a steel liner.[11]

channels are held in place by locknuts on powder-actuated threaded studs. Vertical slots in the hat channels accommodate the studs and allow slight movement along the studs. Strips of 10-gauge material were recessed in the pool walls as backup plates for the horizontal welds. The base molding of the liner is formed by an angle $^{3}/_{16}$ by $2^{1}/_{2}$ by $2^{1}/_{2}$ in., and this molding serves as an expansion joint between the floor and wall sections, Fig. 10. A similar angle trims the top of the liner.

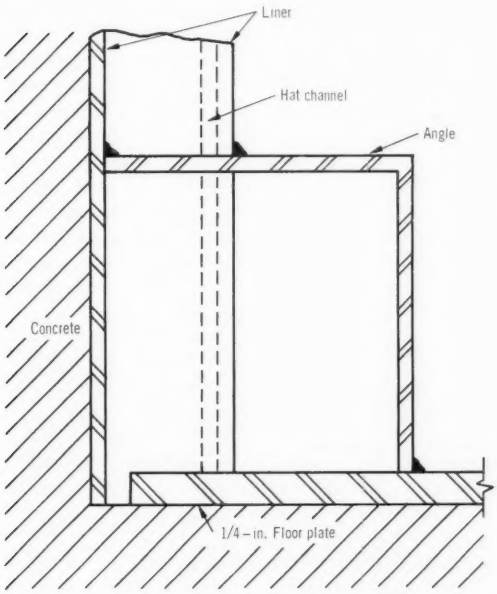

Fig. 10 An expansion joint between pool wall and floor is formed by welding a $^{3}/_{16}$-in.-thick angle to both surfaces.[11]

Installation. The floor was the first section installed. Sheets of $^{1}/_{4}$-in. plate were positioned and welded. Vertical hat channels were installed over the old epoxy coating. The 10-gauge preformed wall sheets were positioned and tack-welded to the hat channels. Gussets were fitted and welded to steel penetrations and to the liner. For cost and strength reasons, the aluminum gate jamb between the two sections of the pool was not replaced. Rather, stainless-steel sheets were formed around the gate and welded to adjacent wall sheets.

Welding. Final welding was done with a short-arc, automatic-feed, inert-gas welding machine after all wall sheets had been tack welded in position. This method proved to be much faster than rod welding; however, it had the disadvantage that the amount of weld material deposited was sometimes inadequate; when the welds were ground flush (to improve the appearance of the liner) some welds were too thin. The short-arc machine was chosen to limit the heat applied and thus reduce buckling. Regardless, considerable buckling of the hat channels occurred at the top and bottom of the liner, but this buckling was corrected (later) by installation of the base angle and top trim angle. Floor plates were rod welded.

A rod-welding technique should be used throughout because the buildup is better and much less splatter is produced. Both factors significantly reduce the amount of grinding required and produce more satisfactory results. Where grinding is not required, the rod weld also produces the better finish.

Testing. First testing of the welds was done with a vacuum bubble-box method—a technique that was not successful. Successful testing was accomplished with a Freon-22 leak-detector system. Gas was introduced through the pool-leakage drain system. After large leaks around pool penetrations were repaired, several smaller leaks were discovered. After several inspection and repair cycles, a raw-water test indicated a leak rate of about 25 gal/day.

Performance. The performance of the liner has been excellent. In addition, facility appearance has been improved. Experience has confirmed that pool leakage is only 25 gal/day. Since the evaporation rate is on the order of 200 gal/day, no attempt has been made to correct the leakage; it presents no operational problem.

References

1. W. K. Alexander, Hydriding of Hanford Production Reactor Zircaloy Process Tubes, *Trans. Amer. Nucl. Soc.*, 10(Suppl.): 12-13 (1967).
2. A. R. Daniel, Terminal Solid Solubility of Hydrogen in Zircaloy-2, Canadian Report AECL-2453, Reprint, June 1966.
3. J. N. Wanklyn and B. E. Hopkinson, The Role of Hydrogen in the High Temperature Corrosion of Zirconium and Its Alloys. I. The Effect of Cathodic Polarization on Corrosion in Water at 325° F., *J. Appl. Chem. (London)*, 8: 496-504 (1958).
4. A. Sawatzky, Hydriding of Zircaloy-2 by Electrolysis, Canadian Report CR-Met-924, June 1960.
5. S. S. Hurt III, Experience with Neutron Damage to Beryllium and Aluminum Lattice Components of the ORR. *Trans. Amer. Nucl. Soc.*,10(Suppl.): 11-12 (1967).
6. J. W. Dykes and J. D. Ford, A Preliminary Report of Beryllium Damage Observed in the MTR Reflector,

USAEC Report IDO-16899, Idaho Operations Office, June 20, 1963.
7. J. P. Waggener and R. C. Herrick, Tube Failure and Analysis Program on the Advanced Test Reactor Primary Heat Exchanger, Phase II, USAEC Report TID-22616, Franklin Institute Research Laboratories, Sept. 3, 1965.
8. G. C. Kinne and P. R. Tichler, Heat Exchanger Tube Vibration and Repair in the High Flux Beam Reactor, *Trans. Amer. Nucl. Soc.*, 10(Suppl.): 8-9 (1967).
9. R. B. DeWitt and R. R. Biggs, Maintenance Experience — Reactor Recirculating Pump, *Trans. Amer. Nucl. Soc.*, 10(Suppl.): 9 (1967).
10. J. H. Collins, Preparations for Replacing the NRU Reactor Vessel, *Trans. Amer. Nucl. Soc.*, 10(Suppl.): 9-10 (1967).
11. D. E. Feltz, P. M. Mason, and J. D. Randall, Design, Installation, and Testing of a Stainless-Steel Liner for a Swimming Pool Reactor, *Trans. Amer. Nucl. Soc.*, 10(Suppl.): 8 (1967).
12. C. W. Garrard and J. D. Randall, A Survey of Pool Liners for Swimming Pool Reactors, Technical Report No. 15, Nuclear Science Center, Texas A&M University, April 1966.
13. H. A. O'Brien, Jr., Fast and Thermal Neutron Flux Measurements in the ORR and LITR, USAEC Report ORNL-TM-1163, Oak Ridge National Laboratory, January 1966.

Thermophysical Properties of Sodium—Recommended Values

By Gerald H. Golden, John V. Tokar, and David Miller

Comparisons of safety studies of sodium-cooled fast breeder reactors will be more meaningful if the various groups making such studies use the same values for the thermophysical properties of sodium. So that "best values" of these properties could be recommended, the literature on the thermophysical properties of the liquid and vapor phases of sodium has been evaluated.[1] The resulting recommended values are reported here.

Interest in sodium as a heat-transfer fluid and as a working fluid for power cycles has triggered numerous studies of its properties. In turn, critical compilations have been necessary every few years.[2–10] The newest compilation, which attempts to update through 1966, includes:

- Liquid density
- Vapor pressure
- Thermodynamic properties (including P – V – T)
- Transport properties (conductivity, viscosity)
- Electrical resistivity
- Surface tension
- Liquid thermal-expansion coefficient
- Liquid compressibility and sonic velocity

In each case the results of different investigators have been compared, and recommended "best" values are presented. The recommended values are presented in tabular form to facilitate engineering use of the property data. Unabridged versions of the thermodynamic charts and tables are available in Ref. 1.

The temperature, pressure, and specific volume at the critical point are not included in the compilation because of the considerable uncertainty about the values reported. However, recent estimates of the critical constants and equations for application in the critical region are given by Miller[11] for sodium and the other alkali metals.

Density of Liquid Sodium

Table 1 lists the methods that various investigators used to measure the density of liquid sodium, the temperature range over which they measured it, and the average extent by which each set of data differs from values calculated by the equation

$$\rho_l(\text{lb/cu ft}) = 59.566 - 7.9504 \times 10^{-3}t - 0.2872 \times 10^{-6}t^2 + 0.06035 \times 10^{-9}t^3 \quad (1)$$

where the temperature, t, is between 208 and 2500°F. Equation 1 was derived by Stone[12] on the basis of the data of the investigators listed in Table 1.

Table 1 SUMMARY OF DENSITY MEASUREMENTS FOR LIQUID SODIUM

Investigators	Method	Temp. range, °F	Av. deviation with Eq. 1, %
Ewing[15]	Dilatometric	M.p. to 503	±0.08
Jackson[47]	Buoyancy	937 to 1314	−0.74
Rinck[48]	Buoyancy	804 to 1183	+0.15
Hagen[49]	Dilatometric	M.p. to 336	±0.05
Stone[12]	Dilatometric (pycnometers)	1577 to 2491	±0.17
Novikov[50]	Buoyancy of		
	Steel sinker	248 to 505	−0.14
	Tungsten sinker	275 to 1324	+0.71
Nishibayashi[51]	Buoyancy	486 to 1580	±1.09

Corroboration. The values obtained with Eq. 1 were corroborated by two other investigations. An equation derived by Thomson and Garelis[5] for the 208.1 to 1184°F range agrees with Eq. 1 within 0.1%. Goltsova[13] used a molybdenum pycnometer for measurements at 212 to 2640°F, from which she derived an equation that agrees with her data within an average of 0.5%; her equation agrees very well with Eq. 1 over the range 212 to 2500°F (at 2500°F, density from the two equations agrees within 0.39%).

Figure 1 plots Eq. 1 and the results of two other investigations.[8,14] The equations derived by Tepper[14] and by Weatherford[8] do not agree as well with Eq. 1 as do the equations derived by Thomson and Garelis[5] and Goltsova.[13] As the source of the graphical data he uses, Weatherford[8] cites Meisl and Shapiro,[6] who in turn cite Miller,[3] who cites Ewing[15] as his source. However, in the experiments, Ewing[15] measured sodium density by a dilatometric technique over the range 225 to 503°F; apparently, the other authors[3,6] extrapolated the original 225 to 503°F data to 1292°F and 2240°F. In view of this large extrapolation, and on the basis of the close agreement of the work of Thomson and Garelis,[5] Goltsova,[13] and Stone,[12] Eq. 1 is recommended as the best representation of the density of saturated liquid sodium over the range 212 to 2500°F.

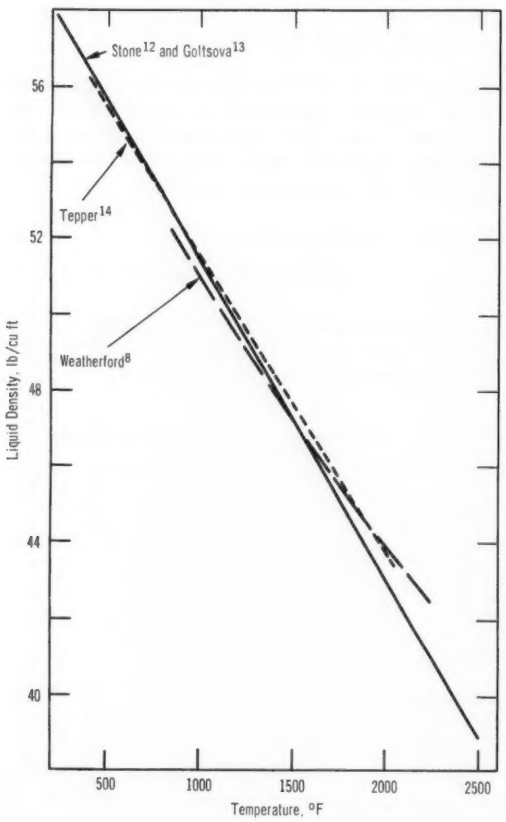

Fig. 1 Density variation of liquid sodium with temperature. The curve of Stone[12] and Goltsova[13] is recommended.

Saturation Vapor Pressure

Comparison of various vapor-pressure equations for sodium is complicated because some equations are fits to specific sets of experimental data, whereas others are "pooled" results.

FITS TO DATA

Stone[12] measured the saturation vapor pressure of sodium with a static-capsule technique. A least-squares fit of the data taken in the range 1624 to 2539°F resulted in the Kirchoff-type equation

$$\log P_s(\text{atm}) = 6.83770 - \frac{9{,}980.94}{T(^\circ\text{R})} - 0.61344 \log T(^\circ\text{R}) \quad (2)$$

This equation gives a normal boiling point of 1618.6°F. The experimental data deviate from values computed with Eq. 2 by an average of 0.37%. An independent "third law check" demonstrated the internal consistency of the vapor-pressure data.

Table 2 summarizes the results of related investigations since 1955. Three of the six equations give normal boiling points that agree to within 0.5°F of that given by Eq. 2. Figure 2 compares these data and shows that four of the six equations agree with Eq. 2 to within 6% in the range 1270 to 2530°F. The Makansi[16] equation agrees best.

POOLED CORRELATIONS

Table 3 summarizes the ranges of applicability of the vapor-pressure correlations, the equations, the predicted normal boiling point, and lists the references cited by each investigator. Figure 3 plots the deviations of six "pooled equation" results from the values predicted by Eq. 2; extrapolations are over wider temperature ranges than intended by some of the authors. As shown in Fig. 3, below 1600°F, most of the pooled correlations differ rather uniformly from Eq. 2. On this basis (and considering the close agreement between the equations of Stone[12] and Makansi[16] above 1600°F), we recommend the Ditchburn and Gilmour[17] equation below 1600°F and the Stone[12] equation for higher temperatures. A similar choice was made earlier by Makansi, Selke, and Bonilla.[18]

Thermodynamic and P-V-T Properties

Sodium vapor is composed of the monomer, dimer, and, reportedly, tetramer; the fraction of each species depends on both temperature and pressure.[12] Saturated vapor contains about 10 mole % dimer at 1500°F and 18 mole % dimer at 2500°F. If the ideal monomeric gas is taken as the base, any deviations from ideality in the vapor are caused by the effect the higher molecular-weight species has on the mean molecular weight of the vapor and on the nonideal compressibility and mixing effects of the individual

Table 2 VAPOR-PRESSURE INVESTIGATIONS SINCE 1955

Investigators	Method	Temp. range, °F	Derived equation for log P_s, atm	Derived normal boiling point, °F
Bowles and Rosenblum[52]	Static capsule	1470 to 3417	$4.51961 - \frac{9{,}363.82}{T(°R)}$	1612.1
Sowa[53]	Evaporation from crucible at fixed pressure	1651 to 2533	$4.56719 - \frac{9{,}491.55^*}{T}$	1618.5
Kirillov and Grachev[54]	Static capsule	1616 to 2372	Authors' smoothed data†	
Makansi[16]	Refluxing capsule	1148 to 2075	$4.521 - \frac{9396‡}{T}$	1618.6
Achener and Jouthas[25]	Flash boiler	1129 to 1752	$4.71924 - \frac{9{,}770.25}{T}$	1610.6
Fischer[55]	Quasistatic variation	971 to 1484	$4.6279 - \frac{9{,}616.14}{T}$	1618.2
Vinogradov and Volyak[56]	Elastic-membrane-sealed static capsule	1096 to 1628	Authors' smoothed data§	1621.1

*Derived from least-squares fit to data.
†Table 1 in Ref. 54.
‡Fit of equation of Kirchhoff-type tried and found to be no better than two-term fit (Ref. 18).
§Table 3 in Ref. 56.

species. Before the P–V–T measurements became available for sodium vapor, its mass specific volume at moderate pressures was computed from ideal-gas thermodynamic properties, generally neglecting the compressibility and mixing effects.

HEAT OF DIMERIZATION

An outline of the thermodynamics of sodium provides a basis for discussing techniques that have been used to analyze pertinent experimental data. Initial assumptions are that the vapor is saturated, consists only of the monomer and dimer, and that these are ideal gases. For the dimerization reaction

$$2\text{Na(gas)} = \text{Na}_2\text{(gas)}$$

$$\Delta F_2^\circ = RT \ln k_2 \qquad (3)$$

where

$$k_2 = \frac{P_{\text{Na}_2}}{P_{\text{Na}}^2} = \frac{N_2}{P_s N_1^2} = \frac{N_2}{P_s(1-N_2)^2} \qquad (4)$$

Dividing Eq. 3 by T and rearranging

$$-R \ln k_2 = \frac{\Delta F_2^\circ}{T} = \left(\frac{F^\circ - H_0^\circ}{T}\right)_2 - 2\left(\frac{F^\circ - H_0^\circ}{T}\right)_1 + \frac{(\Delta H_0^\circ)_D}{T} \qquad (5)$$

For convenience, let $(\Delta H_0^\circ)_D = \Delta D_0^\circ$, the heat of dimerization of the ideal gas at absolute zero.

The thermodynamic properties of ideal gaseous Na and Na_2 were computed by Benton and Inatomi[19] and later by Evans.[20] The values of the free-energy functions $[(F^\circ - H_0^\circ)/T]_1$ and $[(F^\circ - H_0^\circ)/T]_2$ reported by these two groups are in excellent agreement and in accordance with the tables of Stull and Sinke[21] and with the JANAF tables.[22]

The value of ΔD_0° has been determined experimentally by a number of investigators, as described in detail by Thomson and Garelis.[5] The values presented range from -8400 ± 100 to -9300 ± 500 cal/gram atom Na. The vapor composition is extremely sensitive to the value of ΔD_0°.

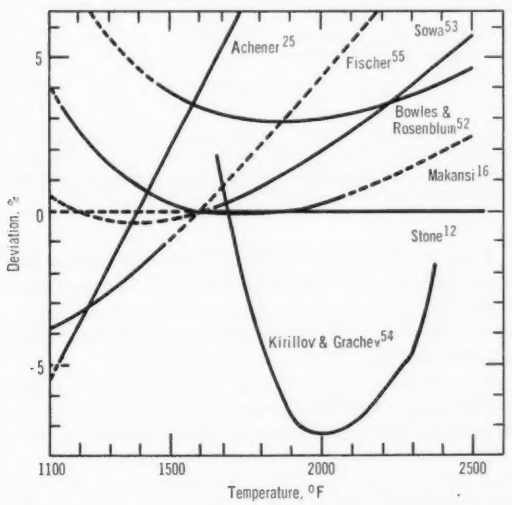

Fig. 2 Deviation of various sodium vapor-pressure values (see Table 2) from those recommended by Stone.[12] Portions of curves based on extrapolations are shown by broken lines.

HEAT OF VAPORIZATION

For vaporization to the ideal monomer

$$\text{Na(liquid)} = \text{Na(gas)}$$

$$\Delta F_v^\circ = -RT \ln P_{\text{Na}} \qquad (6)$$

Table 3 VAPOR-PRESSURE POOLED CORRELATIONS

Investigators	Temp. range, °F	Derived equation for log P_s, atm	Normal boiling point, °F	Refs.
Ditchburn and Gilmour[17]	M.p. to 1790	$6.4818 - \frac{10020.6}{T} - 0.5 \log T$*	1617.5	57–68
Bowles and Rosenblum[52]	1149 to 3418	$4.54025 - \frac{9435.8}{T}$	1618.4	16, 53, 69
Thomson and Garelis[5]	260 to 1250	$4.57791 - \frac{9448.38}{T - 14.65}$		
	1250 to 2240	$4.36383 - \frac{8718.3}{T - 83.16}$	1621.3	16, 57, 59, 60, 63, 64, 66
Meisl and Shapiro[6]	240 to 1040	$8.286 - \frac{10050}{T} - 0.698 \log T$		
Weatherford[8]	1040 to 2240	$8.402 - \frac{10104}{T} - 0.723 \log T$	1630.3	
Kelley[70]	357 to 1620	$9.1882 - \frac{10395}{T} - 1.274 \log T$	1637.3	57–66, 71–75
Stone[12]	1624 to 2539	$6.8377 - \frac{9980.94}{T} - 0.61344 \log T$†	1618.6	(Eq. 2)
Hicks[76]	M.p. to 2070	See Ref. 54	1620.9	16, 57, 58, 63, 66

*Recommended equation for vapor pressure at ≤1600°F.
†Recommended equation above 1600°F.

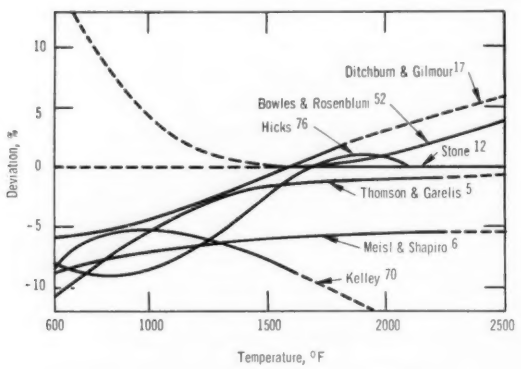

Fig. 3 Deviation of various sodium vapor-pressure values determined by pooled correlations from those recommended by Stone.[12] We prefer the Ditchburn and Gilmour values[17] below 1600°F and those of Stone[12] above 1600°F.

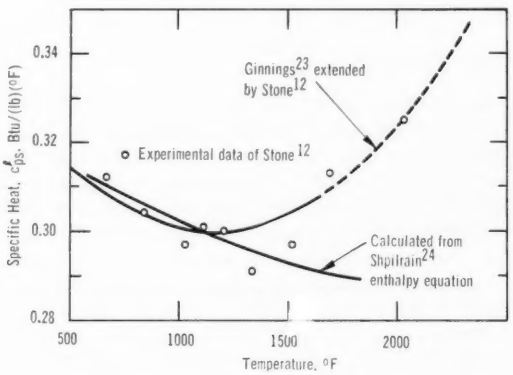

Fig. 4 Ginnings[23] curve (solid portion) of specific heat of saturated liquid sodium was extended by Stone[12] (dashed portion). Other curve was derived from Shpilrain equation for enthalpy of liquid sodium.[24]

Thus

$$(\Delta H_0^\circ)_v = -RT \ln P_{Na} - T\left[\left(\frac{F^\circ - H_0^\circ}{T}\right)_1 - \left(\frac{F^\circ - H_0^\circ}{T}\right)_l\right] \quad (7)$$

where $(\Delta H_0^\circ)_v$ is the heat of vaporization to the ideal monomer at absolute zero.

Ginnings, Douglas, and Ball[23] measured precisely the heat capacity of condensed-phase sodium in the range 547 to 2106°R, from which they derived empirical equations for the enthalpy, specific heat, and entropy of condensed-phase sodium from 492 to 2111°R. Stone[12] measured specific heat at various points between 1062 and 2610°R and extrapolated the Ginnings correlations to 2610°R (Fig. 4). Also shown in Fig. 4 is a curve derived from an equation by Shpilrain[24] for the enthalpy of liquid sodium. Discrepancies in the sodium vapor-pressure data stimulated a number of analyses[4,18,20] to derive values for ΔD_0° and $(\Delta H_0^\circ)_v$.

The heats of vaporization as computed by the virial method with Eq. 8 and by the quasichemical method with Eq. 9 are shown in Fig. 5.

$$\Delta H_v = KT\left(\frac{1}{\rho} - \frac{1}{\rho_l}\right)\frac{dP_s}{dT} \quad (8)$$

$$\Delta H_v = \frac{N_1 \Delta H_{f1}^\circ + N_2 \Delta H_{f2}^\circ + N_4 \Delta H_{f4}^\circ}{\bar{M}} \text{ cal/g} \quad (9)$$

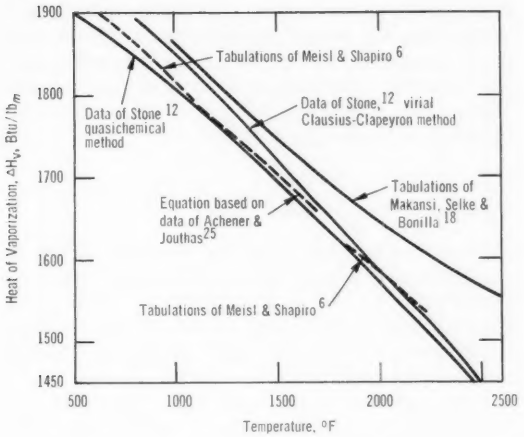

Fig. 5 Heat of vaporization of sodium as computed with virial and quasichemical methods.

Figure 5 also shows values taken from the tabulations of Meisl and Shapiro;[6] Makansi, Selke, and Bonilla;[18] and the recent experimental work of Achener and Jouthas.[25] Reference 25 recommended the relation

$$\Delta H_v = 2023 - 0.2129t \qquad 1100 \le t \le 1700^\circ\text{F} \tag{10}$$

At temperatures below about 1600°F, the quasichemical curve agrees more closely with that of Achener and Jouthas than does the virial curve. Because of this and the close agreement between the virial and quasichemical methods above 1600°F, Eq. 9 is recommended for computations of the heat of vaporization.

ENTHALPY AND ENTROPY OF LIQUID AND VAPOR

For saturated liquid the enthalpy and entropy are computed from Eqs. 11 and 12

$$H_s^l - (H_0^\circ)^s = 22.991(0.389352T - 0.552955 \times 10^{-4}T^2 + 0.113726 \times 10^{-7}T^3 - 20.023) \tag{11}$$

$$S_s^l = 22.991(0.896497 \log T - 1.10557 \times 10^{-4}T + 0.170408 \times 10^{-7}T^2 - 1.792026) \tag{12}$$

For saturated vapor the corresponding properties are computed from the saturated liquid properties and the quasichemical heat of vaporization, Eq. 9. It can be shown however that, with the heat of vaporization defined by Eq. 9, the vapor properties are in fact independent of those of the liquid. The vapor composition is found by solving Eqs. 13 to 20; mean molecular weight is then obtained from Eq. 21.

$$k_2 = \frac{N_2}{N_1^2 P} \tag{13}$$

$$k_4 = \frac{N_4}{N_1^4 P^3} \tag{14}$$

where

$$\log k_2 = -A_2 + \frac{B_2^*}{T} \tag{15}$$

$$\log k_4 = -A_4 + \frac{B_4^*}{T} \tag{16}$$

and

$$N_1 + N_2 + N_4 = 1 \tag{17}$$

$$P^3 k_4 N_1^4 + P k_2 N_1^2 + N_1 - 1 = 0 \tag{18}$$

is solved numerically and values for N_2 and N_4 are computed.

$$N_2 = k_2 P N_1^2 \tag{19}$$

$$N_4 = 1 - N_1 - N_2 \tag{20}$$

Thus

$$\overline{M} = M_1(N_1 + 2N_2 + 4N_4) \tag{21}$$

which is used in Eq. 22 to compute the mass specific volume of the vapor

$$V = RT/\overline{M}P \tag{22}$$

where

$$\overline{M} + M_1 N_1 + M_2 N_2 = M_1(1 + N_2) \tag{23}$$

If given the temperature of the saturated vapor, its composition, mean molecular weight, and specific volume are computed as shown above. Ewing[26] gave the following equations for the enthalpy and entropy of the vapor in state i:

$$H_i^g(T, P) = H^{\circ g}(T) + X_2 \Delta H_2^\circ + X_4 \Delta H_4^\circ \tag{24}$$

and

$$S_i^g(T, P) = S^{\circ g}(T) + \frac{X_2 \Delta H_2^\circ}{T} + \frac{X_4 \Delta H_4^\circ}{T} - \frac{R}{\overline{M}} \ln P + \frac{RX_2}{2\overline{M}} \ln k_2 + \frac{RX_4}{4M_1} \ln k_4 - \frac{R(N_1 \ln N_1 + N_2 \ln N_2 + N_4 \ln N_4)}{\overline{M}} \tag{25}$$

*Ewing discussed techniques for evaluating the constants A_2, B_2, A_4, and B_4 from P–V–T data.[12,26] From the data, Stone[12] obtained $A_2 = 4.3249$, $B_2 = 7204.2$, $A_4 = 10.6798$, and $B_4 = 16{,}325$.

Equations 24 and 25 are used to compute the change in enthalpy and entropy along a constant-temperature path from saturated vapor at T and P_s to an ideal monomeric gas and then to superheated vapor containing monomer, dimer, and tetramer.

The enthalpy and entropy of the subcooled liquid is computed by starting with the corresponding properties of the saturated liquid. The enthalpy change is given by

$$dH_T = \frac{K}{\rho_l}\left[1 + \frac{T}{\rho_l}\left(\frac{\partial \rho_l}{\partial T}\right)_p\right] dp \qquad (26)$$

and the entropy change by

$$dS_T = \frac{K}{\rho_l^2}\left(\frac{\partial \rho_l}{\partial T}\right)_p dp \qquad (27)$$

As an approximation, $(\partial \rho_l / \partial T)_p$ is computed from Eq. 1.

FORTRAN SUBROUTINE

A FORTRAN subroutine was written, based on the quasichemical approach for computing sodium thermodynamic properties in the range 500 to 2500°F. This subroutine was based on data from Refs. 12, 17, 20, and 23. For a given temperature and pressure, the subroutine determines the state and computes the properties. The data of Ref. 17 were used to compute vapor pressure for temperatures ≤1600°F, and those of Ref. 12 for temperatures ≥1600°F.

Table 4 is a listing of the FORTRAN subroutine. It can be used in any compatible computer program calling for the given properties, or as the core of a table-making program. The values shown in Table 5 are the thermodynamic and related properties of the saturated liquid and vapor as computed by the subroutine of Table 4.

SPECIFIC HEAT OF VAPOR

The FORTRAN subroutine (Table 4) was used to compute the specific heat of the vapor at constant pressure along the saturation curve, taking

$$(c_p^g)_s = H^g(T + 1, P_s) - H_s^g(T) \qquad (28)$$

The values thus computed are sensitive to errors in the enthalpy formulation, and hence these results are listed in a separate table on a provisional basis (discussed under "Transport Properties" which follows).

The general thermodynamic approach presented here is tentative; it is based on the best experimental data available. However, if more high-quality experimental data were available, a different approach might be selected. That is, precise P–V–T measurements to temperatures well below 1700°F might lead to the choice of true gas-base calculations, rather than the hybrid approach taken. On the other hand, extension of the precision saturated-liquid specific-heat measurements to temperatures well above 1600°F would probably strengthen the choice of true liquid-base calculations.

Transport Properties

The thermal conductivity and viscosity of both the saturated liquid and vapor phases have been reviewed. For the range 210 to 2500°F, Table 6 summarizes the recommended values for the transport properties; Table 6 also lists liquid-phase Prandtl number (Pr), thermal diffusivity (α), specific heat at constant pressure (c_p), electrical resistivity (ρ_e), and surface tension (σ). Table 7 contains provisional values of specific heat, Prandtl number, and thermal diffusivity for the saturated equilibrium vapor; there are relatively large discrepancies in the supporting data for Table 7.

LIQUID THERMAL CONDUCTIVITY

Nine different reviews and experiments (Fig. 6) were analyzed to determine the best relation for the thermal conductivity (Refs. 4, 5, 14, and 27 to 32). In several instances thermal-diffusivity values were actually measured;[29,32] they were converted to thermal-conductivity values using the specific-heat data of Ginnings.[23] We recommend Ginnings specific-heat relation, which, in engineering units, is

$$c_p[\text{Btu/(lb)(°F)}] = 0.389352 - 1.10599 \times 10^{-4} T + 3.41178 \times 10^{-8} T^2 \qquad (29)$$

where T is in °R.

The analysis of these different reviews showed that the relation

$$k[\text{watts/(cm)(°C)}] = 0.916 - 0.49 \times 10^{-3} t(\text{°C}) \qquad (30)$$

of Evangelisti and Isacchini[27,28] (Fig. 6) was in good agreement with other data from the melting point to 1200°F. Values greater than 1200°F were computed from the Wiedeman–Franz–Lorenz law using a fitted Lorenz value of 2.34×10^{-8} volts^2/°K^2 and recommended electrical-resistivity values taken from Eq. 35. A single relation representing the thermal conductivity over the entire range from the melting point to 2500°F resulted from a smooth least-squares fit that was obtained with the use of values of the two proposed relations evaluated at 100°F temperature intervals from 200 to 2500°F. The result is given by

$$k = 54.306 - 1.878 \times 10^{-2} t + 2.0914 \times 10^{-6} t^2 \qquad (31)$$

where k and t are in Btu/(hr)(ft)(°F) and °F.

Table 4 FORTRAN SUBROUTINE FOR P–V–T AND THERMODYNAMIC PROPERTIES OF SODIUM

```
      SUBROUTINE NAPROP(TEMPR,PATM)
      T=TEMPR
C     CALCULATION OF SATURATION PROPERTIES
  100 IF(T-2059.7)110,110,112
  110 PSAT=(3.03266E6/T**.5)*(EXPF(-2.30733E4/T))                    ATM
  111 GO TO 120
  112 PSAT=(6.8817602E6/(T**.61344))*EXPF(-22981.96/T)               ATM
  113 GO TO 120
  120 HLS=.389352*T-.5529955E-4*(T)**2+.113726E-7*(T)**3-29.02       BTU/LB
  130 SLS=.389344*(LOGF(T))-1.10557E-4*T+.170408E-7*(T**2)-1.792026  BTU/LBR
  140 DL=59.566-7.9504E-3*(T-459.7)-.2872E-6*((T-459.7)**2)+.06035E-9*  LB/FT3
     1((T-459.7)**3)
  150 TWO=EXPF(-9.95845+(16588.3/T))                                 ATM-1
  160 FOUR=EXPF(-24.59115+(37589.7/T))                               ATM-3
  170 U=PSAT*TWO
  180 W=((PSAT)**3)*FOUR
  190 X1=0.8
  200 X1P=X1
  203 X1=X1-(W*(X1)**4+U*(X1)**2+X1-1.)/(4.*W*(X1)**3+2.*U*X1+1.)
  205 IF(ABSF(X1-X1P)/X1-1.E-6)210,210,200
  210 X2=U*(X1)**2
  212 X4=1.-X1-X2
  214 ABAR=22.991*(X1+2.*X2+4.*X4)
  216 VSAT=(.730229*T)/(ABAR*PSAT)                                   FT3/LB
  217 Z=22.991/ABAR
  218 DHF1=25980.7-2.21312*T+7.06278E-4*(T)**2-1.4526E-7*(T)**3      CAL/MNA1
  220 DHF2=2.*DHF1-18304.                                            CAL/MNA2
  222 DHF4=4.*DHF1-41478.                                            CAL/MNA4
  224 DHV=1.8*(X1*DHF1+X2*DHF2+X4*DHF4)/ABAR                         BTU/LB
  226 HGS=HLS+DHV
  228 SGS=SLS+(DHV/T)
C     TEST FOR STATE, I.E., SUBCOOLED, SATURATED, SUPERHEATED
  250 IF(ABSF(PATM-PSAT)/PATM-1.E-4)463,463,260
  260 IF(PATM-PSAT)270,463,410
C     CALCULATION OF SUPERHEATED VAPOR PROPERTIES
  270 UH=PATM*TWO
  272 WH=((PATM)**3)*FOUR
  275 X1H=0.8                                                        MOLEFRX1
  278 X1PH=X1H
  280 X1H=X1H-(WH*(X1H)**4+UH*(X1H)**2+X1H-1.)/(4.*WH*(X1H)**3+2.*UH*
     1X1H+1.)
  282 IF(ABSF(X1H-X1PH)/X1H-1.E-6)284,284,278
  284 X2H=UH*(X1H)**2                                                MOLEFRX2
  286 X4H=1.-X1H-X2H                                                 MOLEFRX4
  288 ABARH=22.991*(X1H+2.*X2H+4.*X4H)
  290 VH=(.730229*T)/(ABARH*PATM)                                    FT3/LB
  292 ZH=22.991/ABARH
  294 BD=X1+2.*X2+4.*X4
  296 B2=2.*X2/BD                                                    WTFRX2S
  297 B4=4.*X4/BD                                                    WTFRX4S
  298 BDH=X1H+2.*X2H+4.*X4H
  300 B2H=2.*X2H/BDH                                                 WTFRX2H
  301 B4H=4.*X4H/BDH                                                 WTFRX4H
  303 HGI=HGS+B2*716.54+B4*811.85
  305 HGH=HGI-B2H*716.54-B4H*811.85
  308 SGI=SGS+B2*716.54/T+B4*811.85/T+(1.987180/ABAR)*LOGF(PSAT)-(B2/
     1 45.982)*(-19.78923+(32963.9/T))-(B4/91.964)*(-48.86704+(74697.5/
     2T))+(1.987180/ABAR)*(X1*LOGF(X1)+X2*LOGF(X2)+X4*LOGF(X4))
  310 SGH=SGI-B2H*716.54/T-B4H*811.85/T-(1.987180/ABARH)*LOGF(PATM)+(
     1B2H/45.982)*(-19.78923+(32963.9/T))+(B4H/91.964)*(-48.86704+(746
     2 97.5/T))-(1.987180/ABARH)*(X1H*LOGF(X1H)+X2H*LOGF(X2H)+X4H*LOGF(
     3X4H))
      PRINT 350
  350 FORMAT(3X,4HTEMP,7X,4HPRES,10X,2HVH,9X,2HZH,7X,3HHGI,8X,3HHGH,7X,3
     1HSGI,9X,3HSGH,5X,5HABARH,8X,3HX2H,9X,3HX4H)
      PRINT 351
  351 FORMAT(2X,5HDEG-F,7X,3HATM,8X,6HFT3/LB,16X,6HBTU/LB,4X,6HBTU/LB,4X
     1,7HBTU/LBF,5X,7HBTU/LBF,15X,6HMOL FR,6X,6HMOL FR)
  360 PRINT 370,T,PATM,VH,ZH,HGI,HGH,SGI,SGH,ABARH,X2H,X4H
  370 FORMAT(/,1X,F7.1,2(2X,E11.4),2X,F8.5,2(2X,F8.2),2X,F8.5,4X,F8.5,2X
     1,F7.3,2(4X,F8.6))
      GO TO 80
C     CALCULATION OF SUBCOOLED LIQUID PROPERTIES
  410 DLP=-7.9504E-3-.5744E-6*(T-459.7)+.18105E-9*(T-459.7)**2
      HLC=HLS+(1./DL)*(1.+(T/DL)*DLP)*(PATM-PSAT)*2.721308
      SLC=SLS+2.721308*(1./(DL**2))*DLP*(PATM-PSAT)
      PRINT 415
  415 FORMAT(8X,4HTEMP,10X,4HPRES,11X,3HHLC,10X,3HSLC,/,8X,5HDEG-F,9X,3H
     1ATM,10X,6HBTU/LB,7X,7HBTU/LBF)
  420 PRINT 450,T,PATM,HLC,SLC
  450 FORMAT(/,6X,F7.1,5X,E11.4,5X,F8.2,5X,F8.5)
      GO TO 80
C      OUTPUT SATURATION PROPERTIES
  463 T=T-459.7
      PRINT 10
   10 FORMAT(1H1,2X,5HTEMPF,6X,4HPSAT,7X,4HVSAT,8X,1HZ,7X,2HDL,6X,3HHLS,
     16X,3HDHV,6X,3HHGS,6X,3HSLS,6X,3HSGS,5X,4HABAR,5X,2HX2,7X,2HX4)
      PRINT 11
   11 FORMAT(2X,5HDEG-F,6X,3HATM,7X,6HFT3/LB,13X,6HLB/FT3,3X,6HBTU/LB,3X
     1,6HBTU/LB,3X,6HBTU/LB,2X,7HBTU/LBF,2X,7HBTU/LBF,10X,6HMOL FR,3X,6H
     2MOL FR)
      PRINT 470,T,PSAT,VSAT,Z,DL,HLS,DHV,HGS,SLS,SGS,ABAR,X2,X4
  470 FORMAT(/,F7.1,1X,E11.5,1X,E11.5,2X,F7.5,1X,F7.3,2X,F7.2,1X,F8.2,1X
     1,F8.2,1X,F8.5,1X,F8.5,1X,F7.3,1X,F8.6,2X,F7.6)
   80 RETURN
   51 END
```

Table 5 SATURATION P–V–T AND THERMODYNAMIC PROPERTIES OF SODIUM

Temp., °F	Saturation vapor pressure, atm	Specific volume, sat. vapor, cu ft/lb_m	Compressibility factor, sat. vapor	Density, liquid, lb_m/cu ft	Enthalpy of sat. liquid, Btu/lb_m	Heat of vaporization, Btu/lb_m	Enthalpy of sat. vapor, Btu/lb_m	Entropy of sat. liquid, Btu/(lb_m)(°F)	Entropy of sat. vapor, Btu/(lb_m)(°F)	Molecular wt. of vapor, av.	Dimer, mole fraction	Tetramer, mole fraction
500.0	3.54292 – 6*	8.55792 + 6*	0.99470	55.527	303.76	1901.06	2204.83	0.79105	2.77194	23.113	0.005328	0.000000
530.0	7.23067 – 6	4.31961 + 6	0.99362	55.281	313.18	1896.57	2209.75	0.80071	2.71702	23.139	0.006425	0.000000
560.0	1.41440 – 5	2.27242 + 6	0.99240	55.034	322.56	1891.94	2214.50	0.81005	2.66543	23.167	0.007656	0.000000
590.0	2.66151 – 5	1.24147 + 6	0.99106	54.788	331.90	1887.14	2219.05	0.81908	2.61687	23.199	0.009025	0.000000
620.0	4.83342 – 5	7.02100 + 5	0.98958	54.541	341.21	1882.20	2223.41	0.82782	2.57108	23.233	0.010533	0.000000
650.0	8.49585 – 5	4.09866 + 5	0.98797	54.293	350.49	1877.10	2227.58	0.83629	2.52783	23.271	0.012181	0.000000
680.0	1.44913 – 4	2.46354 + 5	0.98622	54.046	359.73	1871.84	2231.57	0.84451	2.48691	23.312	0.013968	0.000000
710.0	2.40419 – 4	1.52111 + 5	0.98436	53.798	368.94	1866.43	2235.38	0.85249	2.44814	23.356	0.015892	0.000000
740.0	3.88771 – 4	9.62839 + 4	0.98237	53.550	378.13	1860.88	2239.01	0.86025	2.41137	23.404	0.017950	0.000000
770.0	6.13906 – 4	6.23647 + 4	0.98026	53.301	387.29	1855.18	2242.47	0.86779	2.37643	23.454	0.020139	0.000000
800.0	9.48273 – 4	4.12658 + 4	0.97804	53.053	396.43	1849.34	2245.77	0.87513	2.34321	23.507	0.022454	0.000000
830.0	1.43503 – 3	2.78517 + 4	0.97571	52.804	405.54	1843.38	2248.92	0.88228	2.31159	23.563	0.024890	0.000000
860.0	2.13055 – 3	1.91482 + 4	0.97329	52.555	414.64	1837.30	2251.93	0.88925	2.28146	23.622	0.027441	0.000000
890.0	3.10730 – 3	1.33929 + 4	0.97078	52.305	423.71	1831.10	2254.81	0.89605	2.25272	23.683	0.030100	0.000001
920.0	4.45701 – 3	9.51917 + 3	0.96818	52.056	432.77	1824.80	2257.57	0.90269	2.22529	23.747	0.032862	0.000001
950.0	6.29411 – 3	6.86830 + 3	0.96551	51.806	441.81	1818.41	2260.23	0.90917	2.19910	23.812	0.035719	0.000002
980.0	8.75957 – 3	5.02588 + 3	0.96277	51.556	450.85	1811.94	2262.78	0.91551	2.17406	23.880	0.038663	0.000003
1010.0	1.20248 – 2	3.72657 + 3	0.95997	51.305	459.87	1805.39	2265.26	0.92171	2.15012	23.950	0.041688	0.000004
1040.0	1.62960 – 2	2.79763 + 3	0.95712	51.055	468.88	1798.78	2267.65	0.92778	2.12720	24.021	0.044786	0.000006
1070.0	2.18182 – 2	2.12489 + 3	0.95422	50.804	477.88	1792.11	2269.99	0.93372	2.10526	24.094	0.047950	0.000008
1100.0	2.88803 – 2	1.63174 + 3	0.95129	50.553	486.88	1785.39	2272.27	0.93955	2.08425	24.168	0.051172	0.000012
1130.0	3.78189 – 2	1.26608 + 3	0.94832	50.302	495.87	1778.63	2274.50	0.94526	2.06410	24.244	0.054446	0.000017
1160.0	4.90231 – 2	9.92012 + 2	0.94533	50.051	504.86	1771.84	2276.70	0.95086	2.04479	24.321	0.057765	0.000023
1190.0	6.29393 – 2	7.84477 + 2	0.94231	49.800	513.85	1765.02	2278.88	0.95636	2.02627	24.398	0.061121	0.000032
1220.0	8.00748 – 2	6.25800 + 2	0.93929	49.549	522.85	1758.18	2281.03	0.96176	2.00849	24.477	0.064509	0.000043
1250.0	1.01002 – 1	5.03362 + 2	0.93625	49.297	531.85	1751.32	2283.17	0.96707	1.99142	24.557	0.067922	0.000057
1280.0	1.26364 – 1	4.08062 + 2	0.93320	49.046	540.85	1744.46	2285.30	0.97229	1.97502	24.637	0.071354	0.000076
1310.0	1.56875 – 1	3.33272 + 2	0.93015	48.794	549.86	1737.58	2287.44	0.97742	1.95927	24.718	0.074799	0.000099
1340.0	1.93327 – 1	2.74116 + 2	0.92710	48.542	558.88	1730.69	2289.57	0.98248	1.94413	24.799	0.078253	0.000128
1370.0	2.36589 – 1	2.26975 + 2	0.92404	48.290	567.91	1723.80	2291.71	0.98745	1.92958	24.881	0.081709	0.000164
1400.0	2.87614 – 1	1.89142 + 2	0.92099	48.038	576.95	1716.91	2293.86	0.99235	1.91557	24.963	0.085163	0.000209
1430.0	3.47438 – 1	1.58573 + 2	0.91794	47.786	586.01	1710.01	2296.02	0.99719	1.90210	25.046	0.088611	0.000263
1460.0	4.17182 – 1	1.33714 + 2	0.91488	47.534	595.08	1703.11	2298.19	1.00195	1.88912	25.130	0.092048	0.000329
1490.0	4.98054 – 1	1.13373 + 2	0.91183	47.282	604.18	1696.20	2300.37	1.00665	1.87663	25.214	0.095470	0.000407
1520.0	5.91350 – 1	9.66307 + 1	0.90878	47.030	613.29	1689.28	2302.57	1.01128	1.86459	25.299	0.098872	0.000501

1550.0	6.98453 − 1	8.27734 + 1	0.90572	46.778	622.42	1682.35	2304.78	1.01586	1.85298	25.384	0.102252	0.000613
1580.0	8.20835 − 1	7.12420 + 1	0.90266	46.525	631.58	1675.41	2306.99	1.02039	1.84179	25.470	0.105605	0.000743
1610.0	9.57593 − 1	6.17683 + 1	0.89978	46.273	640.77	1668.72	2309.49	1.02485	1.83112	25.552	0.108706	0.000891
1640.0	1.11237 + 0	5.37706 + 1	0.89688	46.021	649.98	1661.99	2311.97	1.02927	1.82081	25.634	0.111791	0.001061
1670.0	1.28656 + 0	4.70016 + 1	0.89397	45.769	659.22	1655.24	2314.46	1.03364	1.81086	25.718	0.114835	0.001258
1700.0	1.48184 + 0	4.12467 + 1	0.89104	45.517	668.49	1648.46	2316.95	1.03796	1.80124	25.802	0.117838	0.001482
1730.0	1.69998 + 0	3.63330 + 1	0.88809	45.265	677.80	1641.65	2319.44	1.04224	1.79195	25.888	0.120795	0.001737
1760.0	1.94278 + 0	3.21201 + 1	0.88513	45.013	687.14	1634.80	2321.93	1.04648	1.78297	25.975	0.123706	0.002026
1790.0	2.21212 + 0	2.84937 + 1	0.88213	44.761	696.52	1627.90	2324.42	1.05067	1.77428	26.063	0.126567	0.002352
1820.0	2.50993 + 0	2.53603 + 1	0.87910	44.509	705.93	1620.96	2326.89	1.05483	1.76587	26.153	0.129378	0.002717
1850.0	2.83822 + 0	2.26428 + 1	0.87603	44.257	715.39	1613.95	2329.34	1.05895	1.75772	26.245	0.132137	0.003125
1880.0	3.19902 + 0	2.02777 + 1	0.87292	44.005	724.89	1606.89	2331.77	1.06303	1.74982	26.338	0.134841	0.003579
1910.0	3.59441 + 0	1.82124 + 1	0.86976	43.754	734.43	1599.75	2334.18	1.06708	1.74217	26.434	0.137490	0.004083
1940.0	4.02654 + 0	1.64030 + 1	0.86655	43.502	744.02	1592.54	2336.55	1.07110	1.73474	26.532	0.140081	0.004638
1970.0	4.49756 + 0	1.48127 + 1	0.86329	43.251	753.65	1585.24	2338.90	1.07509	1.72754	26.632	0.142612	0.005249
2000.0	5.00968 + 0	1.34108 + 1	0.85996	42.999	763.34	1577.86	2341.20	1.07905	1.72054	26.735	0.145084	0.005919
2030.0	5.56513 + 0	1.21713 + 1	0.85657	42.748	773.08	1570.38	2343.46	1.08299	1.71374	26.841	0.147494	0.006650
2060.0	6.16616 + 0	1.10724 + 1	0.85311	42.497	782.87	1562.80	2345.67	1.08690	1.70713	26.950	0.149840	0.007446
2090.0	6.81505 + 0	1.00955 + 1	0.84958	42.246	792.72	1555.12	2347.84	1.09078	1.70070	27.062	0.152122	0.008309
2120.0	7.51408 + 0	9.22471 + 0	0.84598	41.995	802.62	1547.33	2349.95	1.09464	1.69445	27.177	0.154339	0.009242
2150.0	8.26556 + 0	8.44662 + 0	0.84229	41.745	812.58	1539.43	2352.01	1.09848	1.68836	27.296	0.156490	0.010248
2180.0	9.07179 + 0	7.74965 + 0	0.83853	41.494	822.61	1531.41	2354.02	1.10229	1.68244	27.418	0.158573	0.011329
2210.0	9.93508 + 0	7.12389 + 0	0.83469	41.244	832.69	1523.27	2355.96	1.10609	1.67667	27.544	0.160587	0.012488
2240.0	1.08577 + 1	6.56078 + 0	0.83076	40.994	842.84	1515.01	2357.85	1.10987	1.67105	27.675	0.162533	0.013726
2270.0	1.18420 + 1	6.05297 + 0	0.82676	40.745	853.06	1506.62	2359.68	1.11363	1.66557	27.809	0.164409	0.015045
2300.0	1.28903 + 1	5.59405 + 0	0.82267	40.495	863.34	1498.11	2361.45	1.11738	1.66023	27.947	0.166215	0.016447
2330.0	1.40047 + 1	5.17848 + 0	0.81850	40.246	873.70	1489.47	2363.16	1.12111	1.65502	28.089	0.167950	0.017933
2360.0	1.51877 + 1	4.80143 + 0	0.81425	39.997	884.12	1480.70	2364.82	1.12482	1.64995	28.236	0.169614	0.019504
2390.0	1.64413 + 1	4.45869 + 0	0.80992	39.748	894.62	1471.80	2366.42	1.12852	1.64500	28.387	0.171207	0.021161
2420.0	1.77678 + 1	4.14658 + 0	0.80552	39.499	905.20	1462.77	2367.97	1.13221	1.64017	28.542	0.172728	0.022904
2450.0	1.91693 + 1	3.86185 + 0	0.80104	39.251	915.85	1453.62	2369.47	1.13589	1.63547	28.701	0.174179	0.024733
2480.0	2.06481 + 1	3.60168 + 0	0.79649	39.003	926.58	1444.34	2370.92	1.13956	1.63088	28.865	0.175558	0.026649
2510.0	2.22062 + 1	3.36355 + 0	0.79188	38.755	937.40	1434.93	2372.33	1.14322	1.62641	29.034	0.176867	0.028651

*Power of 10; i.e., 3.54292×10^{-6}, and 8.55792×10^{6}.

Table 6 TRANSPORT AND RELATED PROPERTIES OF SODIUM

Temp., °F	Viscosity, $lb_m/(ft)(hr)$		Thermal conductivity, Btu/(hr)(ft)(°F)		Specific heat, liquid, $Btu/(lb_m)(°F)$	Prandtl number, liquid	Thermal diffusivity, liquid, sq ft/hr	Surface tension, lb_f/ft	Electric resistivity, μohm-cm
	Liquid	Vapor	Liquid	Vapor					
210.0	1.6657	0.03598	50.45	0.006285	0.3305	0.010914	2.636	0.013489	9.67
240.0	1.5374	0.03623	49.91	0.007347	0.3286	0.010122	2.634	0.013375	10.29
270.0	1.4272	0.03647	49.38	0.008391	0.3268	0.009444	2.632	0.013261	10.91
300.0	1.3316	0.03672	48.86	0.009419	0.3250	0.008858	2.630	0.013147	11.53
330.0	1.2480	0.03696	48.33	0.010429	0.3232	0.008347	2.627	0.013032	12.17
360.0	1.1745	0.03721	47.81	0.011421	0.3216	0.007899	2.623	0.012918	12.81
390.0	1.1093	0.03745	47.29	0.012396	0.3200	0.007505	2.619	0.012804	13.46
420.0	1.0512	0.03770	46.78	0.013353	0.3184	0.007155	2.615	0.012689	14.12
450.0	0.9991	0.03794	46.27	0.014293	0.3169	0.006843	2.610	0.012575	14.79
480.0	0.9522	0.03819	45.77	0.015216	0.3155	0.006564	2.604	0.012461	15.47
510.0	0.9098	0.03843	45.27	0.016121	0.3141	0.006314	2.598	0.012346	16.16
540.0	0.8712	0.03868	44.77	0.017009	0.3128	0.006088	2.592	0.012232	16.85
570.0	0.8360	0.03893	44.28	0.017879	0.3116	0.005884	2.585	0.012118	17.56
600.0	0.8038	0.03917	43.79	0.018732	0.3104	0.005699	2.578	0.012004	18.29
630.0	0.7742	0.03942	43.30	0.019567	0.3093	0.005531	2.570	0.011889	19.02
660.0	0.7470	0.03966	42.82	0.020385	0.3082	0.005377	2.562	0.011775	19.76
690.0	0.7218	0.03991	42.34	0.021185	0.3072	0.005238	2.553	0.011661	20.52
720.0	0.6984	0.04015	41.86	0.021968	0.3063	0.005110	2.544	0.011546	21.29
750.0	0.6767	0.04040	41.39	0.022733	0.3054	0.004993	2.534	0.011432	22.08
780.0	0.6564	0.04064	40.93	0.023481	0.3046	0.004886	2.524	0.011318	22.88
810.0	0.6375	0.04089	40.46	0.024212	0.3039	0.004788	2.513	0.011203	23.69
840.0	0.6198	0.04113	40.00	0.024925	0.3032	0.004698	2.502	0.011089	24.52
870.0	0.6033	0.04138	39.55	0.025621	0.3026	0.004616	2.490	0.010975	25.37
900.0	0.5877	0.04162	39.09	0.026299	0.3020	0.004540	2.478	0.010861	26.23
930.0	0.5730	0.04187	38.64	0.026960	0.3015	0.004471	2.466	0.010746	27.11
960.0	0.5592	0.04211	38.20	0.027603	0.3011	0.004407	2.453	0.010632	28.00
990.0	0.5461	0.04236	37.76	0.028229	0.3007	0.004349	2.439	0.010518	28.91
1020.0	0.5338	0.04260	37.32	0.028837	0.3003	0.004296	2.425	0.010403	29.84
1050.0	0.5221	0.04285	36.89	0.029428	0.3001	0.004247	2.411	0.010289	30.79
1080.0	0.5110	0.04310	36.46	0.030002	0.2999	0.004203	2.396	0.010175	31.76
1110.0	0.5004	0.04334	36.03	0.030558	0.2998	0.004163	2.381	0.010060	32.75
1140.0	0.4904	0.04359	35.61	0.031096	0.2997	0.004127	2.366	0.009946	33.75
1170.0	0.4808	0.04383	35.19	0.031617	0.2997	0.004095	2.350	0.009832	34.78
1200.0	0.4717	0.04408	34.78	0.032121	0.2997	0.004066	2.333	0.009718	35.83
1230.0	0.4630	0.04432	34.37	0.032607	0.2998	0.004040	2.317	0.009603	36.90
1260.0	0.4547	0.04457	33.96	0.033076	0.3000	0.004017	2.300	0.009489	37.99
1290.0	0.4468	0.04481	33.56	0.033527	0.3002	0.003998	2.282	0.009375	39.10
1320.0	0.4392	0.04506	33.16	0.033961	0.3005	0.003981	2.264	0.009260	40.24
1350.0	0.4319	0.04530	32.76	0.034377	0.3009	0.003967	2.246	0.009146	41.40
1380.0	0.4249	0.04555	32.37	0.034776	0.3013	0.003955	2.228	0.009032	42.58
1410.0	0.4181	0.04579	31.98	0.035158	0.3018	0.003946	2.209	0.008917	43.78
1440.0	0.4117	0.04604	31.59	0.035522	0.3023	0.003939	2.190	0.008803	45.01
1470.0	0.4055	0.04628	31.21	0.035868	0.3029	0.003935	2.171	0.008689	46.27
1500.0	0.3995	0.04653	30.84	0.036197	0.3036	0.003933	2.152	0.008575	47.55
1530.0	0.3937	0.04677	30.46	0.036509	0.3043	0.003933	2.132	0.008460	48.86
1560.0	0.3882	0.04702	30.09	0.036803	0.3051	0.003935	2.112	0.008346	50.19
1590.0	0.3828	0.04726	29.73	0.037080	0.3059	0.003940	2.092	0.008232	51.55
1620.0	0.3777	0.04751	29.37	0.037339	0.3069	0.003946	2.071	0.008117	52.94
1650.0	0.3727	0.04776	29.01	0.037581	0.3078	0.003955	2.051	0.008003	54.35
1680.0	0.3678	0.04800	28.65	0.037805	0.3089	0.003965	2.030	0.007889	55.79
1710.0	0.3632	0.04825	28.30	0.038012	0.3099	0.003977	2.009	0.007774	57.26
1740.0	0.3587	0.04849	27.96	0.038202	0.3111	0.003991	1.988	0.007660	58.76
1770.0	0.3543	0.04874	27.61	0.038374	0.3123	0.004007	1.967	0.007546	60.29
1800.0	0.3501	0.04898	27.27	0.038528	0.3136	0.004025	1.946	0.007432	61.85
1830.0	0.3459	0.04923	26.94	0.038665	0.3149	0.004044	1.925	0.007317	63.44
1860.0	0.3420	0.04947	26.61	0.038785	0.3163	0.004066	1.904	0.007203	65.06
1890.0	0.3381	0.04972	26.28	0.038887	0.3178	0.004089	1.882	0.007089	66.72
1920.0	0.3343	0.04996	25.95	0.038972	0.3193	0.004114	1.861	0.006974	68.40
1950.0	0.3307	0.05021	25.63	0.039039	0.3209	0.004140	1.839	0.006860	70.12
1980.0	0.3272	0.05045	25.32	0.039089	0.3225	0.004168	1.818	0.006746	71.87
2010.0	0.3237	0.05070	25.00	0.039121	0.3243	0.004198	1.796	0.006631	73.65
2040.0	0.3204	0.05094	24.69	0.039136	0.3260	0.004230	1.775	0.006517	75.47
2070.0	0.3171	0.05119	24.39	0.039134	0.3279	0.004263	1.753	0.006403	77.32
2100.0	0.3139	0.05143	24.09	0.039114	0.3297	0.004298	1.732	0.006289	79.20
2130.0	0.3109	0.05168	23.79	0.039076	0.3317	0.004335	1.711	0.006174	81.12
2160.0	0.3079	0.05193	23.49	0.039021	0.3337	0.004373	1.689	0.006060	83.08
2190.0	0.3049	0.05217	23.20	0.038949	0.3358	0.004413	1.668	0.005946	85.07
2220.0	0.3021	0.05242	22.92	0.038859	0.3379	0.004454	1.647	0.005831	87.10
2250.0	0.2993	0.05266	22.63	0.038752	0.3401	0.004497	1.626	0.005717	89.17
2280.0	0.2966	0.05291	22.35	0.038627	0.3424	0.004542	1.605	0.005603	91.27
2310.0	0.2939	0.05315	22.08	0.038485	0.3447	0.004589	1.585	0.005488	93.41
2340.0	0.2913	0.05340	21.81	0.038325	0.3471	0.004637	1.564	0.005374	95.59
2370.0	0.2888	0.05364	21.54	0.038148	0.3495	0.004686	1.544	0.005260	97.81
2400.0	0.2863	0.05389	21.28	0.037954	0.3520	0.004738	1.523	0.005146	100.06
2430.0	0.2839	0.05413	21.02	0.037742	0.3546	0.004791	1.503	0.005031	102.36
2460.0	0.2816	0.05438	20.76	0.037512	0.3572	0.004845	1.483	0.004917	104.70
2490.0	0.2793	0.05462	20.51	0.037265	0.3599	0.004901	1.463	0.004803	107.08

Table 7 PROVISIONAL VALUES FOR SPECIFIC HEAT, PRANDTL NUMBER, AND THERMAL DIFFUSIVITY OF SATURATED SODIUM VAPOR

Temp., °F	Specific heat, Btu/(lb$_m$)(°F)	Prandtl number	Thermal diffusivity, sq ft/hr
500.0	0.349	0.846	0.387E 06
530.0	0.366	0.846	0.196E 06
560.0	0.384	0.848	0.104E 06
590.0	0.402	0.852	0.569E 05
620.0	0.420	0.857	0.322E 05
650.0	0.438	0.862	0.188E 05
680.0	0.456	0.868	0.112E 05
710.0	0.473	0.874	0.697E 04
740.0	0.490	0.879	0.441E 04
770.0	0.506	0.884	0.286E 04
800.0	0.522	0.888	0.189E 04
830.0	0.536	0.892	0.128E 04
860.0	0.550	0.895	0.883E 03
890.0	0.563	0.897	0.620E 03
920.0	0.574	0.898	0.442E 03
950.0	0.585	0.898	0.321E 03
980.0	0.595	0.897	0.236E 03
1010.0	0.603	0.896	0.176E 03
1040.0	0.611	0.894	0.133E 03
1070.0	0.618	0.891	0.102E 03
1100.0	0.623	0.888	0.794E 02
1130.0	0.628	0.884	0.622E 02
1160.0	0.632	0.879	0.493E 02
1190.0	0.635	0.874	0.394E 02
1220.0	0.637	0.869	0.318E 02
1250.0	0.639	0.863	0.259E 02
1280.0	0.640	0.858	0.212E 02
1310.0	0.640	0.852	0.175E 02
1340.0	0.640	0.845	0.146E 02
1370.0	0.639	0.839	0.122E 02
1400.0	0.638	0.833	0.103E 02
1430.0	0.637	0.827	0.880E 01
1460.0	0.635	0.821	0.752E 01
1490.0	0.633	0.815	0.645E 01
1520.0	0.631	0.809	0.557E 01
1550.0	0.628	0.804	0.483E 01
1580.0	0.626	0.798	0.420E 01
1610.0	0.623	0.793	0.369E 01
1640.0	0.619	0.788	0.325E 01
1670.0	0.616	0.783	0.287E 01
1700.0	0.613	0.779	0.255E 01
1730.0	0.610	0.775	0.226E 01
1760.0	0.607	0.771	0.202E 01
1790.0	0.604	0.768	0.181E 01
1820.0	0.601	0.766	0.162E 01
1850.0	0.599	0.763	0.146E 01
1880.0	0.596	0.762	0.132E 01
1910.0	0.594	0.761	0.119E 01
1940.0	0.591	0.760	0.108E 01
1970.0	0.589	0.760	0.981E 00
2000.0	0.587	0.760	0.892E 00
2030.0	0.585	0.761	0.813E 00
2060.0	0.583	0.762	0.742E 00
2090.0	0.581	0.763	0.678E 00
2120.0	0.580	0.765	0.621E 00
2150.0	0.578	0.768	0.569E 00
2180.0	0.577	0.771	0.523E 00
2210.0	0.575	0.774	0.481E 00
2240.0	0.574	0.778	0.443E 00
2270.0	0.572	0.782	0.408E 00
2300.0	0.571	0.786	0.377E 00
2330.0	0.569	0.791	0.348E 00
2360.0	0.568	0.796	0.322E 00
2390.0	0.566	0.801	0.299E 00
2420.0	0.564	0.807	0.277E 00
2450.0	0.563	0.813	0.257E 00
2480.0	0.561	0.819	0.239E 00

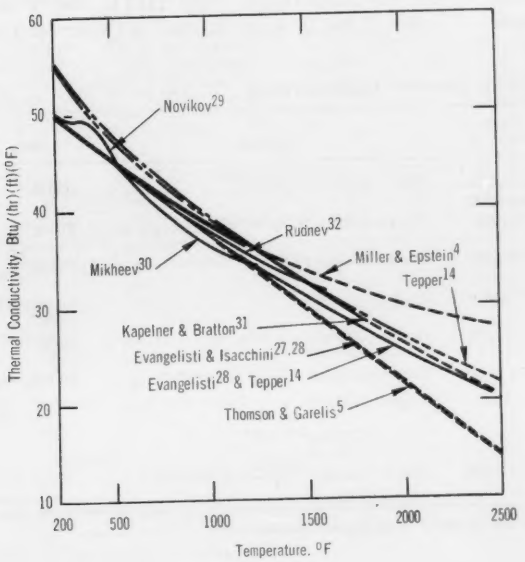

Fig. 6 Comparison of analyses for the thermal conductivity of liquid sodium. Dashed lines are extrapolated or calculated values. Recommended curve of Evangelisti and Isacchini[27,28] includes a high-temperature portion computed from the Wiedeman–Franz–Lorenz law.

VAPOR THERMAL CONDUCTIVITY

To our knowledge the only experimental thermal-conductivity values published for sodium vapor are those of Stefanov.[33] The measurements were made with a dilatometer described by Timrot and Totskii.[34]

A number of experimental and theoretical studies have been conducted (Refs. 7, 8, 35, and 36) or are under way[37–40] to determine vapor conductivity. Figure 7 shows the results reported. There is little

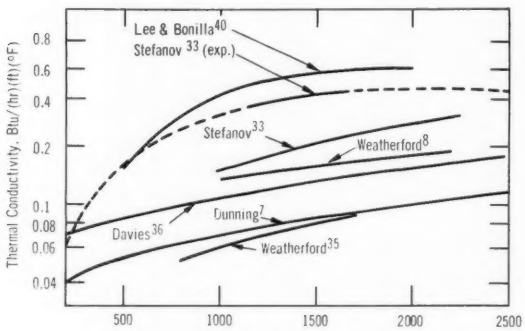

Fig. 7 Curves of thermal conductivity of sodium vapor show little agreement. Data of Stefanov[33] are arbitrarily recommended until the work of Lee[40] becomes available.

agreement among most of the sources; in fact, the predictions of Lee and Bonilla[40] and the experimental results of Stefanov[33] disagree as much as 25%. However, together their results are the best information available. Arbitrarily we recommend the data of Stefanov, at least until the Lee[40] results become available. A second-degree polynomial fit was made of the conductivity values given in Ref. 33 to obtain values for Tables 6 and 7. The result of this fit is

$$k = 0.1639 \times 10^{-2} + 0.3977 \times 10^{-4} t - 0.9697 \times 10^{-8} t^2 \quad (32)$$

where k and t are in Btu/(hr)(ft)(°F) and °F.

LIQUID VISCOSITY

The viscosity of liquid sodium has been measured from the melting point to 1920°F by the investigators shown in Table 8. The methods used to measure the viscosity, the equation, and references are also listed in Table 8.

Several viscosity compilations have appeared in literature, and some are listed in Table V.3 of Ref. 1. The correlations of these data show reasonably good agreement between 212 and 1650°F. Above 1830°F the deviations become larger.

To obtain a relation for the liquid viscosity over the range from melting point to 2500°F required that a smooth curve be drawn through a plot of all data points. The best fit to the curve is given by

$$\log \eta = 1.0203 + \frac{397.17}{T} - 0.4925 \log T \quad (33)$$

where η and T are given in $lb_m/(hr)(ft)$ and °R. A plot of Eq. 33 is shown in Fig. 8; calculated values are given in Table 6.

VAPOR VISCOSITY

Stefanov[33] reported smoothed experimental results for the temperature range 1263 to 1598°F and pressures 0.055 to 0.398 kg/cm². A linear least-squares

Table 8 LIQUID-SODIUM VISCOSITY INVESTIGATIONS

Investigators	Method	Temp. range, °F	Equation	Refs.
Chiong[77]	Oscillating sphere	208 to 672	*$\eta v^{1/3} = 1.183 \times 10^{-3} e^{716.5/vT}$	Hagen[78]
Godfrey[79]	Oscillating sphere	620 to 1612	†	
Ewing[80]	Modified Ostwald glass viscometer	218 to 379	*$\eta v^{1/3} = 1.089 \times 10^{-3} e^{756.9/vT}$	Ewing[15]
Ewing[81]	Nickel viscometer (Ostwald type)	289 to 1267	*$\eta v^{1/3} = 1.142 \times 10^{-3} e^{739.8/vT}$	Ewing[15]
Novikov[82,83]	Oscillating cylindrical capsule	212 to 1470	†	Shvidkovsky[84] Stone[12]
Shpilrain[24]	Oscillating cylinder	320 to 1470	*$\log \eta = -1.6814 - 0.4296 \log T + 234.65/T$	Goltsova[13]
Achener[85]	Oscillating cylinder	208 to 1920	‡$\log \eta = 3.25538 - \frac{10.4126}{T} - 0.96843 \log T$ or ‡$\eta v^{1/3} = 1.54222\, e^{576.151/vT}$	Shvidkovsky[84]
Golden and Tokar[1]	Compilation	M.p. to 2500	§$\log \eta = 0.5108 + \frac{220.65}{T} - 0.4925 \log T$	All the above references

*η is the viscosity in poises, v is the specific volume in cm³/g, and T is in degrees Kelvin.
†Data presented in Table V.2 in Ref. 1.
‡η is viscosity in millipoises.
§η is in centipoises.

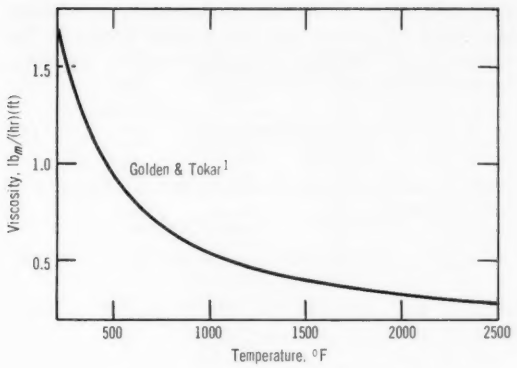

Fig. 8 The viscosity of liquid sodium.

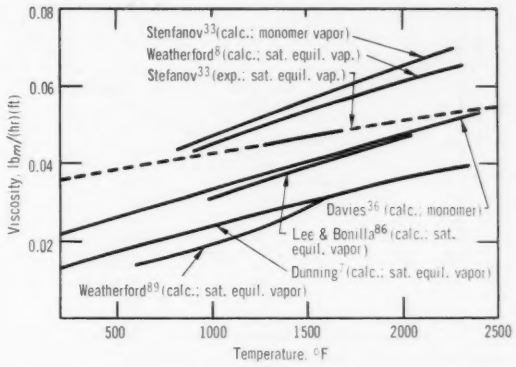

Fig. 9 Curves of viscosity of sodium vapor show little agreement. Data of Stefanov[33] are presently recommended.

fit was made of the already smoothed values to result in

$$\eta[\mathrm{lb}_m/(\mathrm{hr})(\mathrm{ft})] = 0.03427 + 8.176 \times 10^{-6} t(^\circ\mathrm{F}) \qquad (34)$$

The curve calculated from Eq. 34 is plotted in Fig. 9 along with other curves derived by experimental and theoretical investigations. Table 9 lists the investigators, the method used, and the references.

Because there is moderate agreement among most of the recent theoretical and experimental efforts, we recommend that the Stefanov data (Eq. 34) be used until additional experimental information becomes available. Calculated values for the vapor viscosity are given in Table 6.

Table 9 SODIUM-VAPOR VISCOSITY INVESTIGATIONS

Investigators	Method	Ref. sources
Lee and Bonilla[86]	Experimental (preliminary)	87
Dunning[7]	Calculated	88
Weatherford[35]	Calculated	Not clear
Weatherford[8]	Calculated	89
Davies[36]	Calculated	None
Stefanov[33]	Experimental	None

Electrical Resistivity

The electrical-resistivity values from Tepper[14] cover the widest experimental temperature range; they also represent an average of the divergent extrapolated values from other investigators (Table 10). A least-squares fit to the Tepper data is given by

$$\rho_e = 2.1737 + 7.6254 \times 10^{-3} t + 5.8207 \times 10^{-7} t^2 + 1.1262 \times 10^{-9} t^3 \qquad (35)$$

where ρ_e is in μohm-in. and t is in °F.

The electrical-resistivity values from five of the referenced investigators are in very good agreement with the values from Tepper for the range 300 to

Table 10 ELECTRICAL-RESISTIVITY INVESTIGATIONS OF LIQUID SODIUM

Investigators	Method	Temp. range, °F	Equation
Evangelisti and Isacchini[27,90]	Parallel resistor	212 to 1832	$^*\rho_e = 6.56 + 2.868 \times 10^{-2} t + 1.868 \times 10^{-5} t^2 + 9.078 \times 10^{-9} t^3$
Tepper[14]	Parallel resistor	272 to 1989	$^\dagger\rho_e = 2.1729 + 7.6248 \times 10^{-3} t + 5.8313 \times 10^{-7} t^2 + 1.1260 \times 10^{-9} t^3$
Kapelner and Bratton[31]	Parallel resistor	208.4 to 1567	$^*\rho_e = 5.904 + 3.695 \times 10^{-2} t - 9.359 \times 10^{-7} t^2 + 2.291 \times 10^{-8} t^3$
Freedman and Robertson[91]	Parallel resistor	212 to 1022	$^{*\ddagger}\rho_e = 6.3715 + 2.8728 \times 10^{-2} t + 1.8396 \times 10^{-5} t^2 + 5.1593 \times 10^{-9} t^3$
Rahiser[92]	Parallel resistor	392 to 1472	$^{*\ddagger}\rho_e = 7.6986 + 2.3705 \times 10^{-2} t + 3.0095 \times 10^{-5} t^2$
Semyachkin and Solovev[93]	Parallel resistor	212 to 1832	$^{*\ddagger}\rho_e = 6.4525 + 3.3775 \times 10^{-2} t + 9.127 \times 10^{-6} t^2 + 1.12515 \times 10^{-8} t^3$

$^*\rho_e$ is in μohm-cm and t is in °C.
$^\dagger\rho_e$ is in μohm-in. and t is in °F.
‡Curves were fitted to investigators' data.

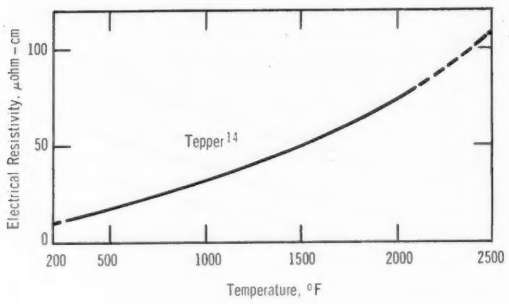

Fig. 10 Recommended electrical-resistivity values for liquid sodium are based on data by Tepper.[14]

1600°F. Also, as stated before, Eq. 35 represents an average of the extrapolated values for temperatures outside the area of agreement. It is recommended that the Tepper relation be used with temperatures from the melting point to 2500°F. Figure 10 plots the recommended Eq. 35; Table 6 lists values of electrical resistivity for various temperatures.

Surface Tension

The surface-tension data are shown in Fig. 11. Except for the Poindexter and Kernaghan[41] curve, there is moderately good agreement among all the correlations both with respect to the temperature coefficient and the actual surface-tension values obtained near the melting point (Table 11). As a result, choosing a recommended fit was difficult. So the data were pooled and the values averaged for surface tension at the melting point and the temperature coefficients (Poindexter and Kernaghan results were excluded). The resulting average melting-point

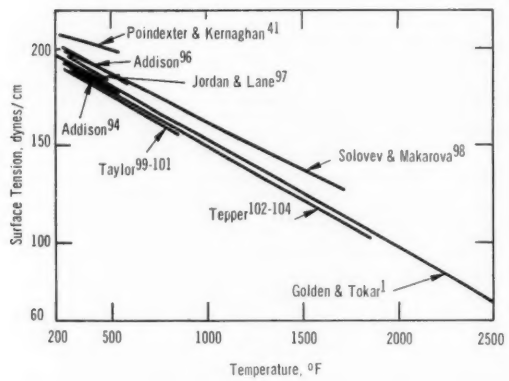

Fig. 11 Surface-tension data for sodium are in good agreement; the recommended curve (Golden and Tokar[1]) is an average of various referenced data.

surface-tension value and temperature coefficient are 196.9 dynes/cm and −0.10 dyne/(cm)(°C). The recommended relation of surface tension and temperature is given by

$$\sigma = 206.7 - 0.10t \tag{36}$$

where σ and t are in dynes/cm and °C. Equation 36 can be rewritten as

$$\sigma = 0.01429 - 3.81 \times 10^{-6} t \tag{37}$$

where σ and t are in units of lb_f/ft and °F. Surface-tension values are given in Table 6.

Table 11 SURFACE-TENSION DATA OBTAINED FROM CORRELATIONS

Investigators	Temp. range, °C	Surface tension,* dynes/cm	Temp. coefficient, dynes/(cm)(°C)
Addison[94]	128 to 180	195	−0.10
Addison[95,96]	110 to 220	202	−0.10
Jordan and Lane[97]	130 to 245	200.2	−0.11 ± 0.01
Poindexter and Kernaghan[41]	103 to 243	206.5	−0.046
Solovev and Makarova[98]	194 to 932	200.7	−0.0894
Taylor[99–101]	110 to 450	190.8	−0.10
Tepper[102–104]	141 to 992	192.5	−0.0986

*At melting point, 98°C.

Thermal-Expansion Coefficient

Table 12 gives values for the thermal-expansion coefficient, together with related data on compressibility and sonic velocity. In the absence of direct dilatometric measurements of thermal expansion at high temperatures, these values of the thermal-expansion coefficient, α_p, have been estimated from Eq. 1 as follows:

$$\alpha_p \equiv \frac{1}{V}\left(\frac{\partial V}{\partial T}\right)_p \cong \alpha_s \equiv \frac{1}{V}\left(\frac{\partial V}{\partial T}\right)_s \tag{38}$$

where the subscript s indicates saturation conditions. Figure 12 shows the thermal-expansion curve computed from this approximation.

Equation 38 is valid only for liquid sodium in equilibrium with its saturated vapor; a small correction can be made if the pressure is significantly greater than the vapor pressure. For this condition the isothermal compressibility

$$\beta_T = -\frac{1}{V}\left(\frac{\partial V}{\partial p}\right)_T = \frac{1}{\rho}\left(\frac{\partial \rho}{\partial p}\right)_T \tag{39}$$

is used in the equation

$$\alpha_p = \alpha_s - \frac{1}{V}\left(\frac{\partial V}{\partial p}\right)_T \left(\frac{\partial p}{\partial T}\right)_s = \alpha_s + \beta_T \left(\frac{\partial p}{\partial T}\right)_s \tag{40}$$

Table 12 THERMAL-EXPANSION, COMPRESSIBILITY, AND THERMAL-PRESSURE COEFFICIENTS FOR LIQUID SODIUM

Temp., °F	Thermal-expansion coefficient, $°F^{-1}$	Isothermal compressibility, atm^{-1}	Thermal-pressure coefficient, atm/°F	Sonic velocity, ft/sec	Adiabatic compressibility, atm^{-1}	Specific heat, const. vol., $Btu/(lb_m)(°F)$
210	1.3930-004*	1.7663-005*	7.89	8285	1.7150-005	0.3573
240	1.4014-004	1.7888-005	7.83	8257	1.7342-005	0.3559
270	1.4098-004	1.8117-005	7.78	8228	1.7537-005	0.3545
300	1.4183-004	1.8350-005	7.73	8199	1.7734-005	0.3530
330	1.4268-004	1.8587-005	7.68	8171	1.7935-005	0.3516
360	1.4353-004	1.8829-005	7.62	8142	1.8140-005	0.3503
390	1.4438-004	1.9075-005	7.57	8113	1.8347-005	0.3489
420	1.4524-004	1.9325-005	7.52	8085	1.8558-005	0.3475
450	1.4610-004	1.9580-005	7.46	8056	1.8772-005	0.3461
480	1.4696-004	1.9840-005	7.41	8027	1.8989-005	0.3447
510	1.4783-004	2.0105-005	7.35	7999	1.9210-005	0.3433
540	1.4870-004	2.0374-005	7.30	7970	1.9435-005	0.3420
570	1.4957-004	2.0649-005	7.24	7941	1.9663-005	0.3406
600	1.5044-004	2.0928-005	7.19	7913	1.9895-005	0.3392
630	1.5132-004	2.1213-005	7.13	7884	2.0131-005	0.3379
660	1.5219-004	2.1503-005	7.08	7855	2.0371-005	0.3365
690	1.5308-004	2.1799-005	7.02	7827	2.0614-005	0.3351
720	1.5396-004	2.2100-005	6.97	7798	2.0862-005	0.3338
750	1.5485-004	2.2406-005	6.91	7769	2.1114-005	0.3325
780	1.5574-004	2.2719-005	6.86	7741	2.1370-005	0.3311
810	1.5663-004	2.3037-005	6.80	7712	2.1630-005	0.3298
840	1.5753-004	2.3362-005	6.74	7683	2.1894-005	0.3285
870	1.5843-004	2.3693-005	6.69	7655	2.2163-005	0.3271
900	1.5933-004	2.4030-005	6.63	7626	2.2437-005	0.3258
930	1.6024-004	2.4373-005	6.57	7598	2.2715-005	0.3245
960	1.6115-004	2.4723-005	6.52	7569	2.2998-005	0.3232
990	1.6206-004	2.5080-005	6.46	7540	2.3286-005	0.3219
1020	1.6298-004	2.5443-005	6.41	7512	2.3578-005	0.3206
1050	1.6389-004	2.5814-005	6.35	7483	2.3876-005	0.3193
1080	1.6482-004	2.6191-005	6.29	7454	2.4179-005	0.3180
1110	1.6574-004	2.6576-005	6.24	7426	2.4487-005	0.3168
1140	1.6667-004	2.6969-005	6.18	7397	2.4800-005	0.3155
1170	1.6760-004	2.7369-005	6.12	7368	2.5119-005	0.3142
1200	1.6854-004	2.7777-005	6.07	7340	2.5444-005	0.3130
1230	1.6947-004	2.8193-005	6.01	7311	2.5774-005	0.3117
1260	1.7042-004	2.8618-005	5.95	7282	2.6110-005	0.3104
1290	1.7136-004	2.9050-005	5.90	7254	2.6452-005	0.3092
1320	1.7231-004	2.9491-005	5.84	7225	2.6800-005	0.3080
1350	1.7326-004	2.9941-005	5.79	7196	2.7154-005	0.3067
1380	1.7422-004	3.0400-005	5.73	7168	2.7515-005	0.3055
1410	1.7517-004	3.0868-005	5.68	7139	2.7882-005	0.3043
1440	1.7614-004	3.1345-005	5.62	7110	2.8255-005	0.3031
1470	1.7710-004	3.1832-005	5.56	7082	2.8636-005	0.3019
1930	1.9237-004	4.0662-005	4.73	6642	3.5435-005	0.2844
1960	1.9340-004	4.1340-005	4.68	6614	3.5950-005	0.2833
1990	1.9443-004	4.2032-005	4.63	6585	3.6475-005	0.2822
2020	1.9546-004	4.2738-005	4.57	6556	3.7010-005	0.2812
2050	1.9650-004	4.3459-005	4.52	6528	3.7556-005	0.2801
2080	1.9754-004	4.4195-005	4.47	6499	3.8113-005	0.2791
2110	1.9859-004	4.4947-005	4.42	6471	3.8680-005	0.2780
2140	1.9964-004	4.5715-005	4.37	6442	3.9259-005	0.2770
2170	2.0069-004	4.6499-005	4.32	6413	3.9849-005	0.2760
2200	2.0175-005	4.7300-005	4.27	6385	4.0451-005	0.2750
2230	2.0281-004	4.8118-005	4.21	6356	4.1065-005	0.2740
2260	2.0388-004	4.8954-005	4.16	6327	4.1691-005	0.2730
2290	2.0495-004	4.9807-005	4.11	6299	4.2330-005	0.2720
2320	2.0602-004	5.0679-005	4.07	6270	4.2982-005	0.2710
2350	2.0710-004	5.1569-005	4.02	6241	4.3647-005	0.2701
1520	1.7872-004	3.2665-005	5.47	7034	2.9285-005	0.2999
1550	1.7970-004	3.3178-005	5.42	7005	2.9684-005	0.2987
1580	1.8067-004	3.3702-005	5.36	6977	3.0091-005	0.2975
1610	1.8166-004	3.4236-005	5.31	6948	3.0505-005	0.2964
1640	1.8264-004	3.4781-005	5.25	6919	3.0927-005	0.2952
1670	1.8363-004	3.5337-005	5.20	6891	3.1356-005	0.2941
1700	1.8463-004	3.5905-005	5.14	6862	3.1794-005	0.2929
1730	1.8562-004	3.6484-005	5.09	6833	3.2240-005	0.2918
1760	1.8663-004	3.7075-005	5.03	6805	3.2694-005	0.2906
1790	1.8763-004	3.7678-005	4.98	6776	3.3156-005	0.2895
1820	1.8864-004	3.8294-005	4.93	6747	3.3628-005	0.2884
1850	1.8965-004	3.8922-005	4.87	6719	3.4108-005	0.2873
1880	1.9067-004	3.9564-005	4.82	6690	3.4598-005	0.2862
1910	1.9169-004	4.0218-005	4.77	6662	3.5097-005	0.2851
2370	2.0782-004	5.2174-005	3.98	6222	4.4098-005	0.2694
2400	2.0890-004	5.3097-005	3.93	6194	4.4786-005	0.2685
2430	2.0999-004	5.4040-005	3.89	6165	4.5488-005	0.2676
2460	2.1108-004	5.5003-005	3.84	6136	4.6205-005	0.2666
2490	2.1218-004	5.5988-005	3.79	6108	4.6937-005	0.2657

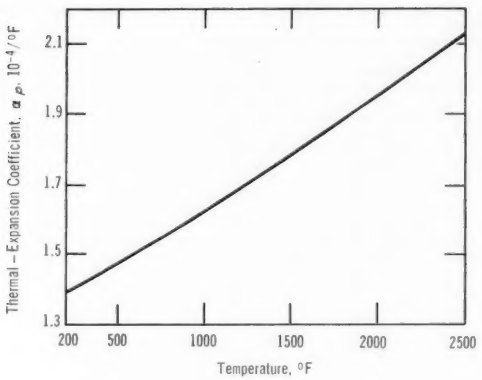

Fig. 12 Estimated thermal-expansion coefficient for sodium.

The derivative $(\partial p/\partial T)_s$ can be obtained from the slope of the vapor-pressure equation using the equations of Ditchburn and Gilmour[17] and of Stone[12] in the appropriate temperature range.

Compressibility

Although there have been many studies of the compressibility of solid sodium, no direct measurements of isothermal compressibility, β_T, have been made over the temperature range of interest, although Bridgeman[42] measured the change in compressibility at the melting point. The isothermal compressibility is related to the easily and accurately measured adiabatic compressibility, β_S, by the relations

$$\beta_T = \frac{c_p}{c_v}\beta_S \tag{41}$$

and

$$\beta_T = \beta_S + \frac{T\alpha_p^2}{\rho c_p} \cong \beta_S + \frac{T\alpha_s^2}{\rho c_p} \tag{42}$$

where the subscript S refers to an adiabatic process. Values of the isothermal compressibility are plotted in Fig. 13.

Adiabatic compressibility is determined from the velocity of sound, C, by

$$\beta_S = 1/\rho C^2 \tag{43}$$

and ρ from Eq. 1.

SONIC VELOCITY

Sonic velocities in sodium have been measured by a number of investigators, as indicated in Table 13.

Pochapsky used triply distilled sodium and an acoustic interferometer to measure the temperature

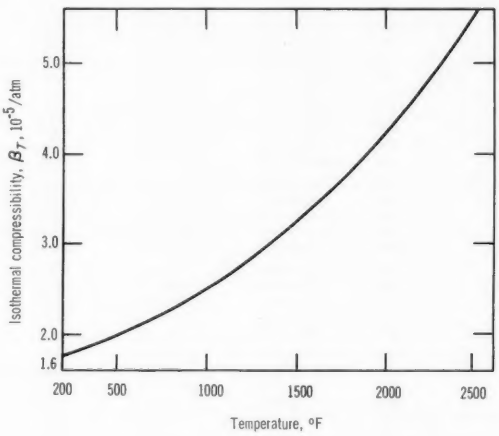

Fig. 13 Calculated isothermal compressibility of sodium.

coefficient with excellent accuracy and consistency.[43] His temperature coefficient has been substantiated by others,[44,45] including the most recent work of Trelin.[46] Therefore a linear equation, based on Pochapsky's constants, for sonic velocity and temperature was used with the density relation (Eq. 1) to calculate the adiabatic compressibility as a function of temperature.

Table 13 EXPERIMENTAL DETERMINATIONS OF SONIC VELOCITY IN LIQUID SODIUM

Investigators	Sonic velocity at melting point, m/sec	Temp. coefficient, m/(sec)(°C)	Temp. range, °C	Comments
Kleppa[105]	2395 ± 25 at 98°C	−0.3	98 to 235	1% calcium and other impurities including gas
Pochapsky[43]	2526 ± 5 at 97.6 ± 0.1°C	−0.524 ± 0.003	97.6 to 272	Acoustic interferometer; good purity
Abowitz and Gordon[44]	2526 ± 5	−0.524 ± 0.003	100 to 140	
Trelin[106]	2595 ± 47	−0.577	100 to 700	Pulsed interferometer
Jarzynski and Litovitz[107]	2526	−0.50	104 to 154	
Letcher and Beyer[108]	2525 ± 25	−0.50	97.8 to 150	
Ilgunas and Barsauskas[109]	2533	−0.66	100 to 180	
Ying and Scott[45]	2526 at 97.8°C	−0.523	97.8 to 315	

THERMAL-PRESSURE COEFFICIENT

The heat capacity at constant volume, c_v, and the thermal-pressure coefficient, γ_V, where c_v can be obtained from Eq. 41 and

$$\gamma_V = \left(\frac{\partial p}{\partial T}\right)_V = \frac{\alpha_p}{\beta_T} \tag{44}$$

were calculated. The thermal-pressure coefficient, which is plotted in Fig. 14, can be used to calculate the pressure change in confined sodium when heat is added from the relation

$$dP = \left(\frac{\partial p}{\partial T}\right)_V dT + \left(\frac{\partial p}{\partial V}\right)_T dV \tag{45}$$

This gives

$$\Delta P \cong \gamma_V \, \Delta T - \frac{1}{\beta_T} \frac{\Delta V}{V} \tag{46}$$

on substitution and integration.

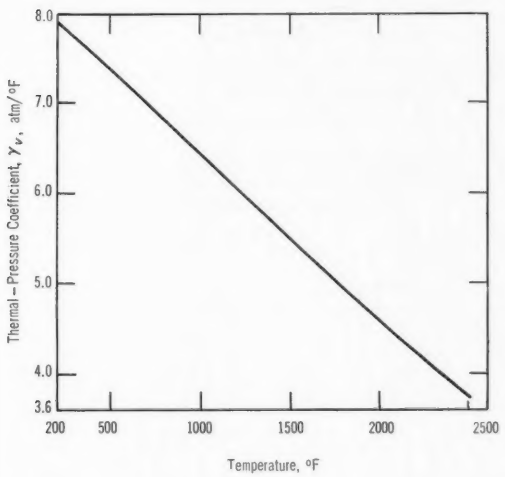

Fig. 14 Calculated thermal-pressure coefficient of sodium.

Summary

The best values for the thermophysical properties of sodium, as presented here, are based on critical evaluations of the literature through 1966. Enthalpies and entropies (Figs. 15 and 16) were computed via a FORTRAN subroutine, as were many related factors. The recommended values have been presented primarily in tabular form to facilitate engineering use.

Nomenclature

C = Sonic velocity; ft/sec
c_p = Specific heat at constant pressure; Btu/(lb)(°F)
c_v = Specific heat at constant volume; Btu/(lb)(°F)
ΔD_0° = Heat of dimerization
E = Internal energy; Btu/lb, Btu/(lb)(mole)
F = Free energy; Btu/lb, Btu/(lb)(mole)
H = Enthalpy; Btu/lb, Btu/(lb)(mole)
K = R'/R = 2.72131, Btu/(atm)(cu ft)
k = Thermal conductivity; Btu/(hr)(ft)(°F), cal/(sec)(cm)(°C)
M = Molecular weight ($M_1 \equiv 22.991$)
N = Mole fraction
P = Pressure; atm abs.
Pr = Prandtl number $\eta c_p/k$
R = Gas constant; 0.730229 (atm)(cu ft)/(lb)(mole)(°R)
R' = Gas constant; 1.98718 Btu/(lb)(mole)(°R)
S = Entropy; Btu/(lb)(°R), Btu/(lb)(mole)(°R)
T = Absolute temperature; °R(≡°F + 459.7), °K(≡°C + 273.15)
t = Temperature; °F, °C
V = Specific volume; cu ft/lb
v = Specific volume; cu ft/(lb)(mole)(monomer), cm^3/g
x = Weight fraction
α = Thermal diffusivity; $k/\rho_l c_p$; sq ft/hr
α_p = Thermal-expansion coefficient; $°F^{-1}$
α_s = Thermal-expansion coefficient for saturation conditions; $°F^{-1}$
β_S = Adiabatic compressibility; atm^{-1}
β_T = Isothermal compressibility; atm^{-1}
γ_V = Thermal-pressure coefficient; atm/°F
η = Dynamic viscosity; $lb_m/(hr)(ft)$
ρ = Vapor density; lb/cu ft, (lb)(mole)(monomer)/cu ft
ρ_l = Liquid density; lb/cu ft, (lb)(mole)(monomer)/cu ft
ρ_e = Electrical resistivity; μohm-cm
σ = Surface tension; lb_f/ft

SUBSCRIPTS

D = Dimerization
f = Formation
i = State
l = Liquid
m = Mass
p = Pressure
s = Adiabatic process; saturation
T = Tetramerization
v = Vaporization
0 = Absolute zero
1 = Monomer
2 = Dimer
4 = Tetramer

SUPERSCRIPTS

° = Standard state
l = Liquid phase
g = Gaseous phase
s = Solid phase

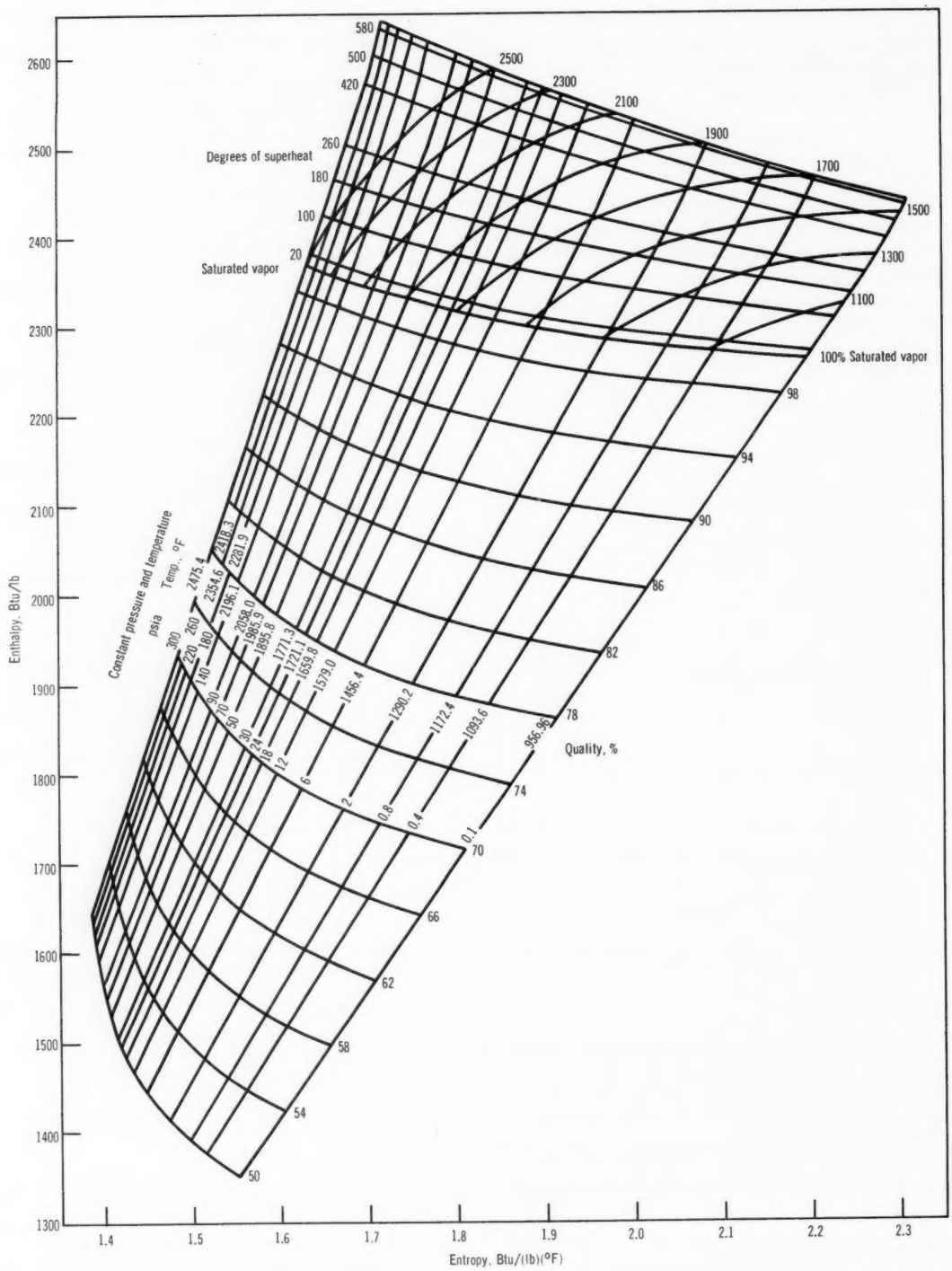

Fig. 15 Mollier diagram for sodium.

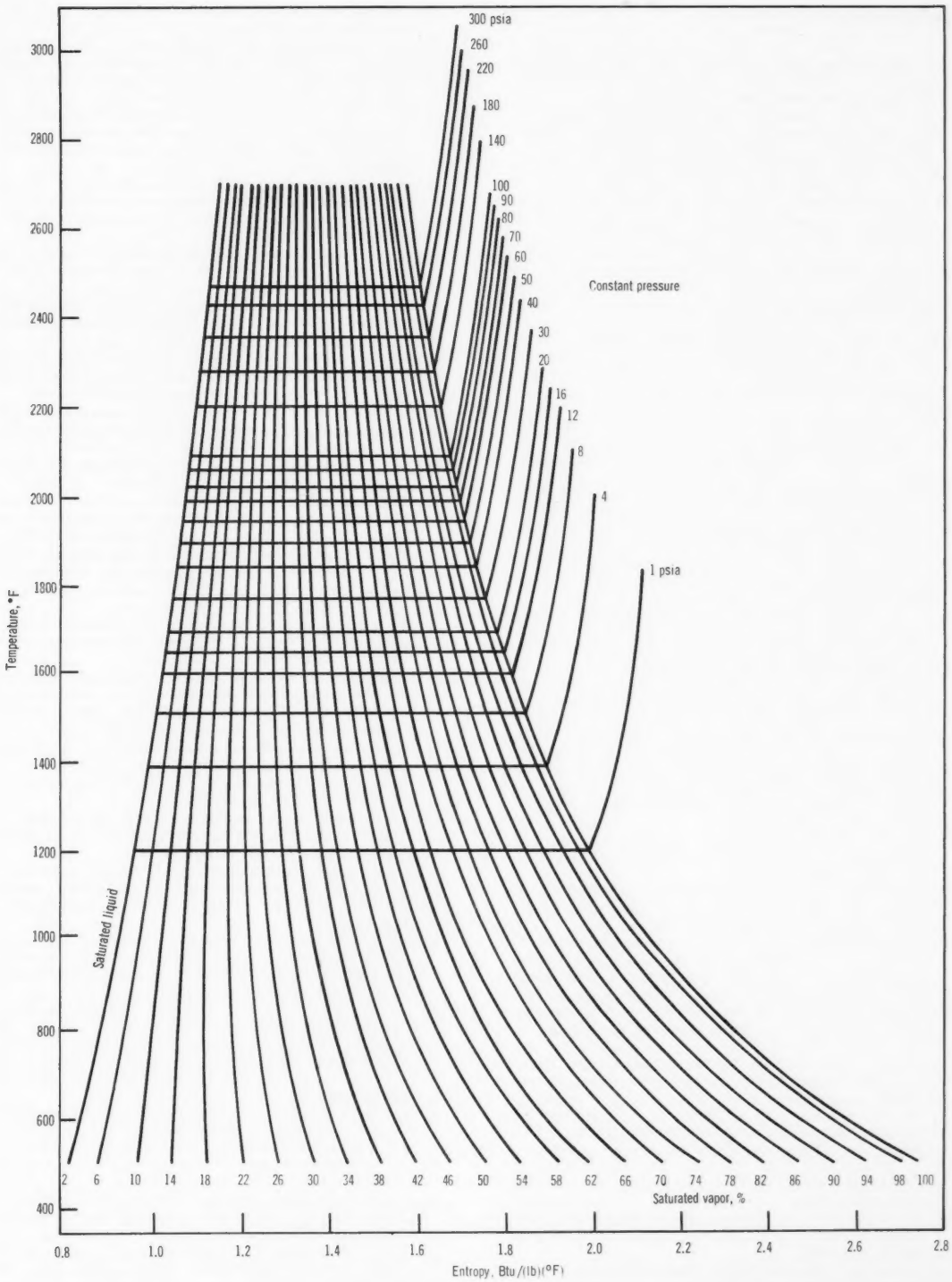

Fig. 16 Temperature–entropy diagram for sodium.

References

1. G. H. Golden and J. V. Tokar, Thermophysical Properties of Sodium, USAEC Report ANL-7323, Argonne National Laboratory, August 1967.
2. R. R. Miller, Physical Properties of Liquid Metals, in *Liquid Metals Handbook*, R. N. Lyon (Ed.), Report NAVEXOS P-733, 1st ed., Chap. 2, June 1952.
3. R. R. Miller, Physical Properties of Liquid Metals, in *Liquid Metals Handbook*, 2nd ed., June 1952.
4. R. R. Miller and L. F. Epstein, Physical Properties—Sodium, in *Liquid Metals Handbook, Sodium (NaK) Supplement*, 3rd ed. (TID-5277), July 1, 1955.
5. G. W. Thomson and E. Garelis, Physical and Thermodynamic Properties of Sodium, Chap. 9 of *Sodium, Its Manufacture, Properties, and Uses*, M. Sittig, Ed., ACS Monograph Series No. 133, Reinhold Publishing Corporation, New York, 1956.
6. C. J. Meisl and A. Shapiro, Thermodynamic Properties of Alkali Metal Vapors and Mercury, 2nd Rev., Report R60FPD358-A, General Electric Company, Flight Propulsion Laboratory Department, Nov. 9, 1960.
7. E. L. Dunning. The Thermodynamic and Transport Properties of Sodium and Sodium Vapor, USAEC Report ANL-6246. Argonne National Laboratory, October 1960.
8. W. D. Weatherford et al., Properties of Inorganic Energy-Conversion and Heat-Transfer Fluids for Space Applications, Report WADD-TR-61-96, Southwest Research Institute, November 1961.
9. G. F. Burdi, SNAP Technology Handbook. Vol. I, Liquid Metals, USAEC Report NAA-SR-8617, Atomics International, Aug. 1, 1964.
10. K. H. Spiller, Zur Kenntnis der Physikalischen Stoffeigenschaften von Flussigmetallen, Teil II: Temperaturbereich Zwischen Siedepunkt und etwa 1300°C, *Atomkernenergie*, 10(H.5/6): 215 (1965).
11. D. Miller, A. B. Cohen, and C. E. Dickerman, Estimation of Vapor and Liquid Density and Heat of Vaporization of the Alkali Metals to the Critical Point, in Proceedings of the International Conference on the Safety of Fast Breeder Reactors, Aix-en-Provence, France, September 19–22, 1967 (to be published).
12. J. P. Stone et al., High-Temperature Properties of Sodium, Report NRL-6241, Naval Research Laboratory, Sept. 24, 1965.
13. E. I. Goltsova, Density of Lithium, Sodium, and Potassium to 1500 to 1600°C, *Teplofiz. Vys. Temp.*, 4(3): 360 (1966).
14. F. Tepper et al., Thermophysical and Transport Properties of Liquid Metals, Report AFML-TR-65-99, MSA Research Corp., May 15, 1965.
15. C. T. Ewing et al., Quarterly Progress Report No. 7 on the Measurements of the Physical and Chemical Properties of the Sodium–Potassium Alloy, Report NRL-C-3287, Naval Research Laboratory, May 1948.
16. M. M. Makansi, C. H. Muendel, and W. A. Selke, Determination of the Vapor Pressure of Sodium, *J. Phys. Chem.*, 59: 40 (1955).
17. R. W. Ditchburn and J. C. Gilmour, The Vapor Pressures of Monatomic Vapors, *Rev. Mod. Phys.*, 13: 310 (1941).
18. M. M. Makansi, W. A. Selke, and C. F. Bonilla, Thermodynamic Properties of Sodium, *J. Chem. Eng. Data*, 5(4): 441 (October 1960).
19. A. Benton and T. H. Inatomi, The Thermodynamic Properties of Sodium Vapor, *J. Chem. Phys.*, 20(12): (December 1952).
20. W. H. Evans et al., Thermodynamic Properties of the Alkali Metals, *J. Res. Nat. Bur. Stand.*, 55(2): (August 1955) (RP-2608).
21. D. R. Stull and G. C. Sinke, Thermodynamic Properties of the Elements, *Advances in Chemistry Series*, Vol. 18, American Chemical Society, November 1956.
22. *JANAF Interim Thermochemical Tables*, Vol. 3, Sodium Data, June 30, 1962.
23. D. C. Ginnings, T. B. Douglas, and A. F. Ball, Heat Capacity of Sodium Between 0° and 900°C, the Triple Point and Heat of Fusion, *J. Res. Nat. Bur. Stand.*, 45 (July 1950) (RP 2110).
24. E. E. Shpilrain et al., Experimental Investigation of Thermal and Electrical Properties of Liquid Alkali Metals at High Temperatures, *High Temp.*, 3: 870 (1965).
25. P. Y. Achener and J. T. Jouthas, The Latent Heat of Vaporization and Vapor Pressure of Sodium, USAEC Report AGN-8191 (Vol. 1), Aerojet-General Nucleonics, July 1966.
26. C. T. Ewing et al., High-Temperature Properties of Potassium, Report NRL-6233, Naval Research Laboratory, Dec. 11, 1964.
27. R. Evangelisti and F. Isacchini, Experimental Determination of the Lorenz Number of Liquid Sodium, *Energ. Nucl. (Milan)*, 12: 601 (1965).
28. R. Evangelisti and F. Isacchini, The Thermal Conductivity of Sodium in the Temperature Range 90 to 850°C, *Int. J. Heat Mass Transfer*, 8: 1303 (1965).
29. I. I. Novikov et al., The Heat-Transfer and High-Temperature Properties of Liquid Alkali Metals, *J. Nucl. Energy*, 4: 387 (1957).
30. M. A. Mikheev (Ed.), Problems of Heat Transfer, USAEC Report AEC-tr-4511, 1959.
31. S. M. Kapelner and W. D. Bratton, The Electrical Resistivity of Sodium, Potassium, Rubidium, and Cesium in the Liquid State, USAEC Report PWAC-376, Pratt & Whitney Aircraft Division, June 30, 1962.
32. I. I. Rudnev, V. S. Lyashenki, and M. D. Abramovich, Diffusivity of Sodium and Lithium, *Sov. J. At. Energy*, 11: 877 (1962).
33. B. I. Stefanov et al., Viscosity and Thermal Conductivity of the Vapors of Sodium and Potassium, *High Temp.*, 4: 131 (1966).
34. D. L. Timrot and E. E. Totskii, Dilatometric Method for the Experimental Determination of the Thermal Conductivity of Corrosive Gases and Vapors at High Temperature, *High Temp.*, 3: 685 (1965).
35. W. D. Weatherford, J. C. Tyler, and P. M. Ku, Properties of Inorganic Working Fluids and Coolants for Space Applications, Report WADC-59-598, Southwest Research Institute, December 1959.
36. R. H. Davies, E. A. Mason, and R. J. Munn, High-Temperature Transport Properties of Alkali Metal Vapors, *Phys. Fluids*, 8: 444 (1965).
37. H. A. Blum, Determination of Thermal Conductivity of Low Vapor Pressure Materials: Sodium Vapor, Southern Methodist University Status Report N66-15614, 1965.
38. W. D. Weatherford, Viscosity Prediction for Alkali Metals, Preprint of paper to be presented at the ASME Symposium on Lubrication in Nuclear Applications, Miami, June 1967.
39. C. F. Bonilla et al., Progress Reports on High-Temperature Thermal Properties of Gases and Vapors, USAEC Reports CU-2660-16, March 1965; CU-2660-26, February 1966; CU-2660-32, February 1967, Columbia University, Department of Chemical Engineering.
40. C. S. Lee, Thermal Conductivity of Alkali Metal Vapors, Doctoral Dissertation, Department of Chemical Engineering, Columbia University, forthcoming.
41. F. E. Poindexter and M. Kernaghan, Surface Tension of Sodium, *Phys. Rev.*, 33: 837 (1929).
42. P. W. Bridgeman, Change of Phase Under Pressure, II. New Melting Curves with a General Thermodynamic Discussion of Melting, *Phys. Rev.*, 6: 94 (1915).
43. T. E. Pochapsky, The Temperature Variation of the Compressibility of Molten Sodium, *Phys. Rev.*, 84: 533 (1951).
44. G. Abowitz and R. B. Gordon, Compressibility of

Liquid Sodium–Potassium Alloys, *J. Chem. Phys.*, 37: 125 (1962).
45. S. P. Ying and C. C. Scott, Attenuation Measurements of Sound and Performance of Ultrasonic Transducers in 600°F Liquid Sodium, USAEC Report APDA-180, Atomic Power Development Associates, Inc., Dec. 15, 1965.
46. Yu. S. Trelin et al., Experimental Data on the Velocity of Sound in Alkali Metals at Temperatures Up to 800°C, *High Temp.*, 4: 352 (1966).
47. C. B. Jackson et al., Density of the System K–Na, Appendix C of Quarterly Progress Report on the Measurement of the Physical and Chemical Properties of the Sodium–Potassium Alloy, No. 1, Report NRL-P-3010, Naval Research Laboratory, September 1946.
48. E. Rinck, *Compt. Rend.*, 189: 39-41 (1929).
49. E. B. Hagen, *Ann. Phys. Chem.*, 19: 436-474 (1883).
50. I. I. Novikov et al., *At. Energ.*, 1(4): 92 (1956).
51. M. Nishibayashi, Density and Viscosity of Molten Materials, Part 1. Density of Sodium and Sodium Hydroxide, Report WADC-TR-53-308(Pt. 1), Cincinnati University, November 1953.
52. K. J. Bowles and L. Rosenblum, Vapor Pressure of Sodium from 0.5 to 120 Atmospheres, Report NASA-TN-D-2849, Lewis Research Center, May 1965.
53. E. S. Sowa, Sodium Vapor Pressure to 25 Atmospheres, *Nucleonics*, 21(10): 76 (October 1963).
54. P. L. Kirillov and N. S. Grachev, Determination of Sodium Vapor Pressure at Temperatures from 880 to 1300°C, *J. Eng. Phys. (USSR)*, 11(5): 3 (1959).
55. A. K. Fischer, Quasistatic Vapor Pressure Measurements on Reactive Systems in Inert Atmosphere Box, *Rev. Sci. Instrum.*, 37(6): 717 (June 1966).
56. Y. K. Vinogradov and L. D. Volyak, Experimental Determination of the Saturated Vapor Pressure of Sodium and Potassium, *Teplofiz. Vys. Temp.*, 4(1): 50 (January–February 1966).
57. C. T. Heycock and F. E. Lamplough, The Boiling Point of Mercury, Cadmium, Zinc, Potassium, and Sodium, *Proc. Chem. Soc. (London)*, 28: 3 (1912).
58. F. Haber and W. Zisch, Anregung von Gasspektren Durch Chemische Reaktionen, *Z. Phys.*, 9: 302 (1922).
59. W. H. Rodebush and T. De Vries, The Vapor Pressure of Sodium, *J. Amer. Chem. Soc.*, 47: 2488 (1925).
60. W. Edmondson and A. Egerton, The Vapor Pressures and Melting Points of Sodium and Potassium, *Proc. Roy. Soc. (London), Ser. A*, 113: 520 (1927).
61. J. Weiler, Die Magnetooptische Bestimmung der Intensitaten der Beiden Eisten Glieder der Kaliumhauptserie und der Dampfdrucke der Kaliums, *Ann. Physik*, 1: 361 (1929).
62. R. Ladenburg and E. Thiele, Neue Dampfdruck-Messungen des Na und die Bestimmung Seiner Chemischen Konstante, *Z. Phys. Chem.*, B7: 161 (1930).
63. W. H. Rodebush and E. G. Walters, The Vapor Pressure and Vapor Density of Sodium, *J. Amer. Chem. Soc.*, 52: 2654 (1930).
64. W. H. Rodebush and W. F. Henry, The Vapor Pressure of Sodium, Low Pressure Measurements with the Absolute Manometer, *J. Amer. Chem. Soc.*, 52: 3159 (1930).
65. L. C. Lewis, Die Bestimmung des Gleichgewichts Zwischen den Atomen und den Molekulen Eines Alkalidampfes mit Einen Molekularstrahlmethode, *Z. Phys.*, 61: 786 (1931).
66. E. Thiele, Untersuchungen uber den Dampfdruck des Natriums, *Ann. Physik*, 14: 937 (1932).
67. R. Ladenburg and R. Minkowski, Der Verdampfungswarme des Natriums und die Ubergangswahrscheinlichkeit des Na-Atoms aus dem Resonanz–in den Normalzustand auf Grund Optischer Messungen, *Z. Phys.*, 6: 153 (1921).
68. H. Rowe, The Vapour Pressures of the Alkali Metals, *Phil. Mag.*, 3: 534 (1927).
69. C. T. Ewing et al., High-Temperature Properties of Sodium, Potassium, and Cesium, Report NRL-6128, Naval Research Laboratory, June 4, 1964.
70. K. K. Kelley, Contributions to the Data on Theoretical Metallurgy—III. The Free Energies of Vaporization and Vapor Pressures of Inorganic Substances, U. S. Bureau of Mines Bulletin 383, 1935.
71. A. Gebhardt, Uber der Dampfdruck von Quecksilber und Natrium, *Ber. Deut. Phys. Ges.*, 3: 187 (1905).
72. L. Hackspill, Recherches sur les Metaux Alcalins, *Ann. Chem. Phys.*, Ser. 8, 8: 613 (1913).
73. C. J. Hansen, Uber Verdampfung und Sublimation, Insbesondere Hochmolecularer Kohlenstoffverbindunger, bei Minimaltemperaturen im Vakuum, *Ber. Deut. Chem. Ges.*, 42: 210 (1909).
74. O. Ruff and O. Johannsen, Die Siedepunkte der Alkalimetalle, *Ber. Deut. Chem. Ges.*, 38: 3601 (1907).
75. H. von Wartenburg, Dampfformig Metallvergindungen, *Z. Electrochem.*, 20: 443 (1914).
76. W. T. Hicks, Evaluation of Vapor Pressure Data for Mercury, Lithium, Sodium, and Potassium, *J. Chem. Phys.*, 38(8): 1873 (1963).
77. Y. S. Chiong, Viscosity of Liquid Sodium and Potassium, *Proc. Roy. Soc. (London), Ser. A*, 157: 264 (1936).
78. E. B. Hagen, *Ann. Phys. Chem.*, 19: 437 (1883).
79. J. Godfrey (see page 12 of Ref. 5).
80. C. T. Ewing, J. A. Grand, and R. R. Miller, Viscosity of the Sodium–Potassium System, *J. Phys. Chem.*, 73: 1168 (1951).
81. C. T. Ewing, J. A. Grand, and R. R. Miller, Viscosity of the Sodium–Potassium System, *J. Phys. Chem.*, 58: 1086 (1954).
82. I. I. Novikov et al., The Heat-Transfer and High-Temperature Properties of Liquid Alkali Metals, *J. Nucl. Energy: Pt. B*, 4: 387 (1957).
83. M. A. Mikheev (Ed.), Problems of Heat Transfer, USAEC Report AEC-tr-4511, p. 33, 1959.
84. Y. G. Shvidkovsky, Certain Problems Related to the Viscosity of Fused Metals, Report NASA-TT-F-88, National Aeronautics and Space Administration, March 1962.
85. P. Y. Achener, Aerojet-General Nucleonics, San Ramon, Calif., personal communication.
86. D. I. Lee, The Viscosity of the Alkali Metal Vapors, Doctoral Dissertation, Department of Chemical Engineering, Columbia University, forthcoming.
87. D. I. Lee and C. F. Bonilla, The Viscosity of the Alkali Metal Vapors, Part I, Cesium Up to 5 Bars and 100°C; The Alkali Metals, *Chem. Soc. (London)*, Special Publication No. 22, pp. 53-74 (1967).
88. A. I. Johnson, C. Huang, and J. D. Kemp, Chart for Getting Vapor Viscosities, *Chem. Eng.*, 61: 195 (1954).
89. W. D. Weatherford, Momentum Dynamics of Gas-Phase Physical Processes, *Bull. Amer. Phys. Soc., Ser. 2*, 6(1): 41-42 (Feb. 1, 1961).
90. R. Evangelisti and F. Isacchini, Una Misura Della Resistivita Elettrica del Sodio ad Elevata Temperatura; per la Verifica Della Legge di Wiedemann–Franz–Lorenz, Italian Report RT/ING-(65)17, November 1965.
91. J. F. Freedman and W. D. Robertson, Electrical Resistivity of Liquid Sodium, Liquid Lithium, and Dilute Liquid Sodium Solutions, *J. Chem. Phys.*, 34: 769 (1961).
92. R. H. Rahiser, Electrical Resistivity of Sodium and Sodium–Potassium Alloys, USAEC File No. NP-4656, Mine Safety Appliances Co., June 17, 1953.
93. B. E. Semyachkin and A. N. Solovev, Experimental Determination of the Electrical Resistivity of Liquid Alkali Metals Up to 1000°C, *Zh. Prikl. Mekh. Tekh. Fiz.*, N.2, 176 (1964).
94. C. C. Addison, D. H. Kerridge, and J. Lewis, Liquid Metals. Part I. The Surface Tension of Liquid Sodium: The Vertical-Plate Technique, *J. Chem. Soc., C*, 2861 (1954).

95. C. C. Addison et al., Liquid Metals. Part II. The Surface Tension of Liquid Sodium: The Drop-Volume Technique, *J. Chem. Soc., C*, 2262 (1954).
96. C. C. Addison, W. E. Addison, and D. H. Kerridge, Liquid Metals. Part III. The Influence of Oxide Films on the Surface Tension of Liquid Sodium, *J. Chem. Soc., C*, 3047 (1954).
97. D. O. Jordan and J. E. Lane, The Surface Tension of Liquid Sodium and Liquid Potassium, *Aust. J. Chem.*, 18: 1711 (1965).
98. A. N. Solovev and O. P. Makarova, Study of the Surface Tension of Liquid Sodium and Potassium, *High Temp.*, 4: 187 (1966).
99. J. W. Taylor, The Surface Tension of Sodium. *J. Inst. Metals*, 83: 143 (1954–1955).
100. J. W. Taylor, The Surface Tension of Liquid Metals and Alloys, British Report AERE-M/TN-24, May 4, 1954.
101. J. W. Taylor, Solid Metal–Liquid Metal Interaction Studies, Part 1. The Surface Tension of Sodium, British Report AERE-M/R-1247, September 1953.
102. F. Tepper and F. Roehlich, Thermophysical and Transport Properties of Liquid Metals, Report AFML-TR-66-206, MSA Research Corp., May 31, 1966.
103. F. Tepper, F. Roehlich, and V. May, Thermophysical and Transport Properties of Liquid Metals, Report MSAR-65-123, MSA Research Corp., Sept. 14, 1956.
104. F. Tepper, F. Roehlich, and V. May, Thermophysical and Transport Properties of Liquid Metals, Report MSAR-65-78, MSA Research Corp., June 11, 1965.
105. O. J. Kleppa, Ultrasonic Velocities of Sound in Some Metallic Liquids. Adiabatic and Isothermal Compressibilities of Liquid Metals at Their Melting Points, *J. Chem. Phys.*, 18: 1331 (1950).
106. Yu. S. Trelin, I. V. Vasil'ev, and V. V. Roshchupkin, Measurement of the Ultrasound Velocity in Molten Alkali Metals, *At. Energ.*, 9(5): 410-411 (November 1960). Translated in *Sov. J. At. Energy*, 9: 955 (1960).
107. J. Jarzynski and T. A. Litovitz, Ultrasonic Absorption in Liquid Sodium–Potassium Alloys, *J. Chem. Phys.*, 41: 1290 (1964).
108. S. V. Letcher and R. T. Beyer, Measurement of Ultrasonic Attenuation in Liquid Sodium and Potassium, *J. Acoust. Soc. Amer.*, 35: 1571 (1963).
109. V. Ilgunas and K. Barsauskas, The Magneto-Acoustic Dispersion in Conductive Fluids, *Kauno Politechn. Inst. Darbai*, 5: 157-172 (1957) (*Chem. Abstr.*, 1960, 9403).

Research and Development on Aqueous Processing

By C. E. Stevenson and D. M. Paige

Caustic decladding followed by HNO_3 dissolution is favored as the feed-preparation method for processing D_2O-moderated organic-cooled reactor (HWOCR) fuels consisting of oxides or carbides clad in sintered aluminum product (SAP). A preliminary study indicates the feasibility of processing stainless-steel-clad oxide fuels from a fast breeder reactor in an existing commercial TBP-process solvent extraction plant. The chemistry and some process methods for transuranium elements are reviewed.

Dissolution of Fuels Clad with Sintered Aluminum Product

A recent report[1] from the Oak Ridge National Laboratory (ORNL) has reviewed potential methods of processing fuels proposed for use in a heavy-water-moderated organic-cooled reactor. Of the fuel materials being considered, carbides or oxides of uranium (or uranium and thorium) clad in SAP appear to be the leading candidates. Work at ORNL on the preparation of these fuels for processing was recently discussed in *Power Reactor Technol. and Reactor Fuel Process.*[2] The current report[1] indicates that caustic decladding of these fuels, followed by HNO_3 leaching, appears to be the most promising head-end process. Nitric acid dissolution of the cladding was very slow; only 18% of a sample of Alcoa XAP 001 material (2.4% O, 1.0% Si + Fe) was dissolved in 4 hr in boiling $8M$ HNO_3 [average rate, 0.17 mg/(min)(cm^2)], and catalysis by Hg^{2+} or F^- did not markedly accelerate the rates of dissolution. It was of interest to note, however, that, when SAP was first heated to a temperature above its melting point, relatively rapid dissolution of the material was effected in $8M$ HNO_3. Rapid dissolution of SAP also occurred in boiling $3M$ to $12M$ HCl. A residue of Al_2O_3 remained after treatment with acids or caustic.

In NaOH or NaOH–$NaNO_3$ solutions (the presence of $NaNO_3$ suppresses evolution of hydrogen and yields NH_3 in its place), the aluminum present in SAP dissolves rapidly. Following removal of the caustic solution, the residual UO_2 or UC may be dissolved in HNO_3 (unirradiated UC appears to be hydrolyzed by caustic, whereas irradiated UC probably is not). In the HNO_3 dissolution the carbon present as carbide is incompletely oxidized to CO_2; the balance is converted to organic acids, which may be extracted from strong HNO_3 solutions before uranium or uranium–thorium extraction by TBP. A feed-preparation flow sheet is shown in Fig. 1.

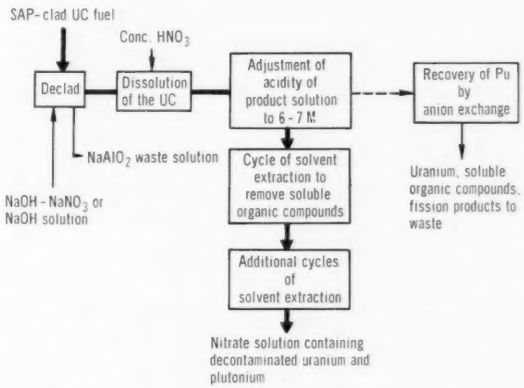
SAP-clad UC fuel
Conc. HNO3
Declad
Dissolution of the UC
Adjustment of acidity of product solution to 6 - 7 M
Recovery of Pu by anion exchange
NaAlO2 waste solution
NaOH - NaNO3 or NaOH solution
Cycle of solvent extraction to remove soluble organic compounds
Uranium, soluble organic compounds, fission products to waste
Additional cycles of solvent extraction
Nitrate solution containing decontaminated uranium and plutonium

Fig. 1 Caustic decladding of SAP-clad UC fuel.[1]

Decladding of SAP-clad or zirconium-clad fuels by fluid-bed hydrochlorination, shearing and leaching, or NH_4F treatment of zirconium cladding is also reviewed in application to HWOCR fuels, but these processes appear to be less promising.

Aqueous Processing of Fast Breeder Reactor Fuels

Nicholson, Oak Ridge National Laboratory, has made a preliminary evaluation of the capability of the Purex processing facility of Nuclear Fuel Services, Inc., at West Valley, N. Y., for the processing of a fast breeder power-reactor fuel.[3] For this purpose he has assumed a plant feed consisting of stainless-steel-clad UO_2–PuO_2 fuel combined with the axial blanket. This plant feed, with a total fission-product content equivalent to an average burnup of 38,500 Mwd/metric ton and an average plutonium content equal to 10% of the heavy metals, corresponds to the fuel specification of a reactor design made by the General Electric Company.[4] A suggested flow sheet for the first-cycle extraction (codecontamination and partition) is shown in Fig. 2.

A daily throughput of 0.52 ton of fuel cooled for 150 days was selected as being compatible with the existing plant operating license and within the capacity of the solvent extraction columns for the specified flow sheet. The shear–leach head-end facility was considered adequate for the previous fuel charge (with its increased heat dissipation and fissile content) without major modifications. However, a new tail-end facility for plutonium purification and packaging was specified to achieve a plutonium throughput as high as required for the selected fuel-processing rate. This tail-end facility would consist of a shielded, continuous, anion-exchange system. Criticality control applied to the selected flow sheet employed both concentration limits and geometrical restrictions for various parts of the plant.

Calculations indicating a solvent irradiation dose (per pass) of 0.017 watt-hr/liter for fuel cooled 150 days and 0.043 watt-hr/liter for fuel cooled 30 days were taken as a basis for the conclusion that solvent damage would be tolerable with the existing system at either cooling time.

The present plant license for the release of ^{85}Kr, ^{131}I, and ^{3}H may be limiting for the processing of such quantities of fast breeder reactor fuel, particularly if short decay cooling periods are involved, but Nicholson indicates that better performance of the off-gas treating equipment can be expected than is assumed in the license application and that greater allowances may be made for dilution. It therefore appears that an upward revision of the plant capacity might result if monitoring verifies the safety-analysis calculations.

Processing of the Actinide Elements

An excellent review article[5] by Los Alamos workers on the chemistry, preparation, and processing of the actinide elements has recently appeared. Production of the higher transuranium elements in the High Flux Isotope Reactor (HFIR) and their recovery in the Transuranium Facility (TRU) at Oak Ridge are discussed. The article also predicts that by the mid 70's we should see the production of about 1 g of ^{252}Cf per year and of significant quantities of other actinides as high as ^{257}Fm.

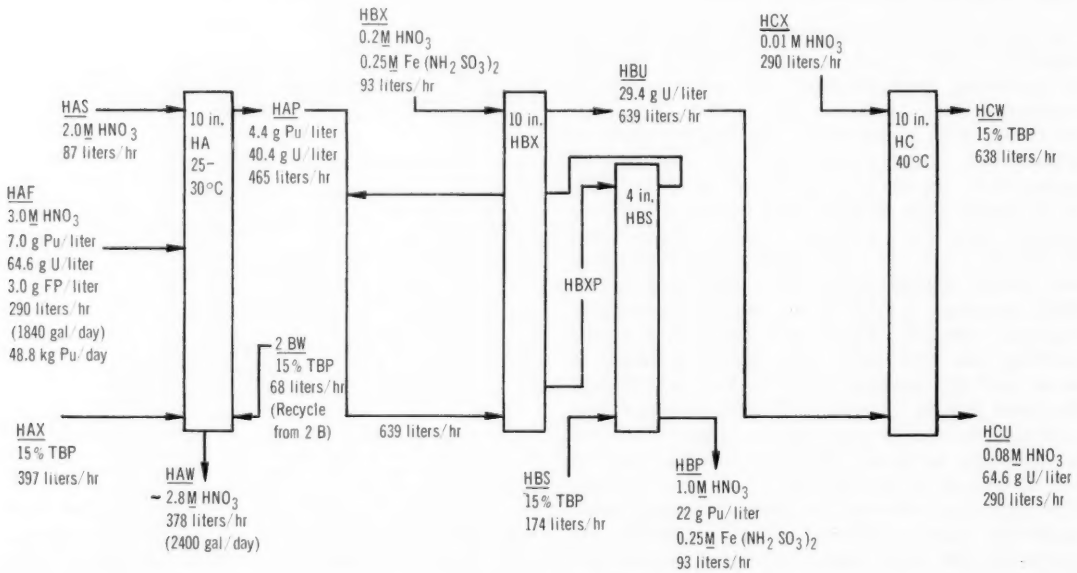

Fig. 2 First-cycle flow sheet for NFS processing of fast breeder reactor fuel.[3]

Watanabe,[6] Japan Atomic Energy Research Institute, has summarized some recent work of that Institute on the solvent extraction of heavy elements ranging from thorium to curium by tributyl phosphine oxide (TBPO) and trioctyl phosphine oxide (TOPO). Distribution-ratio data for both the chloride and nitrate systems, summarized by Watanabe, are shown in Fig. 3. This figure includes new data obtained at the Institute. The data indicate that TBPO may be used for separation of thorium or Np(V) from protactinium, U(VI), Np(IV), or Np(VI) in an HCl system. In the TOPO–HCl system, trivalent actinides may be separated from actinides having higher valences, but the separation of tetra-, penta-, and hexavalent species from each other is difficult. Uranium-VI may be separated from thorium and Np(V) by extracting from $1N$ to $2N$ HCl. In the TOPO–HNO_3 system, americium and curium are separated from tetra- and hexavalent actinides and protactinium, and selective separations of the latter from elements other than actinides are also possible.

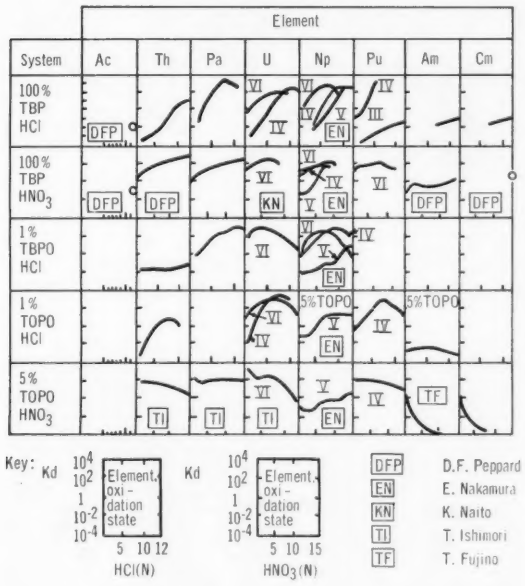

Fig. 3 Extraction of actinide elements from HCl and HNO_3 by TBP, TBPO, and TOPO.[6]

These data were applied to effect various separations. A solvent composed of 1% TOPO in toluene was used to extract ^{233}U and ^{233}Pa from a solution of irradiated thorium dissolved in $6N$ HCl, and ^{233}Pa was scrubbed from the extract with $6N$ HCl saturated with NaF. Americium was separated from rare earths (promethium, samarium, europium, and lanthanum) by reversed phase chromatography using columns containing TOPO or di-(2-ethylhexyl) phosphoric acid (HDEHP) absorbed on Kieselguhr and HNO_3 elution. Although either solvent could be used for separation of lanthanum, HDEHP was found to be better than TOPO for separating americium from promethium and europium.

Plant and Equipment Design and Operation

HYDROCLONES

The work on stacked-clone liquid–liquid contactors has been reviewed previously.[7–11] However, two recent reports are worthy of review since they cover work on a full-scale plant prototype model as well as data on 1.4-scale and 0.5-scale models.

Whatley and Groenier[12] of ORNL discuss the design features and present data on the full-scale (Mark-X size) 18-stage model. This prototype hydroclone is an integral-pump stacked-clone stainless-steel model (Figs. 4 to 7). Figure 8 is a sketch of the assembled 18-unit machine as tested. They also present data on the 0.5-scale plastic model.

Efficiencies for the prototype were compared with those for the 0.5-scale plastic model by using uranyl nitrate as the distribution species. The aqueous phase (continuous) was $1M$ $NaNO_3$–$0.08M$ HNO_3, and the organic phase was 18% TBP in Amsco. The authors report 52 to 82% efficiency for the prototype and 92 to 95% efficiency for the 0.5-scale model.

A general review of hydroclones is also presented in the report.[12]

The effect of geometric scale-up on the performance of stacked-clone contactors is discussed in a report by Finsterwalder,[13] working at ORNL as a guest scientist from West Germany. He presents data on a 1.4-scale model as well as on a 0.5-scale model and compares these with data on the full-scale Mark-X model. Table 1 presents a summary of the data for the three units.

The hydraulic K was determined from pressure-flow characteristics using water. The mathematical form of the relation is a parabola,

$$\Delta p = KF^2$$

The performance index, P, was used to compare the three models and is defined as

$$P = \frac{FE}{r^2}$$

where F is the total flow, E is the stage efficiency, and r is the scale factor.

Table 1 shows the performance index for each of the three contactors. The performance index, P, increases markedly as the size of the model decreases. A log–log plot (not shown) indicates that P is proportional to $r^{-1.08}$.

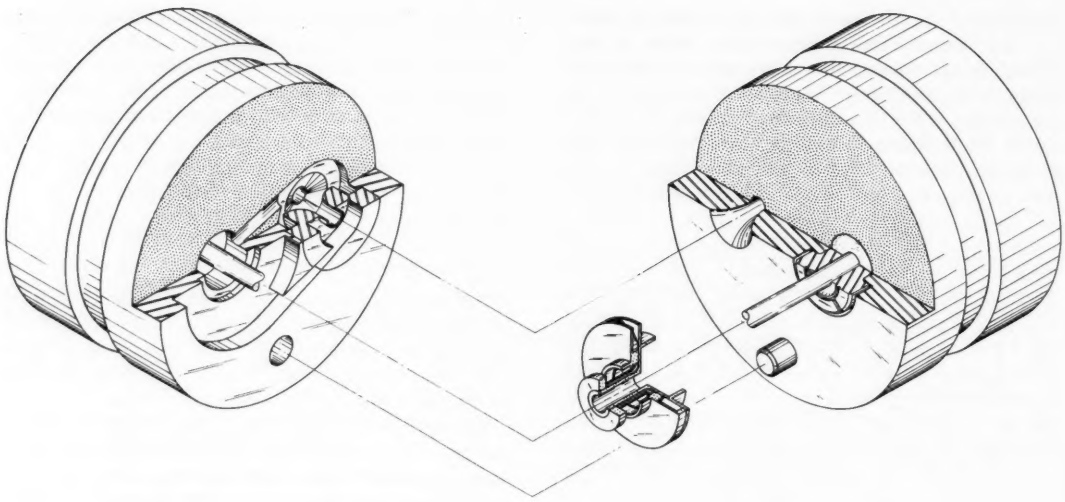

Fig. 4 Integral-pump prototype stacked-clone contactor. Cutaway illustration of adjacent stages.[12]

Fig. 5 Typical extraction stage body of the combined pump–clone contactor.[12]

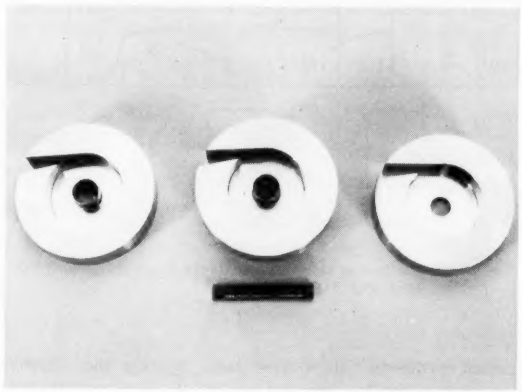

Fig. 6 Inserts for the pump–clone contactor.[12]

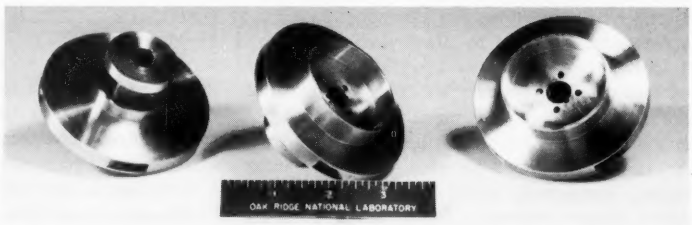

Fig. 7 Pump impellers.[12]

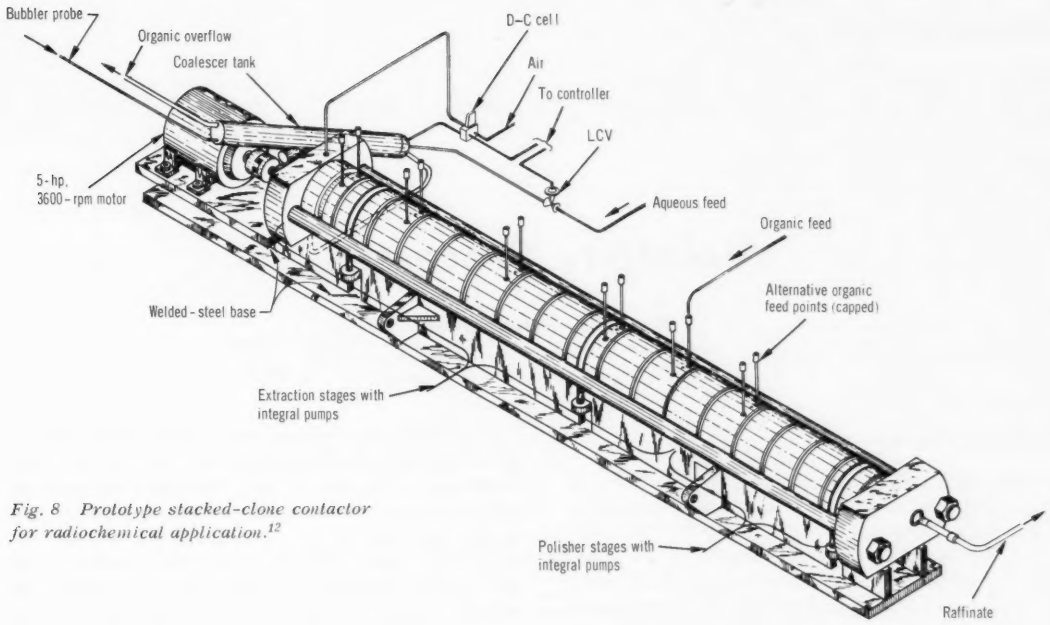

Fig. 8 Prototype stacked-clone contactor for radiochemical application.[12]

Table 1 DATA SUMMARY[13]

	0.5-scale unit	Full-scale unit	1.4-scale unit
Scale factor, r	0.5	1.0	1.4
Hydraulic K	16.7	0.99	0.28
$K \cdot r^4$	1.04	0.99	1.075
Flow capacity (flooding) at 40°C and A/O = 3, liters/min	1.25	3.08	3.67
Typical stage volumes			
Hydroclone cavity, underflow chamber, plenums, ports, and ducts, cm^3	8.5	68.4	186.0
Pump-impeller cavity and ports, cm^3	41.0*	41.0	82.0*
Pump connecting lines, cm^3	50.6*	50.6	184.0*
Total volume per stage, cm^3	100.1	160.0	452.0
Residence time† per stage at flooding, sec	1.0	3.1	7.2
Average stage efficiency, %	85	65	74
Performance index, $P = FE/r^2$	4.24	2.0	1.39

*Not scaled properly; may be varied depending upon design considerations.
†Based on flooding data at a flow ratio (A/O) of 3 and on the volumes of the hydroclone, related parts, and appropriately scaled pump and lines.

References

1. L. M. Ferris, Possible Head-End Processes for Heavy-Water-Moderated Organic-Cooled Reactor (HWOCR) Fuels, USAEC Report ORNL-4109, Oak Ridge National Laboratory, July 1967.
2. *Power Reactor Technol. and Reactor Fuel Process.*, 10(1): 61 (Winter 1966–1967).
3. E. L. Nicholson, Preliminary Investigation of Processing Fast-Reactor Fuel in an Existing Plant, USAEC Report ORNL-TM-1784, Oak Ridge National Laboratory, May 1967.
4. M. J. McNelly, Liquid Metal Fast Breeder Reactor Design Study (1000 MW_e) UO_2–PuO_2 Fueled Plant, Report GEAP-4418, General Electric Company, January 1963.
5. L. B. Asprey and R. A. Penneman, The Chemistry of the Actinides, *Chem. Eng. News*, 45: 75-82 (July 31, 1967).
6. K. Watanabe, Studies on the Solvent Extraction of Actinide Elements by Organophosphorus Compounds, Japanese Report JAERI-1132, November 1966.
7. *Reactor Fuel Process.*, 6(1): 13 (January 1963).
8. *Reactor Fuel Process.*, 6(4): 10, 11 (Fall 1963).
9. *Reactor Fuel Process.*, 8(1): 14-16 (Winter 1964–1965).
10. *Reactor Fuel Process.*, 8(4): 200-202 (Fall 1965).
11. *Power Reactor Technol. and Reactor Fuel Process.*, 10(1): 67 (Winter 1966–1967).
12. M. E. Whatley and W. S. Groenier, Chemical Technology Division Unit Operations Sections Quarterly Progress Report, April–June 1966, USAEC Report ORNL-4074, pp. 4-22, Oak Ridge National Laboratory, April 1967.
13. L. O. Finsterwalder, Geometric Scaling of Stacked-Clone Contactors, USAEC Report ORNL-4088, Oak Ridge National Laboratory, April 1967.

Volatility Processes

By J. J. Barghusen

Nitrofluor Process

The Nitrofluor process for treating reactor fuels is based on dissolution of fuel and cladding in anhydrous HF solutions containing N_2O_4, N_2O_3, or NOF as complexing agents. After the fuel is dissolved, the liquid phase is evaporated and the solid residue is contacted first with liquid BrF_3 and then with gaseous fluorine for recovery of uranium and plutonium, respectively. Recent work at Brookhaven National Laboratory (BNL)[1] has been concerned with engineering-scale demonstrations of the dissolution of UO_2 fuel clad with 30-mil Zircaloy in the 95°C azeotrope solvent ($NOF \cdot 3.1HF \cdot <0.1\ N_2O_3$) and in a NO_2–HF solution.

The dissolution tests using the 95°C azeotrope solvent were performed in a 16-in.-diameter Nickel 200 dissolver using 41 gal of solvent. The experiment involved the processing of an assembly of 20 fuel rods, 30 in. long, and containing 6.8 kg of sintered UO_2 pellets. The fuel bundle was supported within a wire basket. The dissolver solution, in this experiment, was the 95°C azeotrope containing an additional 10% free HF. The NO gas evolved during dissolution was vented continuously at 100 psig. After 20 min the solution temperature remained constant at 50°C and the venting of NO gas ceased, indicating that the Zircaloy cladding had completely dissolved. The solution was then slowly heated to 60°C whereupon dissolution of the UO_2 pellets commenced. After 2.7 hr the pellets had completely dissolved.

Subsequently the liquid phase was vented and the solid residue, mainly $NOUF_6$, was treated three times with BrF_3 to convert the uranium to UF_6. Fluorination of the salt was performed using 27-, 13-, and 23-kg batches of BrF_3 at temperatures (and durations) of 94°C (6 hr), 127°C (13 hr), and 132°C (16 hr), respectively. Owing to the failure of the heaters on the dissolver vessel to provide a temperature of 150°C during fluorination, only one-half of the uranium was recovered as UF_6 in the treatments with BrF_3.

A second experiment[1] involved the processing of 16.33 kg of sintered UO_2 pellets, clad in Zircaloy, in 60 gal of 25 mole % NO_2–75 mole % HF solution. The procedure involved the periodic addition of N_2O_4 to the dissolver already containing HF and the fuel assembly. Upon addition of half the required N_2O_4, the solution temperature and system pressure rose rapidly owing to reaction of the solvent with the cladding. Venting of the system commenced at 150 psig; however, a peak pressure of 230 psig was reached before the system pressure began to decrease. The remaining N_2O_4 was added intermittently, and the dissolution of the fuel was finished in 7 hr. This experiment indicated that the dissolution of oxide fuel in the NO_2–HF solvent can be accomplished without operational problems.

Since the development of the Nitrofluor process has reached the point where meaningful information is available for evaluating the technical and economic potentialities of the process, all work at BNL on the process has been terminated.

Aquafluor Process

General Electric Company has requested a construction permit and operating license for a nuclear fuel-reprocessing facility to be located in Grundy County, Ill.[2] This facility, Midwest Fuel Recovery Plant (MFRP), will utilize the Aquafluor process, which combines aqueous and fluoride-volatility techniques for the separation and recovery of uranium, plutonium, and neptunium from thermal reactor fuels (see Fig. 1). The plant is designed to handle 300 tons of irradiated uranium per year in the form of compacted UO_2 clad in stainless steel or zirconium alloy.

The process employs a single-cycle solvent extraction step to separate uranium, plutonium, and neptunium from the bulk of the fission products. The actinides are stripped from the solvent. Plutonium and neptunium are recovered by anion-exchange techniques. The uranium effluent stream from the ion-exchange contactors is prepared for uranium

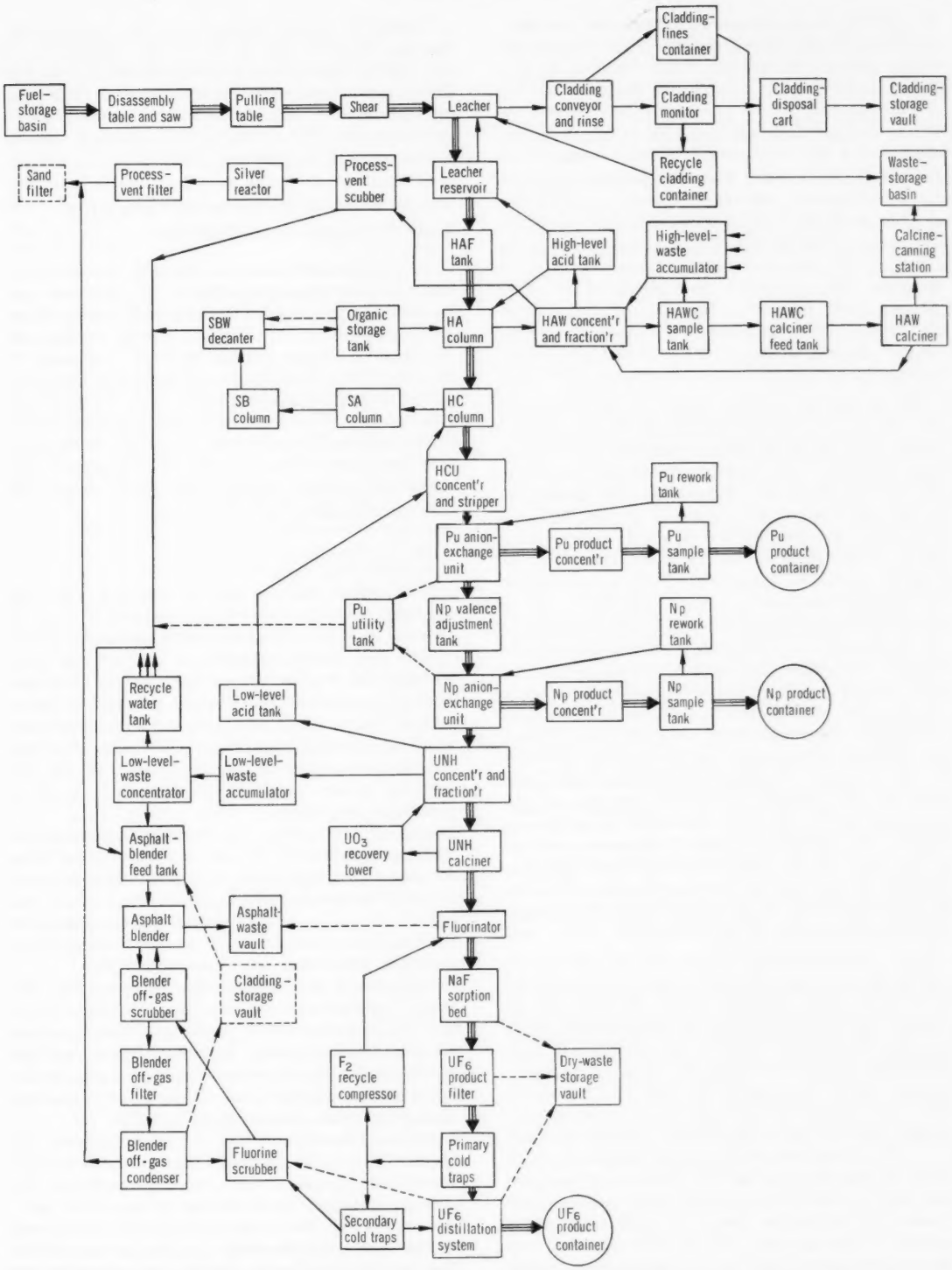

Fig. 1 Proposed Aquafluor-process flow sheet.[2]

recovery by concentration of the solution in a thermosyphon reboiler and calcination of the concentrated uranyl nitrate hexahydrate (UNH) solution to UO_3. The calciner is an electrically heated, fluid-bed reactor similar to the pilot-scale unit operated at Weldon Spring.[3] Conversion of UNH to UO_3 is accomplished at a bed temperature of 300°C using steam as the fluidizing gas. The UO_3 product from the calciner is mixed with inert aluminum oxide powder and the mixture fed by a screw conveyor to a fluid-bed reactor wherein the UO_3 is converted to UF_6 by reaction with fluorine.[2] The fluorinator is 18 in. in diameter and is cooled by circulation of water through coils bonded to the wall of the reactor. Fluorine is fed to the reactor at a rate such that the off-gas stream contains about 18 vol.% fluorine, allowing for a normal rate of UF_6 production.

The off-gas stream will contain, in addition to UF_6 and fluorine, volatile fluorides of fission-product elements such as niobium, ruthenium, and technetium and small quantities of volatile NpF_6 and PuF_6. Partial decontamination from these elements is effected when the off-gas stream is passed through a bed of NaF pellets (2-ft bed diameter) maintained at 400°C. Under these conditions some of the volatile-fluoride impurities (principally PuF_6 and ruthenium and niobium fluorides) are sorbed on NaF, whereas UF_6 is essentially unabsorbed. The gas stream from the sorbent bed is cooled in a finned-tube heat exchanger and then filtered by a system of sintered metal filters to remove particulate material. Uranium hexafluoride is collected in a series of manifolded cold traps. The traps, which are individually heated, are operated in a cyclic manner: on-line operation at low pressure, during which UF_6 is desublimed from the gas stream; and off-line operation at high pressure, during which the solid UF_6 is melted and drained to a product cylinder. Fluorine is recycled to the fluid-bed fluorinator with sufficient gas being bled off for disposal to maintain the desired system pressure. Any UF_6 in the bleed stream is recovered in a duplicate system of cold traps.

Final decontamination of the UF_6 is effected by vaporizing the liquid UF_6 from the product cylinder through a 10-in.-diameter MgF_2 sorption bed (to remove NpF_6 and technetium compounds by selective sorption) followed by a single-stage distillation step. The distillation column is 6 ft long, 4 in. in diameter, packed with a wire-mesh material, and includes a reflux condenser, a heel pot, and a product condenser. The system is designed to operate at 65 psi and 100°C. High-boiling fluoride impurities are collected in the heel pot and are periodically removed and disposed of in the fluorine-waste-gas scrubber system (a bubble-cap tray scrubber using KOH solution). The purified UF_6 product is loaded into shipping cylinders using continuous weighing during filling of the cylinder.

Facilities for the production of 1500 lb of elemental fluorine per day by fused-salt electrolysis of $HF-KHF_2$ solution are provided in the MFRP. The fluorine-generation system employs seven 6000-amp, series-connected cells, each cell containing 3000 lb of electrolyte. The cells are water cooled to provide a uniform cell temperature of 83°C.

Purification of Uranium Hexafluoride and Plutonium Hexafluoride

In the fluid-bed fluoride-volatility processing of reactor fuel materials, volatile UF_6 and PuF_6 are produced by reaction of the fuel with gaseous fluorinating agents such as ClF, ClF_3, BrF_5, and fluorine. In these reactions volatile-fluoride compounds of certain fission products are also produced and appear in the UF_6 and PuF_6 process streams. [See process flow sheets, Figs. 2 and 3, in *Power Reactor Technology and Reactor Fuel Processing*, 10(1): 74 (Winter 1966–1967).] Some of the recent work on developing methods for removing these compounds from process streams is described below.

REMOVAL OF IMPURITIES FROM UF_6

Evaluation of NaF and MgF_2 as Sorbents. The use of solid sorbents that selectively collect fluoride impurities from a UF_6 gas stream while allowing the UF_6 to pass through the system unaffected is being investigated at the Oak Ridge Gaseous Diffusion Plant.[4] A series of tests were performed to evaluate NaF at 344 or 400°C and MgF_2 at 120°C as sorbents for NbF_5, TaF_5, RuF_5, SbF_5, and TiF_4. In these tests UF_6 gas streams containing fluorine and the fluoride impurity were circulated continuously through a packed bed of sorbent.

Both sorbents were satisfactory in reducing the NbF_5 concentration in UF_6 gas streams from 460 ppm to less than 1 ppm prior to breakthrough. Niobium loadings on both sorbents averaged 5 to 7 wt.%. Some caking of NaF was experienced at the inlet to the packed bed in tests in which the NbF_5 concentration was high. This was not observed with MgF_2.

Preliminary data[4] suggest that MgF_2 at 120°C is a satisfactory sorbent for removing TiF_4 from UF_6 if the concentration of TiF_4 in the gas stream is less than 10 ppm. Titanium concentrations in the gas leaving the MgF_2 trap were less than 1 ppm. Meaningful data have not yet been obtained for UF_6 streams containing higher concentrations of TiF_4.

Sodium fluoride at 344°C appears to be a good sorbent for RuF_5, reducing the ruthenium concentration in the gas stream from 250 to 2 ppm. The volatile ruthenium fluoride used in this study (presumably RuF_5) was prepared by direct fluorination of the metal, and therefore the effectiveness of NaF for trapping ruthenium can not be extended with certainty to other volatile ruthenium fluorides or

oxyfluorides produced by fluorination of oxides. It was observed that the $NaF-RuF_5$ complex was unstable and tended to decompose and desorb upon exposure to air. This behavior precluded accurate determination of ruthenium loading and identification of the complex.[4]

Effective trapping of TaF_5 (<1 ppm TaF_5 in the exit gas) was achieved[4] by the use of MgF_2 at 120°C or NaF at 344°C. Preliminary results indicate that MgF_2 at 120°C is a satisfactory sorbent for removing SbF_5 from UF_6.

In general, the quantity of uranium picked up by the sorbent in any of the tests was less than 2×10^{-2} wt.% of the total quantity of uranium passed through the sorbent bed.

Revised Specifications for UF_6. Uranium hexafluoride derived from the reprocessing of highly irradiated power-reactor fuels will contain certain impurities at levels not present in UF_6 derived from both normal uranium and low-burnup reactor fuels. These impurities are ^{232}U and alpha-active transuranium elements. To establish whether the 1958 specification limits for these materials were necessary, AEC appointed a Uranium Hexafluoride Specifications Study Committee in January 1966 to reexamine all UF_6 specifications with respect to the need for these specifications.[5] The examination indicated that all specifications were required for safe and economical operation of the diffusion plants and that all specification limits were economically achievable by manufacturers of normal UF_6. However, the study showed that the limit for ^{232}U of 11 parts per billion parts ^{235}U and the transuranic alpha-activity limit of 150 dis/min per gram of uranium, which were previously in effect, could not be met in UF_6 from spent power-reactor fuels. On the basis of the recommendations from the committee, AEC announced a 10-fold relaxation in the ^{232}U and transuranic alpha-activity limits.[6] The specification limits for UF_6 delivered to AEC, effective July 1, 1967, are presented in Table 1.

Table 1 SPECIFICATIONS FOR URANIUM HEXAFLUORIDE DELIVERED TO THE AEC[6]

(Effective Date July 1, 1967)

Item*	Numerical value
Maximum vapor pressure of filled container at 200°F in pounds per square inch, absolute	75
Minimum weight percent of uranium hexafluoride in material	99.5
Maximum mole percent of hydrocarbons, chlorocarbons, and partially substituted halohydrocarbons	0.01
Maximum number of parts of elements indicated per million parts of total uranium	
Sb	1
Br	5
Cl	100
Nb	1
P	50
Ru	1
Si	100
Ta	1
Ti	1
otal of elements forming nonvolatile fluorides (having a vapor pressure of 1 atm or less at 300°C), e.g., Al, Ba, Bi, Cd, Ca, Cr, Cu, Fe, Pb, Li, Mg, Mn, Ni, K, Ag, Na, Sr, Th, Sn, Zn, and Zr	300
Maximum number of parts of elements or isotopes indicated per million parts of ^{235}U	
Cr	1500
Mo	200
W	200
V	200
^{233}U	500
^{232}U	0.110
Maximum thermal neutron absorption of total impurity elements as equivalent parts of boron per million parts of total uranium	8
Maximum total of gamma activity due to fission products and ^{237}U as percent of gamma activity of aged natural uranium and as measured in a high-pressure ionization chamber (Drawing D-AWM-8796 of Nuclear Division, Union Carbide Corporation)	20
Maximum beta activity due to fission products as percent of beta activity of aged natural uranium	10
Maximum number of parts of plutonium per billion parts of total uranium	1
Maximum alpha activity from all transuranic elements in disintegrations per minute per gram of total uranium	1500

*All specification analyses on uranium hexafluoride shall be performed on samples removed in the liquid state from each cylinder while its contents are liquid and homogeneous.

For several years, UF_6 containing very low concentrations of neptunium and plutonium was fed to the Paducah Gaseous Diffusion Plant. Both neptunium and plutonium have been found on plant-equipment surfaces but neither has been detected in product streams. Since equipment contamination is a cumulative problem, the level of contamination will increase as the total quantity of neptunium and plutonium fed in the UF_6 increases; thus dilution by uncontaminated UF_6 is not a factor. Assessment of methods for removing these species from UF_6 awaits the development of accurate sampling techniques for trace amounts of the materials.[5] Preliminary tests have shown that alkaline-earth and alkali-metal fluorides are promising agents for removal of NpF_6 and PuF_6 from UF_6. Table 2 lists the results of PuF_6 sorption on metal fluorides at several temperature levels.[5] Although these tests involved the sorption of PuF_6 from a flowing fluorine stream at higher plutonium concentrations than will be encountered in a diffusion-plant feed, they indicate that several sorbents merit further studies.

NbF_5 and RuF_5 Removal by Metal Fluorides. At the 36th International Congress on Industrial Chemistry, Prusakov[7] reported the results of a study on the removal of NbF_5 and RuF_5 from UF_6 gas streams by sorption on metal fluorides. The most active sorbents for NbF_5 were NaF at 300°C, LiF at 100°C, and BaF_2 at 100 to 200°C. The interaction of NbF_5 with NaF at 100, 200, and 300°C produced sodium heptafluoroniobate (Na_2NbF_7), whereas hexafluoroni-

Table 2 TEMPERATURE DEPENDENCE FOR RETENTION OF PuF_6 ON GROUP IA AND IIA METAL FLUORIDES[5]

Sorbent	Percentage of plutonium retained at temperature, °C						
	100	200	300	400	500	600	700
LiF	29.4	46.8	87.5	88.7	96.9	89.7	90.4
NaF	98.6	99.8	99.6	99.92	99.94	99.97	98.2
KF	97.1	98.5	97.6	97.5	94.2	94.4	98.0
RbF	83.6	90.4	93.8	99.9	99.9		98.5
CsF	99.6	98.6		97.9	99.8		95.8
BeF_2	29.1	20.1	76.6	70.9	71.0	73.4	87.1
MgF_2	98.8	98.2	96.3	96.9	98.6	98.6	94.5
CaF_2	99.99	99.995	99.994	99.997	99.98		99.996
SrF_2	99.95	99.97	99.7	98.9	99.97	99.96	99.97
BaF_2	99.4	99.95	99.95	99.99	99.97	93.93	99.99

obates were produced by reaction of NbF_5 with LiF, BaF_2, MgF_2, and CaF_2. The reaction of RuF_5 with NaF, LiF, and BaF_2 at 100 to 300°C and with MgF_2 and CaF_2 at 100°C produced hexafluororuthenates of the corresponding metals. At 300°C, RuF_5 may be desorbed from the sodium fluoride complex in a fluorine gas stream. The dissociation pressures of several complex fluorides of niobium and ruthenium were measured by transpiration techniques, and the data are presented in Table 3 as constants for the equation $\log P = A - B/T$, where P is the equilibrium pressure in torrs of the volatile fluoride over the solid phase, and T is °K.

Table 3 THERMAL-DISSOCIATION PRESSURE OF FLUORONIOBATES AND FLUORORUTHENATES AS A FUNCTION OF TEMPERATURE[7]

[$\log P$ (torr) = $A - B/T$ (°K)]

System	Temperature interval, °C	A	B
$LiF-NbF_5$	210–290	5228	2456
$NaF-NbF_5$	330–480	4410	2437
MgF_2-NbF_5	120–218	4881	1659
CaF_2-NbF_5	87–223	3039	864
BaF_2-NbF_5	88–247	1995	464
$LiF-RuF_5$	229–360	5992	2878
$NaF-RuF_5$	313–490	7015	4004
MgF_2-RuF_5	165–301	3821	1445
CaF_2-RuF_5	196–375	2265	845
BaF_2-RuF_5	238–415	3994	2312

METHODS FOR PURIFICATION OF PuF_6

In the fluoride-volatility process flow sheets based on the use of interhalogens for selective fluorination of UF_6, plutonium is recovered as PuF_6 by fluorination with fluorine. Several fission products that form volatile fluorides will accompany the PuF_6, namely, ruthenium, antimony, and niobium; and the PuF_6 stream must be processed further for the preparation of a purified plutonium product.

Sorption of PuF_6 on LiF. Workers at Oak Ridge National Laboratory[8] are investigating the use of LiF as a selective sorbent for PuF_6 since this fluoride, unlike NaF and other metal fluorides, permits nearly quantitative desorption of PuF_6 at elevated temperatures. The rate of PuF_6 sorption on LiF was observed to be affected by the surface area of the sorbent. High PuF_6 sorption was achieved at 175°C with LiF having a surface area >20 m^2/g, whereas a temperature of 300°C was required to achieve a similar sorption rate with low-surface-area (3 m^2/g) LiF. The complex formed at 100°C with high-surface-area LiF has an average plutonium valence of 4.55. Tests to demonstrate the effectiveness of LiF in recovering PuF_6 from simulated process gas streams are being carried out in fluid-bed systems.

Sorption of PuF_6 on NaF. Experimental results reported by Prusakov[7] and by Argonne National Laboratory (ANL)[9] have indicated that the reaction between PuF_6 and NaF at 100 to 150°C produces the complex compound $3NaF \cdot PuF_4$. Other experiments at ANL[9] have shown that the complex salt $7NaF \cdot 6PuF_4$, prepared by aqueous chemistry, upon contact with fluorine at temperatures up to 550°C releases PuF_6 to produce the compound $2NaF \cdot PuF_4$. This material is highly stable in fluorine up to 550°C, and further recovery of plutonium from this compound by volatility techniques would be difficult.

A technique for purifying PuF_6 process gas streams based on the sorption of PuF_6 on NaF at 100°C is being explored at ANL.[10] Under the sorption conditions considered for PuF_6, UF_6, NpF_6, Tc, and small amounts of Ru, Nb, and Sb are also sorbed. Removal of uranium, neptunium, and technetium from the NaF bed is achieved by passing fluorine through the bed at 400°C. The resulting NaF bed, containing plutonium, is leached with anhydrous HF at 20°C. Sodium fluoride is soluble in liquid HF. Plutonium tetrafluoride, which is insoluble, appears as a precipitate and is recovered by filtration of the solution.

BrF_3 Reduction of PuF_6. An alternative method[10] for purifying PuF_6 streams involves the selective reduction of PuF_6 to PuF_4 with BrF_3. The procedure involves contacting the mixture of PuF_6, actinide hexafluorides, and fission-product fluorides with BrF_3 for 1 hr at 80°C. The reaction vessel is then evacuated and the temperature of the vessel increased to 150°C to volatilize the fission products and bromine fluorides. Remaining traces of uranium, neptunium, and fission products are removed from the PuF_4 product by contact with BrF_5 gas at 300°C.

Experiments have been performed[11,12] to evaluate the reduction of PuF_6 from mixtures containing gram quantities of UF_6, NpF_6, SbF_5, NbF_5, and RuF_5. Reduction of PuF_6 to PuF_4 was complete. The major portion of uranium, antimony, and niobium was separated from plutonium in the evacuation step. Even higher decontamination from these elements was achieved in the step in which the PuF_4 was contacted with BrF_5 for 6 hr at 300 to 400°C.

Essentially no decontamination from ruthenium was observed after the reduction-evacuation step.

The decontamination factor for ruthenium after the BrF_5 fluorination step was approximately 540. No significant separation of neptunium was achieved. Preliminary experiments[12] using tracer quantities of niobium and ruthenium showed unsatisfactory removal of these elements from plutonium.

Thermal Decomposition of PuF_6. Thermal decomposition of PuF_6 to PuF_4 at 300°C is being considered as a technique for separating plutonium from mixtures containing UF_6 and other fluorides. Since neptunium may be present in these mixtures as NpF_6, the behavior of NpF_6 during thermal decomposition of PuF_6 was determined at ANL.[13] Gaseous mixtures of NpF_6 and PuF_6 were circulated through a vessel at 300°C. It was observed that a small fraction of the neptunium (~0.2 wt.%) codeposited with the plutonium. The concentration of neptunium in the deposited solids was constant throughout the entire experiment. The fraction of the total neptunium in the gas mixture that codeposited with plutonium was found to be dependent upon the total quantity of plutonium deposited.

Thermal decomposition of PuF_6 has been demonstrated at ANL on an engineering scale using a fluid-bed reactor to carry out the decomposition reaction. Three experiments[14] were made to examine the feasibility of separating plutonium from UF_6-PuF_6 mixtures by thermal decomposition. In the process a mixture of gases is passed through a fluidized bed of sintered, refractory alumina (a bed of PuF_4 might be used in a large-scale continuous operation) at 300°C, and PuF_4 deposits on the bed material. In each experiment 10 kg of a PuF_6-UF_6 mixture (up to 0.4 wt.% plutonium), diluted to 40 vol.% hexafluoride with nitrogen, was processed in 8 hr.

The results of the experiments indicated that the decomposition process is very efficient as evidenced by the low plutonium content of the UF_6 off-gas stream. On the basis of analyses of process streams, a plutonium separation of about 99.9% was achieved. The final alumina bed contained 1.46 wt.% plutonium and only 0.19 wt.% uranium. The decomposition of PuF_6 to PuF_4 occurred preferentially on the sintered alumina-bed particles rather than in the gas phase.

Since the UF_6-PuF_6 feed stream to the fluid-bed decomposer was derived from fluorination of sintered UO_2-PuO_2 pellets containing synthetic fission products, the mixed feed contained some ruthenium fluoride. Analyses of the bed material and process gas streams indicated that no ruthenium was deposited with the PuF_4 on the bed and that the ruthenium passed through the decomposer with the UF_6 (Ref. 15). The ruthenium content of the PuF_4–alumina bed was 0.2 ppm.

References

1. Brookhaven National Laboratory, Nuclear Engineering Department Annual Report, December 31, 1966, USAEC Report BNL-50023, May 1967.
2. General Electric Company, Design and Analysis Midwest Fuel Recovery Plant, AEC Docket 50-268, 1966, available at AEC Public Document Room (revised Apr. 17, 1967).
3. S. Simecek and W. T. Trask, The Integrated Fluid-Bed System, USAEC Report MCW-1478, Mallinckrodt Chemical Works, June 10, 1963.
4. M. J. Stephenson, J. R. Merriman, and H. L. Kaufman, Removal of Impurities from Uranium Hexafluoride by Selective Sorption Techniques. Progress Report for 1966, USAEC Report K-1713, Union Carbide Corporation, Nuclear Division, Oak Ridge Gaseous Diffusion Plant, July 17, 1967.
5. E. D. Arnold, J. C. Barton, E. L. Keller, R. W. Levin, and F. S. Voss (Comps. and Eds.), Uranium Hexafluoride Specifications Studies. An AEC Program Status Report, USAEC Report ORO-656, Oak Ridge Operations Office, July 12, 1967.
6. *Federal Register*, 31(250): 16584 (Dec. 28, 1966).
7. V. N. Prusakov, V. K. Ezhov, O. G. Lebedev, and V. K. Popov. Some Aspects of Nuclear Fuel Reprocessing by Fluorination Method, paper presented at the 36th International Congress on Industrial Chemistry, Brussels, Sept. 10–21, 1966.
8. R. P. Milford, G. I. Cathers, R. W. Horton, and W. H. Carr, Fluoride Volatility Processing Semiannual Progress Report for Period Ending November 30, 1966, USAEC Report ORNL-TM-1849, Oak Ridge National Laboratory, July 1967.
9. R. M. Adams and A. Glassner (Comps.), Reactor Development Program Progress Report, November 1966, USAEC Report ANL-7279, pp. 68-69, Argonne National Laboratory, Dec. 21, 1966.
10. R. M. Adams and A. Glassner (Comps.), Reactor Development Program Progress Report, January 1967, USAEC Report ANL-7302, p. 75, Argonne National Laboratory, Feb. 24, 1967.
11. R. M. Adams and A. Glassner (Comps.), Reactor Development Program Progress Report, March 1967, USAEC Report ANL-7317, p. 85, Argonne National Laboratory, Apr. 28, 1967.
12. R. M. Adams and A. Glassner (Comps.), Reactor Development Program Progress Report, April 1967, USAEC Report ANL-7329, p. 72, Argonne National Laboratory, June 16, 1967.
13. R. M. Adams and A. Glassner (Comps.), Reactor Development Program Progress Report, December 1966, USAEC Report ANL-7286, pp. 52-53, Argonne National Laboratory, Jan. 26, 1967.
14. Argonne National Laboratory, Chemical Engineering Division Research Highlights, May 1966–April 1967, USAEC Report ANL-7350, 1967.
15. R. M. Adams and A. Glassner (Comps.), Reactor Development Program Progress Report, May 1967, USAEC Report ANL-7342, p. 101, Argonne National Laboratory, June 30, 1967.

Compact Pyrochemical Processes

By W. E. Miller and R. K. Steunenberg

Pyrochemical processes employ high-temperature nonaqueous methods for separations of fissile, fertile, and fission-product elements in irradiated reactor fuels. In most cases liquid metals and/or salts are used as process solvents. The required separations may be effected by selective volatilization, precipitation from a solvent, liquid metal–salt extraction, or electrolysis. Processes for ceramic (oxide or carbide), metallic, and molten-salt fuels are currently being developed. Much of the development work is directed toward the reprocessing of fast breeder reactor fuels. Processes of this type are expected to be capable of handling high-burnup, short-cooled fuels in compact equipment.

Salt-Transport Process for Fast Breeder Reactor Fuels

Current work at Argonne National Laboratory is directed toward the development of a pyrochemical process for the recovery of irradiated core and blanket fuel from fast breeder reactors. A conceptual flow sheet for this process was presented in detail in an earlier issue of *Power Reactor Technology and Reactor Fuel Processing*.[1] The process represented by the flow sheet is for UO_2-PuO_2 fuels clad with stainless steel. The oxide is first declad by selectively dissolving the stainless steel in liquid zinc at 800°C. The oxide is then separated from the zinc phase, suspended in a molten salt (47.5 mole % $MgCl_2$–47.5 mole % $CaCl_2$–5.0 mole % CaF_2), and reduced by contacting the salt with a liquid Cu–33 wt.% Mg alloy at 800°C. The gaseous fission products are released to the system atmosphere during the reduction step. The alkali, alkaline-earth, and rare-earth fission products and the MgO by-product of the reduction reaction appear in the salt, which is discarded as waste. The metallic uranium, plutonium, and the remaining noble and refractory fission products appear in the liquid-metal phase. The plutonium is then separated from the uranium and the fission products by cycling a new molten salt (50 mole % $MgCl_2$–30 mole % NaCl–20 mole % KCl) between the Cu–33 wt.% Mg alloy and a Zn–2 wt.% Mg alloy at 600°C. With this salt-transport step, the plutonium can be selectively transferred to the Zn–2 wt.% Mg alloy. The zinc and magnesium are removed from the metallic plutonium product by vacuum distillation (retorting). The uranium, which is present in the Cu–33 wt.% Mg alloy as precipitated metal, is recovered by decanting the supernatant liquid-metal alloy and washing the precipitate with liquid magnesium. Residual magnesium is removed from the uranium by retorting. Mixed UO_2-PuO_2 is prepared from the product metals by direct oxidation.

DEMONSTRATION OF SALT-TRANSPORT PROCESS STEPS

Recently reported work on the salt-transport process[2,3] has been concerned primarily with a demonstration of the flow sheet, with the exception of the decladding and oxide reconversion steps. The equipment[4] used in this demonstration, which consists of two resistance-heated reaction vessels interconnected by a heat-transfer line to permit the movement of process solvents between the vessels, is shown in Fig. 1. The starting material consisted of 233 g of PuO_2, 458 g of UO_2, and 52 g of oxides of inactive fission-product elements. The oxide-reduction and salt-transport steps of the process were easily done. In the salt-transport step, which was described in a previous issue of *Reactor and Fuel-Processing Technology*,[5] preliminary analyses indicate that 99.4% of the plutonium was transported in 14 cycles. An additional processing step was carried out to remove any copper that may have been transported with the plutonium product. In this step $ZnCl_2$ was added to the Zn–2 wt.% Mg alloy to convert the plutonium to $PuCl_3$, which was extracted into the salt phase. The plutonium was then extracted from the salt by a Zn–4 wt.% Mg alloy. The plutonium recovery in this step was 99.9%, and the copper content of the Zn–4 wt.% Mg alloy was 20 ppm, which corresponds to the amount of copper in the reagents making up the alloy.

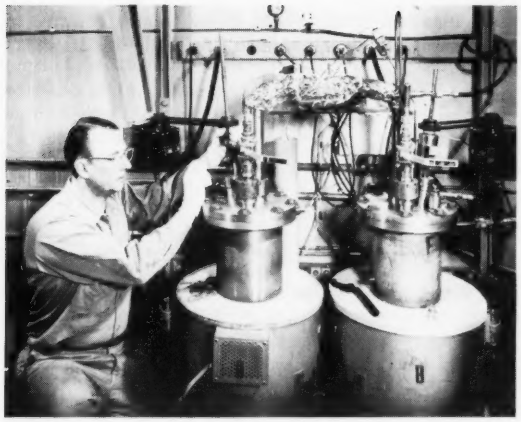

Fig. 1 Equipment for testing salt-transport process.[4]

TWO-PHASE THERMAL-CONVECTION LOOP FOR CORROSION TESTING

A two-phase thermal-convection loop made from 1-in.-diameter tubing is being developed for corrosion tests of potential container materials for pyrochemical processes.[2] The equipment consists of two loops, one on top of the other, in the form of a modified figure "8." The upper loop is filled with salt, and the lower one is filled with metal. The interface between these two immiscible phases is contained in a horizontal leg common to both loops. Temperature gradients are maintained between the vertical legs of each loop so that countercurrent thermal-convection flow occurs between the metal and salt phases.

In the first test the loop was constructed of type 304 stainless steel. The purpose of this test was to study the operating characteristics of the double-loop design. The metal phase was Cu–33 wt.% Mg, and the salt phase was 50 mole % $MgCl_2$–30 mole % NaCl–20 mole % KCl. The salt-phase temperatures were 819°C in the hot leg and 736°C in the cold leg. The metal-phase temperatures were 830°C in the hot leg and 650°C in the cold leg.

After 7 days of operation, the circulation rate of the metal phase decreased. The loop was then shut down and sectioned, and deposits of iron and chromium from the wall of the loop were found in the cold leg of the metal loop. This mass transfer of wall material from the hot leg to the cold leg was similar to that observed when liquid metals, such as bismuth, lead, and mercury, are contained in chrome–nickel steels with a temperature gradient.

This test has demonstrated the feasibility and usefulness of the double-loop design for studying corrosion in two-phase systems. Loops made from more promising container materials, such as tantalum and niobium, will be used to study corrosion of these materials.

NEPTUNIUM SOLUBILITY STUDIES

Experiments were performed to determine the solubility of neptunium in liquid cadmium and the distribution coefficient of neptunium between a molten salt (50 mole % $MgCl_2$–30 mole % NaCl–20 mole % KCl) and various cadmium–magnesium alloys.[2,3] With this information the possibility of recovering neptunium in pyrochemical processes for fast breeder reactor fuels was investigated. Initial results of the solubility experiments indicated a solubility of about 0.3 at.% neptunium in liquid cadmium at 393°C. The values of the distribution coefficient* at 650°C ranged from 3 to 0.15 for Cd–Mg alloy compositions ranging from 0.7 to 81 wt.% magnesium, respectively. These results indicate that a neptunium recovery step may be feasible.

Processes for Molten-Salt Breeder Reactor (MSBR) Fuel

Oak Ridge National Laboratory (ORNL) is developing a thermal breeder reactor in which the core fuel is a molten fluoride salt (66 mole % LiF–34 mole % BeF_2) containing ^{235}U or ^{233}U fluoride as the fissile material and ZrF_4 as the stabilizing agent to prevent uranium oxide precipitation. The blanket, which contains fertile thorium, is a molten fluoride salt of the nominal composition 71 mole % LiF–2 mole % BeF_2–27 mole % ThF_4. Nonaqueous techniques are being developed to reprocess both the core and the blanket. The objective of reprocessing the core fuel is to remove rare-earth fission products, which are thermal-neutron poisons. The objective of blanket processing is to recover fissile ^{233}U and bred ^{233}Pa, which decays to ^{233}U. Research and development work on these processes is discussed in a recent ORNL report.[6]

The major steps[6] in the present conceptual process for treating molten-salt breeder reactor fuel are shown in Fig. 2. Core fuel is first contacted with fluorine to oxidize uranium to UF_6, which volatilizes from the liquid salt. Fluorination also removes certain fission-product fluorides, such as fluorides of Mo, Te, Ru, Zr, and Nb, which volatilize along with the UF_6. The UF_6 stream is passed through salt-sorber beds to remove fission-product fluorides from the UF_6. The barren fuel-carrier salt leaving the fluorinator is LiF–BeF_2 containing rare-earth fission products. The carrier salt is purified by vacuum distillation of LiF–BeF_2. The still residue consists of a highly concentrated solution of rare earths in LiF, which is discarded as waste. The core fuel is reconstituted in a single operation in which UF_6 and H_2 are introduced into the purified molten salt and the UF_6 is reduced to UF_4. After some feed adjust-

*Distribution coefficient (K_d) = (wt.% neptunium in salt phase)/(wt.% neptunium in metal phase).

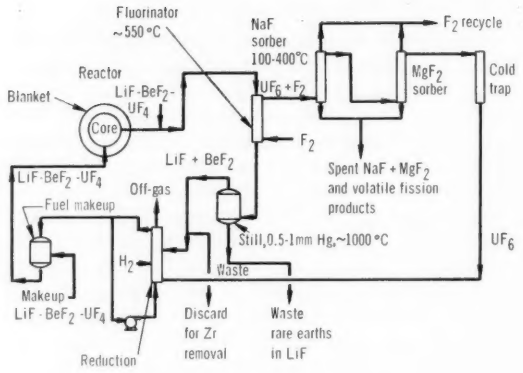

Fig. 2 Principal steps in processing irradiated fuel from a molten-salt breeder reactor.[6]

ment, the processed fuel salt is returned to the reactor core.

The feasibility of distilling fluoride salts was established in batch laboratory experiments by Kelly.[7] Equipment has now been designed for an engineering-scale demonstration of vacuum distillation of molten-salt reactor fuel. This demonstration will show that molten salt containing fission products can be fed continuously to the still at the same rate at which it is being distilled with the simultaneous accumulation of fission products in the bottoms. The still can also be operated batchwise to concentrate fission products in some small fraction of the original charge. The vacuum-distillation equipment is shown in Fig. 3.

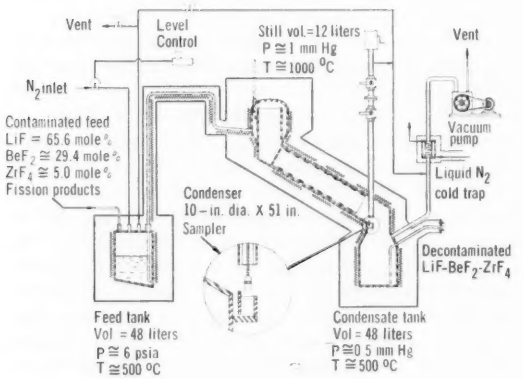

Fig. 3 Vacuum distillation[6] *of LiF–BeF_2–ZrF_4.*

To design a still requires knowledge of the relative volatilities of the rare-earth fluorides and LiF, which is the major constituent in the still pot. The volatilities of four of the rare-earth trifluorides, which have been obtained from recent experiments, relative to that of LiF at 1000°C and 0.50 mm Hg are listed as follows:

Rare-earth fluoride	Mole fraction	Relative volatility with respect to LiF
CeF_3	0.02	3×10^{-3}
LaF_3	0.02	3×10^{-4}
NdF_3	0.05	6×10^{-4}
SmF_3	0.05	2×10^{-4}

These relative volatilities show that rare-earth fluoride removals of the required efficiencies can be obtained in a still of simple design without rectification.

Two other methods of separating rare-earth fission products from the molten fuel-stream carrier salt are under investigation: (1) the rare-earth fission products may be reduced and extracted into a molten-metal phase that is immiscible with the salt or (2) they may be removed by the formation of insoluble solid solutions with UF_3.

When the molten fuel-stream carrier salt is contacted with a Bi–Li alloy, rare-earth fluorides are reduced, and the resulting rare-earth metals deposit in the alloy. Experimental results have indicated that much more than the theoretical amount of lithium disappears from the metal alloy when the alloy and the salt are contacted. It is suspected that lithium reduces some of the BeF_2 in the salt.

With the other method of rare-earth removal, the rare-earth fluorides can be precipitated with UF_3 as solid solutions by adding solid UF_3 to the molten salt. Results obtained for the removal of NdF_3 are illustrated in Fig. 4. Material-balance calculations for

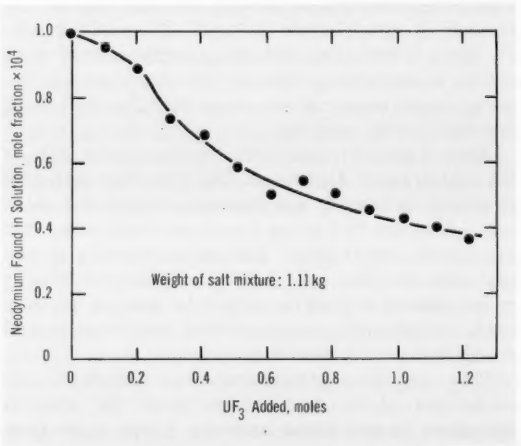

Fig. 4 Removal[6] *of NdF_3 from LiF–BeF_2 (66 to 34 mole %) at 550°C by precipitation on solid UF_3.*

the system indicate that the composition of the solid phase, resulting from the addition of UF_3, varied from 0.54 to 0.22 mole % NdF_3 in UF_3. Subsequent changes in the concentrations of NdF_3 and UF_3 in the salt mixture, as the temperature was varied from 550 to 800°C, indicated a constant solid-phase composition of 0.22 mole % NdF_3 in UF_3.

Measurements of the solubilities of rare-earth fluorides in mixtures of molten $LiF-BeF_2$ have been resumed to supplement earlier data. The purpose of this experimental program is to investigate the behavior of those rare earths which are of interest to fuel-reprocessing studies for the reference design MSBR and whose solubilities in the proposed MSBR fuel solvent have not been previously measured. The solubility of SmF_3 in 66 mole % $LiF-34$ mole % BeF_2 was determined for comparison with previous SmF_3 solubility data in a similar fluoride solvent (62.8 mole % $LiF-36.4$ mole % $BeF_2-0.8$ mole % UF_4) and with anticipated measurements of SmF_2 solubilities in the $LiF-BeF_2$ solvent. Experimental values for the solubility of SmF_3 at 600, 700, and 800°C were 0.013, 0.024, and 0.040 mole fraction, respectively. Solubilities of NdF_3 in the same solvent were 0.010, 0.019, and 0.035 mole fraction at 600, 700, and 800°C, respectively. Heats of solution calculated from the linear dependence of the logarithm of the solubility values on the reciprocal of the absolute temperature were 10.5 kcal/mole for SmF_3 and 11.5 kcal/mole for NdF_3.

The solubility values for SmF_3 in $LiF-BeF_2$ coincide only at 650°C with those obtained previously for the $LiF-BeF_2-UF_4$ solvent. The heat of solution of SmF_3, based upon the previous data, is about 13.9 kcal/mole. Although no discrepancies in the two experimental procedures are apparent, further studies would be required to investigate possible solvent effects.

Thorium is the fertile material in the MSBR blanket. Fissile ^{233}U is produced in the blanket by the reactions

$$^{232}Th + n \rightarrow {}^{233}Th \xrightarrow{\beta^-} {}^{233}Pa \xrightarrow{\beta^-} {}^{233}U$$

The concentration of ^{233}U in the blanket must be maintained at a low level to avoid appreciable parasitic neutron captures. A recent issue of *Reactor and Fuel-Processing Technology*[8] reviewed processing methods for removal of protactinium from blanket salt.

In one of the processes under study, blanket salt is contacted with Th–Bi amalgam to reduce the protactinium fluoride to metal. In another process solid thorium metal is added to the blanket salt, and the protactinium metal formed by the reduction of the fluoride is collected on steel wool. Difficulties in collecting the reduced protactinium metal have been experienced in both processes. Work on these processes is continuing.

Miscellaneous Developments

Zone-melting experiments[9] were conducted at Kernforschungszentrum, Karlsruhe, Germany, to investigate the removal of fission products and other impurities from UCl_4. In all cases the impurities distributed strongly toward the molten zone, thus moving toward the end of the sample. The separation factors (C/C_0) were between 10^{-4} and 5×10^{-2} and were in the following order: $RuCl_3 < BaCl_2 < CsCl < CeCl_3 < NaCl < ZrCl_4$. (The separation factor in this case is defined as the ratio of concentration of solute after zone melting to the concentration of solute prior to zone melting.) The values were computed for conditions after 20 passes of the molten zone at 10 mm/hr. Separations with tracer concentrations showed the same results as those obtained with higher concentrations (0.1–1 wt.%). Zone-refining experiments with a UCl_4-KCl eutectic yielded less favorable results. Separation factors under comparable conditions were less favorable by one to three orders of magnitude. For instance, for the solute $RuCl_3$, C/C_0 values were 2.0×10^{-4} and 0.12 in UCl_4 and UCl_4-KCl, respectively. In the UCl_4-KCl eutectic, zirconium tetrachloride was the only compound that distributed toward the solid phase, and it did so only when it was present in macro concentrations.

In other studies at Karlsruhe,[10] zone melting and column crystallization were compared as separative methods in the system KNO_3-NaNO_3, the binary eutectic $KCl-LiCl$, the ternary eutectic $MgCl_2-NaCl-KCl$, and the binary eutectic UCl_4-KCl. The results showed that both purification methods are, in principle, satisfactory for inorganic fused-salt separations. Zone melting appears to be well suited for the purifications of certain substances, but it requires a long period of time and only small amounts of material can be handled. Column crystallization, on the other hand, is rapid and is suitable for large throughputs. It offers the best separation efficiency in those systems in which the components are present in large concentrations. However, serious mechanical problems are encountered in applying this method to melts that have high freezing points or are highly corrosive.

Glasses, which have been used for cation exchange in molten-salt solvents, show a remarkable selectivity in certain systems. Investigations were conducted on the distribution behavior of radioactive tracers between molten salts and clean crushed glasses.[11] In a system in which the glass composition was 21.8 mole % $Na_2O-60.2$ mole % $B_2O_3-18.0$ mole % NaCl and the salt was molten $NaNO_3$, order-of-magnitude values of K_d* at 550°C for the solutes Cs^+, Ba^{2+}, and Eu^{3+} were 10^{-3}, 1, and 10^3, respectively.

*K_d is defined as (specific activity in glass phase)/(specific activity in salt phase) for the adsorption process.

References

1. *Power Reactor Technol. and Reactor Fuel Process.*, 10(1): 80 (Winter 1966–1967).
2. R. M. Adams and A. Glassner (Comps.), Reactor Development Program Progress Report, June 1967, USAEC Report ANL-7349, pp. 85-87, Argonne National Laboratory, July 31, 1967.
3. R. M. Adams and A. Glassner (Comps.), Reactor Development Program Progress Report, July 1967, USAEC Report ANL-7357, pp. 90-93, Argonne National Laboratory, Aug. 31, 1967.
4. Argonne National Laboratory, Chemical Engineering Division Research High-lights, May 1966–April 1967, USAEC Report ANL-7350, p. 19, 1967.
5. *Reactor Fuel-Process. Technol.*, 10(4): 314 (Fall 1967).
6. Oak Ridge National Laboratory, Molten-Salt Reactor Program. Semiannual Progress Report for Period Ending February 28, 1967, USAEC Report ORNL-4119, July 1967.
7. M. J. Kelly, Removal of Rare-Earth Fission Products from Molten-Salt Reactor Fuels by Distillation, *Trans. Amer. Nucl. Soc.*, 8: 170 (May 1965).
8. *Reactor Fuel-Process. Technol.*, 10(3): 235 (Summer 1967).
9. R. von Ammon, Use of Zone Melting for Purification of Irradiated Nuclear Fuels, *Nukleonik*, 9(2): 65-69 (February 1967).
10. R. von Ammon, Studies on Nuclear-Technology Application of Column Crystallization and Comparison with Zone-Melting Methods, German Report KFK-502, October 1966.
11. M. H. Rowell, Ion Exchange in Fused Salts. III. The Cation Exchange Characteristics of Some Borate, Borosilicate, and Borophosphate Glasses in Fused Sodium Nitrate, USAEC Report USNRDL-TR-1091, Naval Radiological Defense Laboratory, September 1966.

Progress in Waste-Disposal Research and Development

By Phillip Fineman

Conversion of High-Level-Activity Wastes to Solids

FLUID-BED CALCINATION

Radioactive aqueous wastes resulting from the reprocessing of spent reactor fuel are being converted to a granular, free-flowing solid in a heated, fluid-bed calciner in the Waste Calcining Facility (WCF) of the Idaho Chemical Processing Plant (ICPP).[1] The calcined solids are removed continuously from the calciners and transported pneumatically to underground storage bins. Reductions in volume (liquid to solid) of 9 to 11 are being achieved.[1,2] Presented in the following paragraphs are further results of the second radioactive-waste-processing campaign, currently in progress, and a discussion of the operating difficulties encountered.[3-13] Also discussed are possible modifications to the WCF which would improve its operating reliability and increase throughput rates. In addition, laboratory and pilot-plant investigations related to the following are described: calcination of zirconium fluoride wastes, storage of calcine, high-temperature performance of various stainless steels in NaK, and a valveless control system.

Second Waste-Processing Campaign. Since the last report on the current processing campaign,[1] the WCF has continued to calcine successfully the aqueous plant wastes presently being produced and stored at the ICPP.[3-13] The wastes calcined during this period were aluminum nitrate solutions containing high concentrations of nitric acid and acid-deficient aluminum nitrate solutions containing high concentrations of ammonium nitrate. Some 372,000 gal of these two wastes were converted into 4800 cu ft of solids. In general, operation of the WCF was highly satisfactory. Operating problems, which are discussed below, appear to be readily solvable. Preconcentrating the blended wastes (to 85% of the original volume) made it possible to increase the net throughput of the calciner by about 15% (based on the rate of waste depletion from the tank farm).[9,11,12] The overall net feed rate* has averaged about 70 gal/hr, which exceeds the design feed rate of 60 gal/hr. The off-gas from the calciner was effectively decontaminated; the release rates to the atmosphere of ^{90}Sr and ^{106}Ru remained consistently well below the established safe release limits.

Operating Problems. Although a greater number of operating problems were encountered in this campaign[5] than in the first one,[2] the relative ease with which these problems can be solved has demonstrated the considerable flexibility of the WCF. The principal problems encountered and the means for their solutions are as follows:

1. *Plugging of the Feed System.* Sand, present in the alumina starting-bed material, and silica gel collected in the feed evaporator and then released to the feed stream, caused recurring feed-control problems early in the present campaign.[5] During the first few days after initial start-up, finely divided sand was elutriated from the fluidized bed and carried into the WCF scrubbing system. This sand then found its way into the feed system by way of the scrub solution, which is recycled to the calciner. Here the sand tended to stop or impede the flow of the feed solutions. In the future it is planned to use bed substances other than sand to eliminate this problem. One of the substances being considered is dolomite,† which is soluble in the scrubbing solution. The results of recent pilot-plant work[3,4,5] have shown that dolomite can be used as a starting-bed material. Pilot-plant work is also under way to identify the best

*The feed rate for the WCF calciner is also stated in terms of gross values. The gross feed rate has averaged about 93 gal/hr; it includes about 5% jet dilution that results during transfer of the waste solutions to the WCF and about 22.5 gal/hr of recycle from the off-gas scrubbing system.[8]

†Dolomite is composed of calcium and magnesium carbonates.

means of modifying the WCF feed system to eliminate plugging tendencies when feed solutions contain significant quantities of solids.

2. *Difficulties in Processing of $Al(NO_3)_3-NH_4NO_3$ Wastes*

> Early in July 1966, while processing aluminium nitrate waste containing a high concentration of ammonium ion, the pressure drop across the final filters increased about 4 inches, to 10.5 inches of water, during a four-day period of operation. The off-gas filters were replaced, and ammonium-free waste was started into the WCF because it was believed that the rapid rise in pressure drop was related to the ammonium waste. However, a rapid pressure drop rise occurred with the new filters until the temperature of the off-gas entering the filters was decreased from 85 to 80°C. After the temperature change, a dramatic four-inch decrease in pressure drop across the filters was observed. An analysis of the operation indicates that trace quantities of ammonium nitrate (first from the waste during calcination and later—while ammonium-free waste was being calcined—from residual material in the calciner, scrubbing system, and/or silica gel absorbers in the off-gas train) may deposit on the filters and form crystals to partially plug the filter gas passages. The connection between temperature and pressure drop could be due to a temperature effect on the size of ammonium nitrate crystals. At 84.5°C, a marked change occurs in dimensions of ammonium nitrate crystals.[5a]

3. *NaK Heating System Problems.* During the first and second processing campaigns, problems involving the NaK heating system have caused the greatest amount of downtime.[5] Several weld failures on a section of piping near one of two expansion tanks[1] and a failure in one of the duplex tubes in the calciner vessel have necessitated shutdowns for repairs.[5] In all cases a thorough review of the circumstances has linked the failures to stress conditions related to the design of the system. Some of the sources of excessive stress were eliminated by removing one expansion tank and making some piping changes. A long-range study is now under way to determine the best design to replace the existing heating system. Operating experience has shown that the entire system can be simplified and that greater reliability and increased capacity can be designed into a new system without any sacrifice in safety.

Possible Modifications to the WCF. The following modifications for improving the WCF operating reliability and processing flexibility are under consideration:[11]

1. *NaK Heating System.* Several methods of heating the WCF are being examined for the purpose of finding a replacement for the liquid-metal heating system. These methods include electric heaters, directly fired tubes using combustion gases, fluidizing air at very high temperatures, and in-bed combustion of hydrocarbons. The most promising method, which is currently under investigation, is in-bed combustion of kerosene. A 10-day run[12] made in the 12-in.-diameter pilot-plant calciner showed that in-bed burning provides a satisfactory means of heating while calcining either aluminum nitrate or zirconium fluoride wastes. Equipment inspection after the run revealed no obvious corrosion effects. Analysis of run results is under way.

2. *Reduction of Solids Carry-over.* Essentially all solids elutriated from the calciner bed are removed from the off-gas in the calciner cyclone or in the scrubbing system.[11] About 20% of the elutriated solids enter the scrubbing system where they dissolve and periodically are recycled to the feed, thus reducing the overall calciner throughput. Elimination of the solids from the off-gas by dry filtration would greatly reduce, if not eliminate, the recycle of scrubbing solution. Currently, stainless-steel filters are being considered as replacement for the calciner cyclone. Corrosion tests on applicable sintered stainless-steel fiber material and decontamination tests with filters exposed to the WCF off-gas are being conducted.

Laboratory and Pilot-Plant Investigations. A number of laboratory and pilot-plant investigations are being carried out: WCF product storage, zirconium waste calcination, effect of NaK at high temperatures on stainless steels, and the testing of a valveless feed-control system.

1. *Effect of Storage on WCF Solids Product.* The calcined solids from the WCF are stored underground in large stainless-steel bins.[14] The center-line temperature of the stored calcine may be as high as 700°C during storage due to the radioactive decay of the stored fission products. Constituents of the waste that are volatile at this center-line temperature migrate to a cooler zone where they condense. This results in a change in the distribution of the volatile constituents during the period of high heat generation.

Long-term (up to 1 year) heating experiments[5,7,10] were conducted in which heated 2-g samples of actual WCF calcine were maintained at three temperatures: 525, 700, and 800°C. The results of these experiments were as follows:

(a) Essentially no cesium volatilizes at 700°C or lower, but significant amounts volatilize at 800°C or higher.

(b) Appreciable quantities of ruthenium volatilize at temperatures as low as 525°C.

(c) The originally amorphous alumina converts to either gamma or alpha crystalline alumina, depending upon the temperature. Gamma alumina is the only crystalline form at 700°C or lower, whereas alpha alumina is the predominant crystalline form at 800°C or higher.

(d) No strontium or cerium is volatilized during storage at 800°C or lower.

All the results obtained thus far indicate that no radionuclides will escape from the solids stored at high temperatures; instead, movement of the heat sources due to radionuclide migration may result in a stable situation in which the maximum tempera-

ture of the solids is lower than that without migration. Results of future studies planned to determine the interrelation between radionuclide migration and the resulting temperature distribution may show the feasibility of using even larger, lower-cost bins for storing calcined solids than the bins in the second storage facility[14] currently being filled at ICPP.

2. *Calcination of Zirconium Wastes.* Wastes containing zirconium fluoride will be generated as a result of processing reactor fuels containing zirconium as one of the constituents. Studies[6–11] are in progress to determine the possibility of calcining zirconium fluoride wastes near the end of the current WCF processing campaign. Tests are being conducted in the 12-in.-diameter pilot-plant calciner with a simulated zirconium fluoride waste solution being used as feed. Tests are also being carried out in a corrosion–erosion test loop to determine the effects of solids from the calcination of the zirconium fluoride wastes in the off-gas scrub solution.

3. *Performance of Stainless Steels in NaK at High Temperatures.* A service test evaluation was conducted on a welded assembly* containing 304, 316, and 348 stainless steel.[15] The assembly was inserted as a section of the NaK transmission return line from the pilot-plant calciner and was exposed to NaK for 14,200 hr without failure at temperatures from slightly below 1000 to 1400°F. There was no general corrosion damage on the materials. Appreciable carbide precipitation at the grain boundaries and sigma phase (a hard intermetallic compound of the general formula Fe_mCr_n) were observed in the 304 and 348 stainless steel; only carbide precipitation was noted in the 316 stainless steel. The appearance of the sigma phase, which is probably the most significant deleterious effect, does not appear to affect the serviceability of the steel so long as the sigma-phase particles and the concentration are small.† These observations, together with evaluations of physical-property tests, indicate that these three stainless steels appear to be equally suitable from a corrosion standpoint for service with NaK in the temperature range and for the exposure time reported.

4. *Valveless Feed-Control System.* Because of the plugging and erosion of valves in the WCF feed system, a valveless, nonrestrictive control system is being sought for future application.[8–10,12] Two approaches were tested: air injection and a vortex-flow restrictor. Air injection alone is not satisfactory because it produces slugging flow. Results of small-scale tests of an air-operated vortex-flow restrictor have been very encouraging. Additional tests will be made in a full-scale mock-up of the WCF feed system.

Selected Current Literature

FEED-INJECTION STUDIES

An important feature in the operation of the WCF calciner is the feed injection of waste solutions into the heated, fluidized bed with pneumatic atomizing nozzles. In a recent article, Legler,[16] Idaho Nuclear Corporation, reports on the feed-injection studies made in connection with the development of the WCF before the first waste-processing campaign. Of several schemes tested for injecting feed solution into the bed, best results were obtained with a two-fluid pneumatic atomizing nozzle unconventionally submerged in a heated, fluidized bed. Three such nozzles (two-fluid, external-mixing atomizing nozzles of conventional design) were installed in the WCF calciner and successfully used in injecting plant wastes (first processing campaign) into the calciner. Their operation was considered very satisfactory. The author believes that this and other types of conventional pneumatic atomizing nozzles may be suitable for injecting feed into other fluid-bed processes where conversion of liquids to granular solids is desired.

ASPHALT IMMOBILIZATION OF INTERMEDIATE-LEVEL-ACTIVITY WASTES

Oak Ridge National Laboratory (ORNL) is developing a process for the asphalt-immobilization of intermediate-level-activity wastes (ILW).[17–20] Two reports[21,22] related to the development of this process have become available. The first report[21] summarizes the laboratory studies conducted at ORNL on this process. It covers laboratory work concerned with the determination of process stoichiometry and parameters and with the testing of asphalt‡ products for leaching rate of various elements, radiation stability, and safety evaluation. The other report[22] presents the results of safety tests carried out by a commercial laboratory,[18] under subcontract to ORNL, on asphalt products. Samples of pure asphalt (plus emulsifying agent) and asphalt products containing 20, 40, and 60 wt.% salts§ were subjected to various laboratory tests, including those of stability (drop weight, autoignition, and shock sensitivity) and flame propagation. Included as part of the testing program were large-scale burning tests of 30-gal drums of asphalt products. In the laboratory

*The assembly (nominal diameter of 2 in.) consisted of a schedule-40 348 stainless-steel elbow, one end of which was welded to a schedule-40 316 stainless-steel nozzle and the other end to a schedule-80 304 stainless-steel pipe.

†In applications where sigma-phase growth is undesirable, the author suggests the use of a fully austenitic stainless steel with low carbon content.

‡The asphalts used in these studies contain nominally 63 wt.% asphalt, 35 wt.% water, and 2 wt.% emulsifying agent.

§In the process proposed by ORNL, the ILW is first concentrated in a waste evaporator. This concentrate[21] is principally a nitrate solution of sodium, potassium, aluminum, and iron and often contains sulfate, chloride, fluoride, and phosphate as well.

tests all materials tested proved to be insensitive to both impact and shock. However, it was not possible to establish the autoignition temperature and burning rate for any of the materials. In the large-scale burning tests, the salt–asphalt mixtures burned vigorously; they did not explode or show a significant increase in burning rate over that for the pure asphalt.

The Nuclear Safety Information Center at ORNL has issued an indexed bibliography[23] containing abstracts of articles dealing with the following subjects: shipping containers, shipping regulations, criticality safety as related to shipping and handling, transportation accidents, and all other items dealing with safety during the transportation and/or handling of radioactive materials.

References

1. *Power Reactor Technol. and Reactor Fuel Process.*, 10(1): 89 (Winter 1966–1967).
2. R. E. Commander, G. E. Lohse, D. E. Black, and E. D. Cooper, Operation of the Waste Calcining Facility with Highly Radioactive Aqueous Waste, Report of the First Processing Campaign, USAEC Report IDO-14662, Phillips Petroleum Co., June 1966.
3. J. A. Buckham, Idaho Nuclear Corporation, unpublished, Oct. 5, 1966.
4. *Ibid.*, Nov. 3, 1966.
5. *Ibid.*, Dec. 3, 1966.
   a. Idaho Nuclear Corp., Chemical Technology Branch Annual Report for Fiscal Year 1967, USAEC Report IN-1087, p. 34, October 1967.
6. J. A. Buckham, Idaho Nuclear Corporation, unpublished, Jan. 4, 1967.
7. *Ibid.*, Feb. 2, 1967.
8. *Ibid.*, Mar. 1, 1967.
9. *Ibid.*, Mar. 5, 1967.
10. *Ibid.*, May 3, 1967.
11. *Ibid.*, June 2, 1967.
12. *Ibid.*, July 5, 1967.
13. *Ibid.*, Aug. 2, 1967.
14. *Reactor Fuel Process.*, 9(4): 232 (Fall 1966).
15. T. L. Hoffman, Performance of Types 304, 316, and 348 Stainless Steel in NaK at High Temperatures, USAEC Report IN-1089, Idaho Nuclear Corporation, May 1967.
16. B. M. Legler, Feed Injection for Heated Fluidized Beds, *Chem. Eng. Progr.*, 63(2): 75-82 (February 1967).
17. *Reactor Fuel Process.*, 9(3): 171 (Summer 1966).
18. *Reactor Fuel Process.*, 9(4): 227 (Fall 1966).
19. *Power Reactor Technol. and Reactor Fuel Process.*, 10(2): 176 (Spring 1967).
20. *Reactor and Fuel-Process. Technol.*, 10(3): 253 (Summer 1967).
21. H. W. Godbee, R. E. Blanco, E. J. Frederick, W. E. Clark, and N. S. S. Rajan, Laboratory Development of a Process for Incorporation of Radioactive Waste Solutions and Slurries in Emulsified Asphalt, USAEC Report ORNL-4003, Oak Ridge National Laboratory, July 1967.
22. J. A. Herickes and W. Schicker, Summary Report Safety Characteristics of Waste-Asphalt Products, Report TR-PL-9278, Atlantic Research Corporation, Dec. 28, 1966.
23. L. B. Shappert and R. S. Burns, Indexed Bibliography on Transportation and Handling of Radioactive Materials, USAEC Report ORNL-NSIC-33, Oak Ridge National Laboratory, June 1967.

LEGAL NOTICE

This journal was prepared under the sponsorship of the U. S. Atomic Energy Commission. Neither the United States, nor the Commission, nor any person acting on behalf of the Commission:

A. Makes any warranty or representation, expressed or implied, with respect to the accuracy, completeness, or usefulness of the information contained in this journal, or that the use of any information, apparatus, method, or process disclosed in this journal may not infringe privately owned rights; or

B. Assumes any liabilities with respect to the use of, or for damages resulting from the use of any information, apparatus, method, or process disclosed in this journal.

As used in the above, "person acting on behalf of the Commission" includes any employee or contractor of the Commission, or employee of such contractor, to the extent that such employee or contractor of the Commission, or employee of such contractor prepares, disseminates, or provides access to, any information pursuant to his employment or contract with the Commission, or his employment with such contractor.

NUCLEAR SCIENCE ABSTRACTS

The U. S. Atomic Energy Commission, Division of Technical Information, publishes *Nuclear Science Abstracts* (*NSA*), a semimonthly journal containing abstracts of the literature of nuclear science and engineering.

NSA covers (1) research reports of the U. S. Atomic Energy Commission and its contractors; (2) research reports of government agencies, universities, and industrial research organizations on a worldwide basis; and (3) translations, patents, books, and articles appearing in technical and scientific journals.

Complete indexes covering subject, author, source, and report number are included in each issue. These are cumulated quarterly, semiannually, and annually providing a detailed and convenient key to the literature.

Availability of *NSA*

SALE *NSA* is available on subscription from the Superintendent of Documents, U. S. Government Printing Office, Washington, D. C., 20402, at $30.00 per year for the semimonthly abstract issues and $22.00 per year for the four cumulated-index issues. Subscriptions are postpaid within the United States, Canada, Mexico, and all Central and South American countries, except Argentina, Brazil, Guyana, French Guiana, Surinam, and British Honduras. Subscribers in these Central and South American countries, and in all other countries throughout the world, should remit $37.00 per year for subscriptions to semimonthly abstract issues and $25.00 per year for the four cumulated-index issues.

EXCHANGE *NSA* is also available on an exchange basis to universities, research institutions, industrial firms, and publishers of scientific information. Inquiries should be directed to the Division of Technical Information Extension, U. S. Atomic Energy Commission, P. O. Box 62, Oak Ridge, Tennessee, 37830.

TECHNICAL PROGRESS REVIEWS may be purchased from Superintendent of Documents, U. S. Government Printing Office, Washington, D. C., 20402. *Nuclear Safety* at $3.50 per year (six issues) for each subscription or $0.60 per issue; each of the other journals at $2.50 per year (four issues) or $0.70 per issue. The use of the coupon below will facilitate the handling of your order.

POSTAGE AND REMITTANCE: Postpaid within the United States, Canada, Mexico, and all Central and South American countries except Argentina, Brazil, Guyana, French Guiana, Surinam, and British Honduras. For these Central and South American countries and all other countries: add, for each annual subscription, $1.00 for *Nuclear Safety* and $0.75 for each of the other journals; for single issues, add one-fourth of the single-issue price. Payment should be by check, money order, or document coupons, and MUST accompany order. Remittances from foreign countries should be made by international money order or draft on an American bank payable to the Superintendent of Documents or by UNESCO book coupons.

order form

SUPERINTENDENT OF DOCUMENTS
U. S. GOVERNMENT PRINTING OFFICE
WASHINGTON, D. C., 20402

Enclosed:

document coupons ☐ check ☐ money order ☐

Charge to Superintendent of Documents No. _____

Please send a one-year subscription to

☐ ISOTOPES AND RADIATION TECHNOLOGY
☐ NUCLEAR SAFETY
☐ REACTOR AND FUEL-PROCESSING TECHNOLOGY
☐ REACTOR MATERIALS

SUPERINTENDENT OF DOCUMENTS
U. S. GOVERNMENT PRINTING OFFICE
WASHINGTON, D. C., 20402

(Print clearly)

_____
Name

_____
Street

_____
City, State, ZIP Code